Microfluidic perfusion culture for controlling the stem cell microenvironment

by

Lily Y. Kim

S.B. Electrical Engineering
Massachusetts Institute of Technology, 1997
M.Eng. Electrical Engineering
Massachusetts Institute of Technology, 1998

SUBMITTED TO THE HARVARD-MIT DIVISION OF HEALTH SCIENCES AND TECHNOLOGY IN PARTIAL FULFILLMENT OF THE REQUIREMENTS FOR THE DEGREE OF

DOCTOR OF PHILOSOPHY IN BIOMEDICAL ENGINEERING
AT THE
MASSACHUSETTS INSTITUTE OF TECHNOLOGY

June 2008

Signature of author:_____
Harvard-MIT Division of Health Sciences and Technology
April 14, 2008

Certified by:_____
Professor Joel Voldman
Department of Electrical Engineering and Computer Science
Thesis Supervisor

Accepted by:_____
Professor Martha L. Gray
Edward Hood Taplin Professor of Medical and Electrical Engineering
Director, Harvard-MIT Division of Health Sciences and Technology

Microfluidic perfusion culture for controlling the stem cell microenvironment

by

Lily Y. Kim

Submitted to the Harvard-MIT Division of Health Sciences and Technology
on April 14, 2008 in Partial Fulfillment of the Requirements for the
Degree of Doctor of Philosophy in Biomedical Engineering

ABSTRACT

In multicellular organisms, cells do not exist in isolation but communicate with other cells via extracellular signaling molecules, many of which diffuse into the microenvironment. More than most cell types, embryonic stem cells (ESCs) are critically sensitive to their microenvironment, which plays an important role in determining whether an ESC will self-renew or differentiate. Although conventional methods exist for controlling the soluble microenvironment, they are able to exert only limited control over diffusible signaling. Especially in conventional static culture, the content of the cell culture media changes constantly over time as cells interact with and modify their surroundings.

This thesis explores the use of microfluidic perfusion as a tool for modulating diffusible cell-cell signaling in mESC culture, thus enabling more control over the soluble microenvironment over time. Non-recirculating microfluidic perfusion culture can effect a more defined microenvironment by continuously controlling the supply and removal of soluble factors, with minimal use of expensive reagents.

We describe development of the first successful protocol for culturing mouse ESCs in microfluidic perfusion over several days. To optimize flow-rate conditions such that proliferation is achieved while avoiding nutrient deprivation and high shear stress regimes, we developed novel logarithmic flow-rate devices for characterizing mESC behavior across a wide range of flow rates simultaneously. We observed both flow-rate and location-dependent proliferation and investigated the role of glucose depletion in generating these effects.

Finally, we demonstrate that perfusion culture can significantly affect diffusible cell-cell signaling in the soluble microenvironment, and thus the cell's biological state. We first show that typical flow rates are able to remove secreted factors by collecting leukemia inhibitory factor (LIF) from the output of microfluidic ESC cultures perfused with LIF-free media. We then show that two well-established serum-free media: N2B27 (neuronal differentiation media) and N2B27+LIF+BMP4 (self-renewal media) are not sufficient for successful perfusion culture of mESCs at typical densities, although they are able to support cultures in static conditions. These results suggest the presence of autocrine/paracrine loops that support ESC propagation in serum-free media when cultured under static conditions.

Thesis supervisor and thesis chair: Joel Voldman
Title: Associate Professor of Electrical Engineering and Computer Science

Thesis committee member: George Q. Daley
Title: Associate Professor of Biological Chemistry and Molecular Pharmacology and Associate Professor of Pediatrics, Harvard Medical School, Children's Hospital Boston

Thesis committee member: William Deen
Title: Professor of Chemical Engineering

Acknowledgements

Working on this thesis has been a privilege. Not often do we get the chance to explore the universe in this way, and it has been immensely rewarding. I would like to thank my advisor, Joel Voldman, for giving me the opportunity to work on this project and for all the guidance and encouragement over the years. I would also like to thank Professors Bill Deen and George Daley of the thesis committee for their valuable feedback and assistance. The Harvard-MIT Division of Health Sciences and Technology has provided me with memorable experiences in world of medicine. Dr. Tom Weaver and the Hertz Foundation have been very supportive, both financially as well as through their advice.

I would like to thank everyone in the Voldman group for all those late-night discussions, their collective scientific and engineering wisdom, as well as their great sense of humor. There's nothing like having someone there to understand what it's like when the cells on chip have died for the third week in a row, or the exhilaration when they finally live and actually do something interesting. Especial thanks to Katarina Blagović for her contributions to the neuronal differentiation work.

I would like to thank my family—my mom, Sunyim, and sister, Connie, for their enthusiasm and optimism, and especially my father, Yoobong, for inspiring me with intellectual curiosity and a desire for lifelong learning. Finally, I would like to thank my husband, Ben, who has been my best friend and cooked fantastic meals for me for the past five years, and Lucy and Gigi, who have been extremely supportive cats.

Table of Contents

Table of Figures

List of Variables

τ: Shear stress (kg m^{-1} s^{-2})
μ: viscosity (kg m^{-1} s^{-1})
Q: flow rate (m^3 s^{-1})
h: channel height (m)
w: channel width (m)
L: channel length (m)
P: pressure (kg m^{-1} s^{-2})
R: fluidic resistance (kg m^{-4} s^{-1})
x: distance along the long axis of the channel, parallel to flow (m)
y: distance along the vertical direction of culture channel, perpendicular to flow (m)
v_x: fluid velocity in the x-direction (m s^{-1})
v_{max}: maximum fluid velocity in x-direction (m s^{-1})
U: mean channel velocity (m s^{-1})
$\tau_{singlecell}$: conservative estimate for shear experienced by single cell attached to wall (kg m^{-1} s^{-2})
c_g: glucose concentration (mol m^{-3})
c_0: initial glucose concentration (mol m^{-3})
D_g: glucose diffusivity (m^2 s^{-1})
$\boldsymbol{N}$: glucose flux (mg m^{-2} s^{-1})
$\boldsymbol{n}$: normal vector
k_{ads}: coefficient (mL s^{-1})
$f(C_G)$: relative magnitude of cell proliferation as a function of glucose concentration (unitless)
m: cell density (m^{-2})
m_{coeff}: fitting parameter for model (m^{-2} s^{-1})
κ: rate constant for trapping strength for single cell (m s^{-1})
κ_{eff}: effective rate constant for ligand-receptor binding over cell-covered surface (m s^{-1})
σ: fraction of the plane occupied by traps
N_A: Avogadro's number
R_{total}: total number of receptors on cell surface
k_{on}:ligand-receptor binding constant (L s^{-1} mol^{-1})
r_{cell}: cell radius (m)
D_L: ligand diffusivity (m^2 s^{-1})
$F(r)$: Cumulative probability density function
n: 1/(inter-cell spacing)^2 (m^{-2})

Chapter 1. Introduction

This thesis explores the use of microfluidic perfusion as a tool for modulating diffusible cell-cell signaling in mouse embryonic stem cell (mESC) culture, thus enabling more control over the soluble microenvironment. I define "soluble microenvironment" to be the biochemical composition of the liquid media in the cell culture microenvironment. This study also describes the development of microfluidic devices for perfusion culture of mESCs and investigates methods for achieving successful culture of mESCs in those devices.

This chapter first defines diffusible signaling and relates the importance of the microenvironment in determining stem cell fate, both in self-renewal and in neuronal differentiation. The chapter continues with an overview of conventional and microsystem technologies for modulating diffusible cell-cell signaling and presents concepts behind using perfusion culture to modulate the soluble microenvironment. The chapter concludes with an outline of the rest of the thesis.

1.1 Diffusible cell-cell signaling

In multi-cellular organisms, cells do not exist in isolation but constantly communicate with other cells in the environment. This communication can occur through direct cell-cell contact via junctions, or it can occur indirectly via extracellular signaling molecules. Cells use a large variety of signaling molecules to communicate, including small molecules as well as peptides and larger proteins[1]. In order for communication to occur, a cell must secrete a signaling molecule and another cell must have a receptor to bind and detect this molecule. When the secreting cell is the same cell that binds the signaling molecule, this type of signaling is called autocrine signaling. When the receiving cell is a different cell, this type of signaling is called paracrine signaling. Some signaling molecules, such as Wnts, have a strong propensity to bind to the extracellular matrix (ECM)[2]. In these cases, the signaling molecules are not freely diffusible and instead participate in ECM-mediated signaling. In this thesis, "diffusible signaling" describes all extracellular signaling involving freely diffusible molecules (including both autocrine and paracrine signaling). The closed-loop nature of diffusible signaling makes it challenging to probe experimentally[3]. Computational modeling of autocrine/paracrine signaling is an active area of research, but there is still much to be learned[4]. Diffusible signaling is an essential part of cell-cell communication and can affect metabolism, proliferation, and differentiation[1].

1.2 Mouse embryonic stem cells and the soluble microenvironment

More than most cell types, embryonic stem cells (ESCs) are critically sensitive to their surroundings. ESCs are typically derived from the inner cell mass of a blastocyst-stage, pre-implantation embryo[5] and have the ability divide indefinitely *in vitro* while maintaining a pluripotent state. Pluripotency is the ability to differentiate into any cell type of the adult body [5, 6]. Therefore, ESCs have two principal fates: to self-renew, or to differentiate into mature cell types. It is the combination of self-renewal and pluripotency that makes ESCs attractive for cell-transplantation therapies and drug discovery, because of the possibility of expanding ESCs to create large numbers, then controlling their differentiation into the desired adult cell type.

Understanding the mechanisms behind self-renewal and differentiation are key areas of stem cell research.

In particular, much research has been done to explore the role of the cellular microenvironment, or "stem cell niche", in determining ESC fate[5]. The microenvironment is complex and, in addition to soluble molecules, also includes direct cell-cell interactions with the surroundings, mechanical stimuli, and ECM. The ability to control the complex interactions of the microenvironment during *in vitro* culture is important for learning how external stimuli affect stem cell fate.

As in other fields, mouse models have been used extensively in ESC research to gain a better understanding of ESC biology[7, 8]. It was from mice that the first ESCs were derived and cultured *in vitro* in 1981[7]. Since then, the field of mESC research has grown extensively and provides a rich background for the application of biomicrosystems technologies.

1.2.1 Microenvironments for maintaining self-renewal of mESCs

There has been much progress in developing methods for maintaining mESCs in a self-renewing, pluripotent state, as well as in understanding the mechanisms behind self-renewal. However, it is still not completely understood how pluripotency is maintained in mESCs.

Since 1981, researchers have worked to simplify mESC culture methods and have moved toward finding minimal, chemically defined culture conditions that will maintain pluripotency. The reason for moving toward simplified, defined conditions, is that it not only improves understanding of how to practically optimize culture protocols, but it adds to our understanding of the mechanisms behind pluripotency.

When mESCs were first derived, initial methods involved growing mESCs on a layer of mouse embryonic fibroblasts (MEFs)[7]. It was found that culturing on MEFs preserved pluripotency, and that media conditioned by MEFs was sufficient to maintain pluripotency. Thus, it was assumed that MEFs provided nutritional/secreted factors that supported the mESCs, and the MEFs became known as "feeder cells". It was then discovered that leukemia inhibitory factor (LIF) was sufficient for culturing mESCs without feeders, while maintaining pluripotency[7].

Removing the necessity of feeders greatly reduced the complexity of the system by removing one set of interacting cells (changing the system from a coculture to a monoculture). However, mESCs were still being cultured in media containing fetal bovine serum (FBS). FBS is extracted from the blood of fetal calves and contains an uncharacterized mixture of proteins that can vary from lot to lot. FBS is used because, on a practical level, it works to maintain cell cultures. However, any medium containing serum is not a defined medium, because it contains unknown components in unknown quantities, and makes it difficult to tell what external factors are truly necessary for maintaining pluripotency. In 2003, Ying *et al.* discovered that by adding bone morphogenic protein 4 (BMP4), it was possible to maintain mESCs in serum-free media[9]. This established the ability to maintain mESCs in a self-renewing state using chemically defined media.

For example, it has generally been observed that different mESC lines have variable responses when cultured in such feeder-free conditions, with some lines exhibiting more spontaneous differentiation than others. This implies that although LIF can replace the need for feeders in general, there may be other unidentified factors that have a significant effect on mESC self-renewal. Although feeder-free and even serum-free techniques are available, culture on feeder layers is still common.

Finally, in addition to the composition of the media, it is generally known that the cell-culture substrate and the cell density can have a significant effect on stem cell fate. For example, Prudhomme *et al.* demonstrated that culturing mESCs on different ECMs can cause variable amounts of differentiation[10]. And it is well known that culturing ESCs at low densities can cause increased differentiation, or even death[5, 11]. Thus, the microenvironment is important not only in determining a stem cell's fate to self-renew or differentiate, but in establishing cell survival. In addition, there is evidence that other secreted factors not included in the formulation of Ying *et al.*, such as the ECM-mediated Wnt-signaling pathway, may be involved in mESC self-renewal[12], although conflicting evidence from hESCs sheds some doubt on the true role of Wnt signaling in maintaining pluripotency in mESCs. In short, there are a host of other stimuli that may affect the stem cell fate, in addition to the molecules present in the chemically defined media. Some of these stimuli are known; some remain unidentified. For some signaling molecules, such as LIF, BMP4, and fibroblast growth factor (FGF), it is known that mESCs have both the ability to secrete these molecules and the receptors to bind them, making autocrine/paracrine signaling a possibility. It is not known the extent to which autocrine/paracrine signaling affects self-renewal.

To understand why these conditions produce self-renewing cells, researchers have worked to elucidate the intracellular signaling pathways involved in ESC self-renewal and differentiation. The interactions of the pathways are complex and poorly understood, with many cytokines having both pro- and anti-pluripotent effects depending on the context. While BMP4 does preserve pluripotency in the right amounts in combination with LIF, BMP4 also causes differentiation under other circumstances[5]. Figure 1.1 summarizes some of the ways extracellular signaling can influence stem cell fate. These complex interactions lend themselves to systems-biology-type approaches, where signaling pathways are modeled quantitatively to give more insight into dynamics and interactions[10, 13, 14]. Having the experimental means to significantly control the microenvironment over time would enable testing of the finer points of these systems-biology models[15].

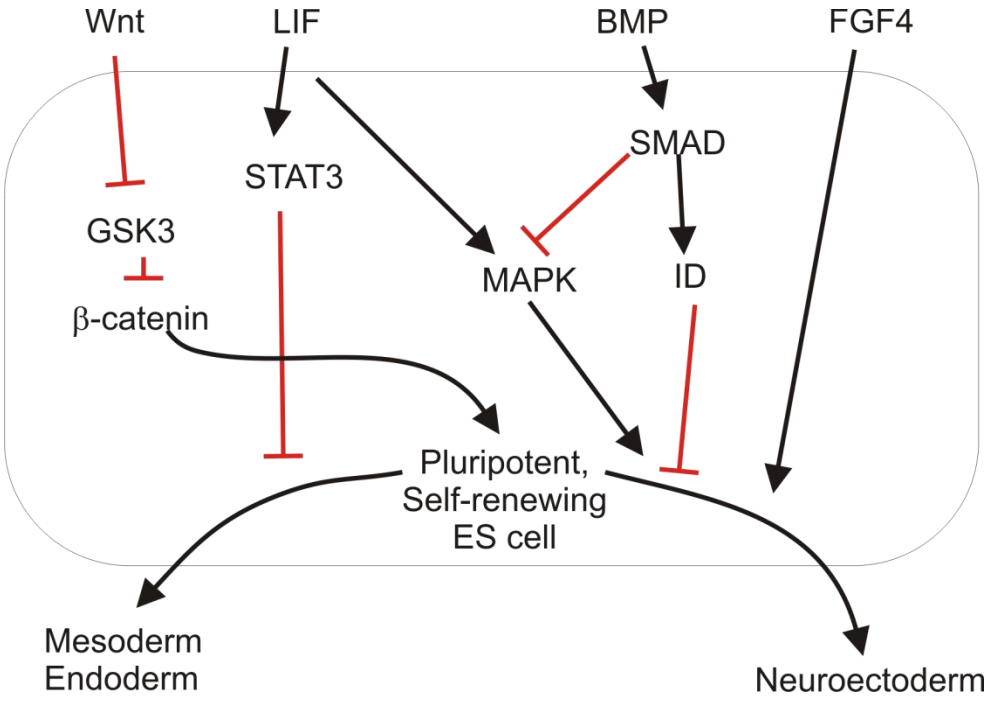

Figure 1.1: Influences of extracellular and intracellular signaling on mESC fate. This diagram shows only some of the known pathways involved in determination of mESC fate. Fate decisions are determined not solely through presence or absence of a single factor, but through a sensitive balancing act between different pathways[5, 9]. More control over the soluble microenvironment would enable greater understanding of exactly how these pathways interact.

1.2.2 Microenvironments for inducing neuronal differentiation of mESCs

As with self-renewal, mESC differentiation to neuroectodermal lineages can be specified by controlling the culture conditions. There are three main techniques for achieving differentiation *in vitro*: 1) creating multicellular aggregates of mESCs (called embryoid bodies), 2) culturing mESCs on a layer of stromal cells 2) culturing mESCs on a known ECM in defined conditions[16, 17]. As in the case of self-renewal, using monoculture and chemically defined protocols reduces the complexity of the system, giving insight into the essential mechanisms behind differentiation. To achieve this goal, Ying *et al.* developed a protocol for feeder-free, serum-free, neuronal differentiation of mESCs.

Like with self-renewal, cell density and substrate type are important for achieving neuronal differentiation[17], indicating the complex nature of interactions which ultimately determine cell fate. In particular, Ying *et al.* found that autocrine production of FGF was involved in neuronal determination[17]. Thus, autocrine/paracrine signaling may be important in neuronal differentiation.

1.3 Conventional methods for controlling the soluble microenvironment

There are several conventional methods for controlling diffusible signaling. These methods have been successful in contributing to our knowledge of the stem cell microenvironment; however there are limitations to the extent of control available through these techniques.

1.3.1 Controlling media composition

The most direct way of controlling the microenvironment is by controlling the initial composition of the cell culture media (Figure 1.2(a)). These methods can be used to either inhibit or enhance specific autocrine/paracrine signals. Antibodies and/or small-molecule inhibitors can be added to inhibit the action of specific ligands and/or receptors. A large concentration of a specific factor can be added to saturate the response of a particular signaling pair. However, while these methods may be effective for a known ligand/receptor pair with known blockers, they are not able to modulate diffusible signaling in general, including that of unknown ligand/receptor pairs. In addition, cells are constantly interacting with the microenvironment, taking up substances and secreting signals and waste. Although the media may have been chemically defined at the start of culture, over time the soluble microenvironment becomes a complex, spatially and temporally varying system.

1.3.2 Controlling cell density and cell type

Controlling cell density and cell type (monoculture vs. coculture) are two of the main conventional techniques for modulating diffusible signaling *in vitro* (Figure 1.2(b)). By culturing cells at a variety of densities, one assumes that at low densities, there will be a lower concentration of soluble factors, and thus decreased autocrine/paracrine signaling[11, 17]. As mentioned above, another method for controlling diffusible signaling with other cells is by controlling the *type* of other cells in the culture (for examples, MEFs during self-renewal or stromal cells during differentiation)[5, 16]. One can also control the relative densities of different types of cells in the coculture. However, as mentioned earlier, although coculture undoubtedly changes the diffusible signaling environment, it does so in an uncontrolled manner.

1.3.3 Controlling media delivery: macroscale perfusion culture

Macroscale perfusion is generally used in bioreactor culture for maintaining large numbers of cells, for maintaining especially metabolically demanding cells such as hepatocytes, and for culture of 3D tissues where perfusion is needed to adequately deliver nutrients to the bulk of a dense, 3D culture. While these methods have not been adopted for the purpose of affecting diffusible signaling, they do significantly impact the content of the soluble microenvironment and provide context for microfluidic perfusion studies. Since one eventual application of stem cells is for use in cell transplantation therapies, there has been much interest in developing methods for scaling up stem cell cultures, typically using macro-scale perfusion culture or stirred-suspension bioreactors[18-20]. For example, Fong *et al.* of Andre Choo's group have investigated conditions for macroscale, perfused, high-density cultures of mESCs and hESCs,

and found that perfusion enhanced hESC cultures by 70% when compared with static controls[18]. Work is also being done to scale up mESC culture using microcarriers in stirred-suspension bioreactors[19, 21]. Li *et al.*[22] have also worked on culturing mESCs in 3D matrices using perfusion bioreactors.

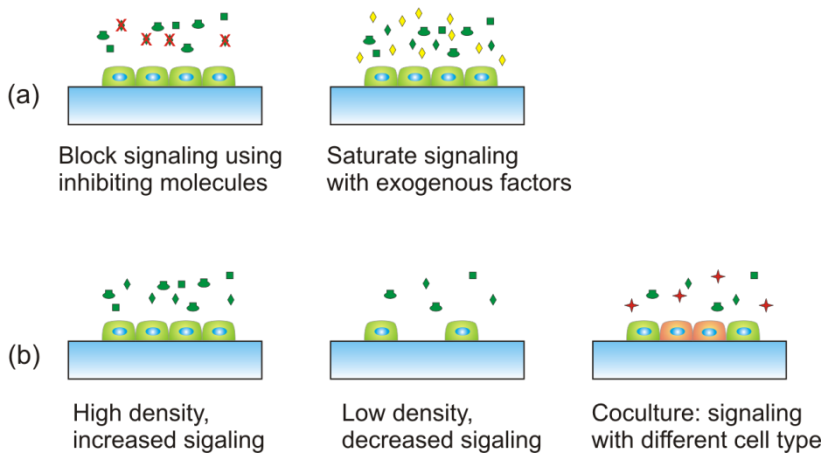

Figure 1.2: Conventional methods for modulating diffusible signaling *in vitro*. The green shapes represent a mixture of endogenous signaling molecules. The red X's represent blocking antibodies that inhibit the action of endogenous factors. The yellow diamonds represent exogenously added factors. Finally, the red stars show endogenous factors produced by a cocultured cell type. (a) shows methods that control diffusible signaling by controlling the media content. (b) shows methods that control diffusible signaling by controlling density and cocultured cell type.

1.4 Microfabricated methods for controlling the soluble microenvironment

Because microscale cell culture offers capabilities unavailable or difficult to implement in conventional culture, there has been much interest recently in microsystems for cell culture [23, 24]. Microscale tools enable more precise control of the microenvironment by allowing precise control of direct cell-cell interactions, cell-ECM interactions, soluble factors and mechanical forces[24]. However, microsystems offer other advantages in addition to greater control over the microenvironment. Microscale cell cultures also support higher-throughput experimentation[25] and enable integration of on-chip assays for dynamic profiling [26, 27].

Here I focus on microsystem techniques for controlling cell-cell diffusible signaling in the soluble microenvironment. Some of these methods have been demonstrated with cell types other than ESCs, however they are in principle applicable to ESCs.

1.4.1 Controlling media composition

Microsystems enable greater control over the composition of media in the microenvironment through techniques such as application of chemical gradients and targeted delivery of molecules using laminar streams (Figure 1.3(a)). In perfused microfluidic systems, low Reynold's numbers mean that fluid flow is laminar, a property used to advantage in many microfluidic designs.

Much work has been done on developing systems to establish chemical gradients using laminar streams[28, 29]. Methods have also been developed to generate stable chemical gradients without flow[30]. Such gradients have been used to explore phenomena such as chemotaxis[28] and neural stem cell differentiation[31]. Microsystems have also been used to deliver multiple laminar streams of different soluble molecules at the cellular or sub-cellular levels[32]. In addition to being able to generate constant gradients, microsystems have also been developed to apply time-varying gradients to cell cultures[29].

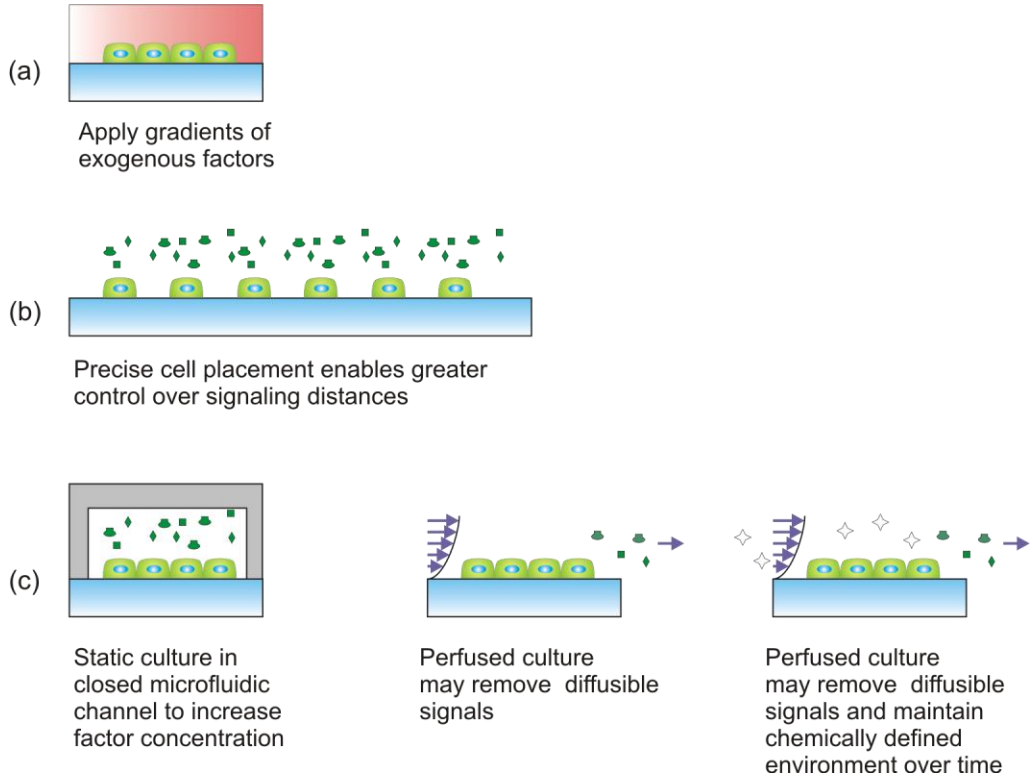

Figure 1.3: Microsystem-enabled methods for controlling diffusible signaling *in vitro*. The green molecules represent endogenous factors, whereas the white molecules represent exogenous, defined factors. (a) Microsystems enable more precise control over the spatial and temporal distribution of media content. Gradients can be applied, as well as laminar streams of molecules that are small enough to target only a portion of a single cell[31, 32]. (b) Microsystems also allow precise placement of cells, enabling greater control over signaling distances. Many different types of patterns can be created, from single cells[33], to organized circular colonies[15], to patterned cocultures[34]. (c) Microsystems can also be used to concentrate (left) or remove secreted factors from the culture using non-recirculating perfusion (middle), as well as constantly remove general diffusible factors to maintain a chemically defined environment over time (right).

Particularly relevant to this study is work by Chung *et al.*, who have used laminar flow to generate stable gradients of a growth factor mixture to apply to neural stem cells (NSCs) [31]. Their goal was to use this method to optimize conditions for neural differentiation. In their work, they observe that NSCs grown without added growth factors in flow have poor proliferation when compared with cells in conventional static culture (Figure 1.4(B,E)). They also demonstrate that adding growth factors to the perfused media restores the NSC culture (Figure

1.4(D,F)). This behavior is consistent with disruption of proliferative autocrine/paracrine signaling by flow. However, they did not estimate whether they were likely to remove secreted factors at the flow rates used, did not measure any factors removed by flow, and did not perform control experiments by perfusing conditioned media to verify that their observations were in fact due to removal of proliferative factors by flow.

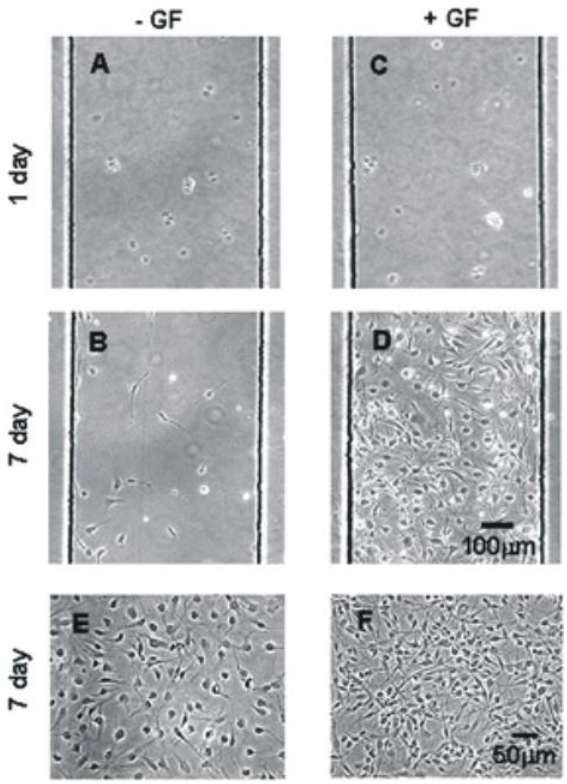

Figure 1.4: Microfluidic culture of neural stem cells by Chung *et al.*[31] shows culture of neural stem cells in a perfused device (A-D) without added growth factors (A-B) and with added growth factors (C-D) on day 1 and 7 of culture. (E-F) show corresponding results in static conditions. Interestingly, they observed poor proliferation in perfusion without growth factors (B), although static culture in that same media resulted in good proliferation (E). When they added growth factors to both the perfused and static conditions, they observed good proliferation in both perfused (D) and static (F) conditions. These results are interesting and imply that the perfusion culture may have removed proliferative secreted factors from the culture. However, they did not perform other experiments to verify that that was the actual mechanism behind this behavior.

1.4.2 Controlling cell placement

Microscale cell culture systems have also enabled novel experiments by using cell patterning technologies to control cell-cell interactions (Figure 1.3(b))[15, 33, 35]. Although cell patterning is often used to control direct cell-cell interactions[33], because it affects cell density and spacing, it also affects the cell-cell communication via diffusible signaling, especially in static culture. Many different approaches have been used for patterning cells, including dielectrophoretic traps[36, 37], microwells[33], elastomeric stencils in contact with the substrate[34, 38, 39], stencils removed from the substrate[40], and encapsulating cells in photo-patternable hydrogels[41].

Particularly relevant to this study is work by Davey *et al.*[15], who have used cell patterning to investigate the effects of cell-secreted gp130 ligands on mESC self-renewal by patterning mESCs in monolayer flat circles and assessing stem cell fate by measuring Oct-4, Nanog, and STAT3 levels at various physical locations throughout the circle. They found a radial expression of these signals, with higher expression in the center of the circles, and suggested that these results were due to a higher concentration of self-renewal factors in the center of the circle (Figure 1.5). While more work remains to be done to verify the effects (for example, to rule out cell migration as the cause of the radial patterns), this approach contributes to the set of tools for investigating diffusible signaling. However, because this approach is entirely in static culture, it does not have the same capabilities as microfluidic perfusion in controlling the soluble microenvironment. It would be interesting to observe what might happen if these experiments were repeated in a perfused or agitated setting as a control condition.

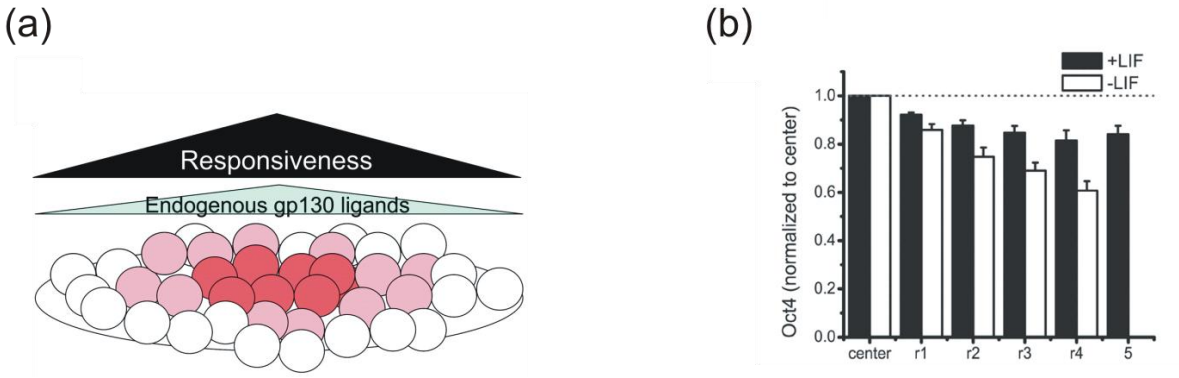

Figure 1.5: Static microfluidic culture of patterned circular mESC colonies by Davey *et al.*[15]. (a) shows a schematic of a typical circularly-patterned mESC colony and the supposed concentration of cell-secreted gp130 ligands (darker red in the middle, where there is likely a higher concentration, and lighter pink toward the periphery where there is likely a lower concentration). (b) shows the percentage of Oct4+ cells at various distances from the center of the colony in +LIF (black) and –LIF (white) conditions. Without added LIF (white), they observed a higher Oct4 expression in the center of the colony, consistent with higher levels of diffusible signaling. This effect was not observed as much in the +LIF case, perhaps due to the fact that that added LIF may have saturated the effect.

1.4.3 Controlling media delivery: microfluidic perfusion culture

Because of the difference in scale, microfluidic perfusion culture offers many benefits not available at the macroscale. Using microfluidics can reduce culture volumes by orders of magnitude, thus reducing consumption of costly reagents. In particular, microfluidics enables the use of non-recirculating perfusion for continuously sweeping away cell-secreted factors during culture (Figure 1.3(c,middle)) and continuously perfusing in chemically defined media (Figure 1.3(c,right)). In non-recirculating perfusion culture systems, new media is continuously perfused through the cell culture and then sent to waste instead of being recirculated back to the cells. Although it is theoretically possible to sweep away secreted factors using non-recirculating macroscale perfusion, the media volumes needed would be prohibitively large, making this option impractical. This thesis explores the use of non-recirculating perfusion culture for modulating cell-cell diffusible signaling by removing cell-secreted factors and maintaining chemically defined microenvironments over time (Figure 1.3(c, middle, right)).

Recently there has been much work involving microfluidic perfusion culture of cells[31, 42-50]. Work in microfluidic perfusion culture can be broadly classified into the following groups: 1) multiplex perfusion arrays for parallel culture under a variety of conditions [27, 47] 2) perfusion of metabolically demanding cells (such as hepatocytes) in 3D constructs[48, 50, 51] 3) devices where perfusion culture is a secondary function 4) devices where perfusion culture (or lack thereof) is used to manipulate the microenvironment. There also has been work on modeling how perfusion affects the content of the soluble microenvironment, to provide more insight into how these changes may affect cells[49, 52-56].

Of particular relevance, Figallo *et al.* [49] have developed a micro-bioreactor array for non-recirculating perfusion culture of adherent cells (C2C12 myoblasts and hESCs). They have shown using modeling that their device can operate in two modes: 1) convection-dominated transport for large molecules and diffusion-dominated transport of small molecules 2) diffusion-dominated transport of both small and large molecules. (They use oxygen as an example small molecule, and albumin as a large molecule.) However, they did not confirm this with experiments, and they did not apply this to their experimental results, which dealt more with shear effects. They did demonstrate vascular differentiation of hESCs cultured in the reactor, and found that cells cultured under higher levels of shear showed more vascular differentiation (Figure 1.6). However, they did not demonstrate biological effects due specifically to the influence of perfusion on the soluble microenvironment that were not related to shear. They reported that perfusion culture of hESCs was significantly more challenging than culture of C2C12 cells, which readily adhered to the glass surfaces in the microbioreactor. Interestingly, they encapsulated the hESCs in a hydrogel layer in the perfused culture, and it is not clear whether their system is capable of supporting perfused hESC culture without encapsulation in hydrogels.

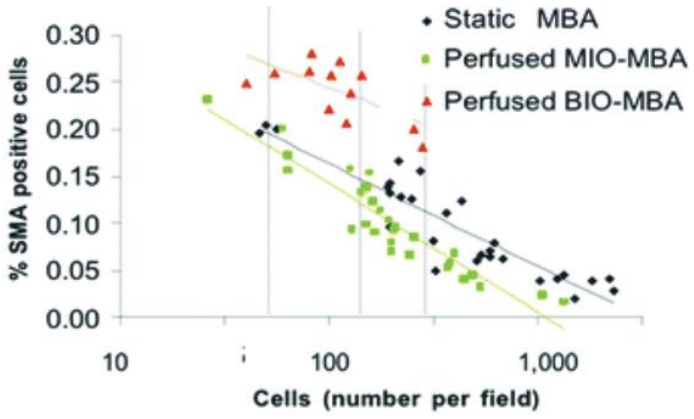

Figure 1.6: Microfluidic perfusion culture of hESCs by Figallo *et al.*[49] compares the percentage of cells expressing Smooth Muscle Actin (SMA), an indicator of vascular differentiation. The x-axis shows the effective cell density, and the three colors show the different experimental conditions: Static, Perfused MIO (slow flow), and Perfused BIO (high flow). Figallo *et al.* observed that the cells in the high flow conditions exhibited higher %SMA expression and attributed these observations to the known role of hydrodynamic

shear in vascular differentiation. While these results are interesting, they do not explore how the contents of the soluble microenvironment may have affected the results.

Finally, using the opposite tactic, Yu *et al.*[57] have cultured cells in completely closed, static microfluidic channels to control the microenvironment by increasing the cell-to-media-volume ratio (Figure 1.3(c, left)). They assume that cell-cell diffusible signaling will be enhanced in this environment. However, such an approach can only be used with cell types with low metabolic requirements and is not suited to ESCs, which require daily feeding even in conventional culture.

1.4.4 Hydrodynamic shear stress

Shear stress is an inherent part of microfluidic perfusion culture systems and is often perceived as a limiting factor in microfluidic perfusion culture due to its detrimental effects on cells at high levels. However, it is possible to design and operate microfluidic perfusion culture systems such that applied shear stresses are orders of magnitude below those at which adverse effects are observed[31, 58]. Methods for mitigating shear stress include lowering fluid velocities, designing high aspect ratio cell culture chambers,[58] and including micropillars or microwells[59] to shield cell cultures. On the other hand, some microfluidic perfusion systems use high levels of shear stress to investigate biological phenomena, such as endothelial cell function[60] or cell adhesion[61]. In addition, acceptable levels of shear stress can vary widely depending on cell type[50] For microfluidic perfusion culture in 2D Poiseuille flow systems, the resulting parabolic flow profile yields a simple estimate of shear stress at the wall[62]:

$$\tau = \frac{6\mu Q}{h^2 w} \tag{1.1}$$

where μ = viscosity (kg m^{-1} s^{-1}), Q = flow rate (m^3 s^{-1}) , h = chamber height (m), and w = chamber width (m). For a given flow rate, Q, the shear stress may be reduced to acceptable levels by increasing the channel height (lowering the fluid velocity). Since these changes (increasing the height and lowering the fluid velocity) affect not only the shear stress, but the content of the soluble microenvironment, the effects on nutrient delivery and secreted factors must also be considered. The parallel-plate shear stress estimate is useful when dealing with simple rectangular cell culture chambers; however, finite-element simulations may be used to estimate shear stress in devices with more complicated geometries[58]. Another method for assessing the effect of shear stress on cells in a microfluidic perfusion culture system is to assay for stress-induced markers[63].

As shown in Figure 1.7, the shear stresses applied throughout this thesis to sustain mESC cultures were typically between 0.1-1 dyn/cm^2 and are well below typical arterial shear stresses of ~15 dynes/cm^2[64] and shear stresses applied during differentiation studies: 1.5-10 dyn/cm^2 used by Yamamoto *et al.*[65] and 15 dyn/cm^2 used by Wang *et al.*[66]. Recently Fok and Zandstra demonstrated that the proliferation and developmental potential of mESCs grown in a stirred suspension bioreactor under continuous shear stresses of 6.25 dyn/cm^2 – 9.86 dyn/cm^2 was comparable to that of controls, and they cited a minimum threshold of 6.5 dyn/cm^2 for removing adherent cells from surfaces[19]. Even the absolute highest shear levels applied in this thesis were ~3 dyn/cm^2 (highest flow condition in Chapter 4) were lower than these thresholds, and the cells

grown under those conditions proliferated well, with no observable differences in morphology from the cells grown at lower flow rates. These results suggest that shear stresses applied in this study should have minimal effect on the mESC cultures.

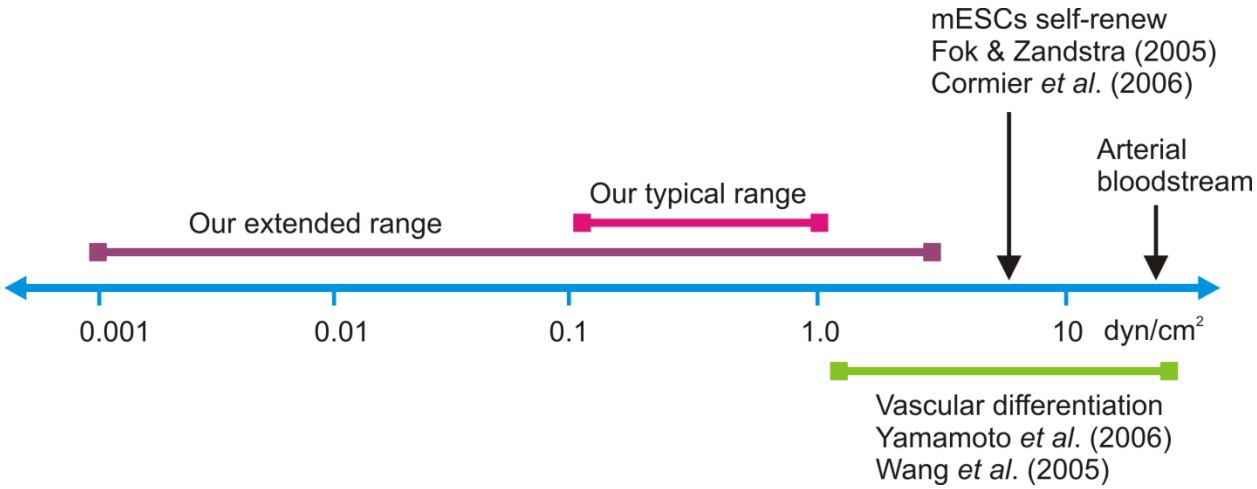

Figure 1.7: Typical shear stresses applied in this thesis (pink bar).

1.5 Scope of this thesis

Although methods exist for controlling the soluble microenvironment, they are able to exert only limited control over diffusible signaling and over the content of the soluble microenvironment over time. Non-recirculating microfluidic perfusion culture has the potential to create a more defined microenvironment by continuously controlling the supply and removal of soluble factors, with minimal use of expensive reagents (Figure 1.3(c, right)). Indeed, perfusion culture may enable "superdefined" environments when compared with static culture in chemically defined media, where the background of soluble factors and nutrients changes constantly over time. While there has been some work mentioning the effects of microfluidic perfusion culture on diffusible signaling[31, 49], these studies have not experimentally demonstrated the capability of their systems to remove soluble factors, and have not conclusively demonstrated that perfusion-mediated changes in the content of the soluble microenvironment can have a biologically significant effect on cells.

Because mESCs are critically sensitive to the microenvironment, methods for enabling greater control over the microenvironment would be especially beneficial to the study of mESC self-renewal and differentiation. In particular, the existence of defined, feeder-free protocols for both self-renewal and neuronal differentiation form a basis from which to explore the notion of creating "superdefined" conditions using perfusion. In addition, when this study began there was no prior work in the literature on microfluidic perfusion culture of ESCs, and thus a need to establish such methods before further studies could be pursued.

The scope of this thesis is in three parts: 1) to *develop technology* that enables microfluidic perfusion culture of mESCs, and 2) to *establish conditions* for successful culture of mESCs in microfluidic perfusion 3) to demonstrate the use of microfluidic perfusion in *modulating the soluble microenvironment* in mESC culture.

Microfluidic technology was developed throughout the entire work of the thesis and customized to each application. In the first part of the thesis (Chapter 2-3) I focus on aim 2, whereas in the latter half (Chapters 4-5) I focus on aim 3.

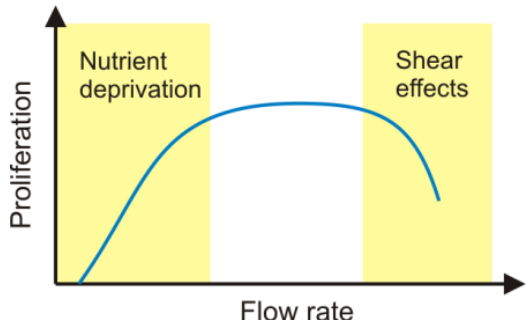

Figure 1.8: Schematic graph of potential mESC behavior in perfusion culture. The goal of Chapter 3 was to apply a wide range of flow rates and observe mESC growth to characterize the general behavior of mESCs under microfluidic perfusion.

Because there was no prior work in the literature on microfluidic perfusion culture of mESCs, the first task was to establish basic conditions for maintaining a viable culture, described in Chapter 2. In Chapter 3, I develop a novel microfluidic device for applying a logarithmic range of flow rates to the mESC cultures to better understand the overall behavior of mESCs across a wide range of flow rates. Figure 1.8 shows a schematic of general behavior of cells in perfusion culture. The goal here was to establish a range of flow rates that avoided nutrient deprivation at low flow and shear effects at high flow. While gathering these results, I noticed that proliferation varied not only as a function of the applied flow rate, but also as a function of the downstream distance from the channel inlet. At low flow rates, colonies at the channel inlets were large, but decreased in size as one traveled further downstream in the same channel.

The results from Chapter 3 were suggestive of depletion of growth-enhancing molecules and/or accumulation of growth-inhibiting molecules at downstream locations at low flow rates. To explore the mechanisms behind the results from Chapter 3, in Chapter 4 I investigate the role of glucose in causing these flow-rate dependent colony area patterns. I developed and characterized an improved logarithmic flow-rate device to enable this investigation.

Having established flow-rate ranges for successful microfluidic perfusion culture of mESCs, in Chapter 5 I estimate and measure whether perfusion culture at typical flow rates found in Chapters 2-4 can sweep away large molecules such as LIF. I then demonstrate that perfusion-mediated removal of secreted factors can affect the biological state of the cells, specifically, survival of mESCs in neuronal differentiation media. Finally, I explore the question of whether serum-free defined media (as formulated by Austin Smith's group[9, 17]) is sufficient for non-recirculating perfusion culture of mESCs (both in self-renewal and neuronal differentiation conditions). Chapter 6 summarizes the thesis contributions and describes areas for future work.

Chapter 2. Establishing microfluidic perfusion culture of embryonic stem cells

Microfluidic perfusion culture has been demonstrated on a variety of cell types, including primary rat hepatocytes[43], human hepatocytes[48], and endothelial cells[58], as well as on a variety of adult stem cell types such as neural stem cells[31], bone marrow stem cells[48], and C2C12 myoblasts[45, 67]. A year after publication of work from this thesis[68], Figallo *et al.* demonstrated microfluidic perfusion culture of hESCs[49]. However at the time of this work there was no precedent in the literature for microfluidic perfusion culture of embryonic stem cells, so the first goal was to establish conditions for such a culture. To date, this work remains the only published work on microfluidic perfusion culture of mESCs in self-renewal conditions[68]. This chapter describes the basic requirements to attain a viable, proliferating mESC culture in non-recirculating microfluidic perfusion. The system must allow cell attachment, then provide sufficient conditions for survival and proliferation. In addition, if essential secreted factors are removed by the flow, they must be replaced in the media. Finally, the system must maintain sterility and bubble-free operation. Because 3T3 fibroblasts are generally easier to culture than mESCs, I initially demonstrated microfluidic perfusion culture in this system with fibroblasts, then with a coculture of fibroblasts and mESCs. Finally, I developed experimental methods for achieving a viable mESC self-renewal monoculture in a perfused microfluidic system.

2.1 Experimental

2.1.1 Cell culture

3T3 murine fibroblasts were cultured in 3T3 media: Dulbecco's Modified Eagle's Medium (DMEM, 11960044, Invitrogen, Carlsbad, CA) supplemented with 5% bovine calf serum (SH30072.03, Hyclone), 4 mM L-glutamine (25030081, Invitrogen, Carlsbad, CA), 100 U/mL penicillin and 100 μg/mL streptomycin (15140122, Invitrogen, Carlsbad, CA). I maintained the cells in a 37°C humidified environment with 7.5% CO2, fed cells every other day with 3T3 media and passaged when 90% confluent using a solution of 0.25% trypsin with 3.8 g/L EDTA·4Na (25200056, Invitrogen, Carlsbad, CA).

Two mESC lines were used: D3 and ABJ1 (with a stably integrated GFP reporter for Oct-4). The ABJ1 cells were generously donated by George Daley's lab. Both lines were cultured without feeders in ES media: DMEM (11960044, Invitrogen, Carlsbad, CA) supplemented with 15% ES-qualified fetal bovine serum (16141079, Invitrogen, Carlsbad, CA), 4 mM L-glutamine (25030081, Invitrogen, Carlsbad, CA), 1 mM non-essential amino acids, 50 U/mL penicillin, 50 μg/mL streptomycin (15140122, Invitrogen, Carlsbad, CA), 100 μM β-mercaptoethanol (M7522, Sigma,St. Louis, MO), and 500 pM leukemia inhibitory factor (LIF, ESGRO, Chemicon, Temecula, CA). I cultured cells directly on tissue-culture plastic (430639, Corning, Corning, NY) in a 37° C humidified environment with 7.5% CO_2. For maintenance of mESCs, we fed cells daily and passaged every other day using 0.25% trypsin with 3.8 g/L EDTA·4Na (25200056, Invitrogen, Carlsbad, CA) at a density of ~8×10^4 cells/cm^2.

2.1.2 Single-channel microfluidic device

For simplicity, the experiments in this chapter were performed using an existing single-channel device design (Figure 2.1). This channel had dimensions of 30 mm × 3 mm × 85 μm and had previously been successfully used to culture 3T3 fibroblasts in static culture (personal communication: Brian Taff).

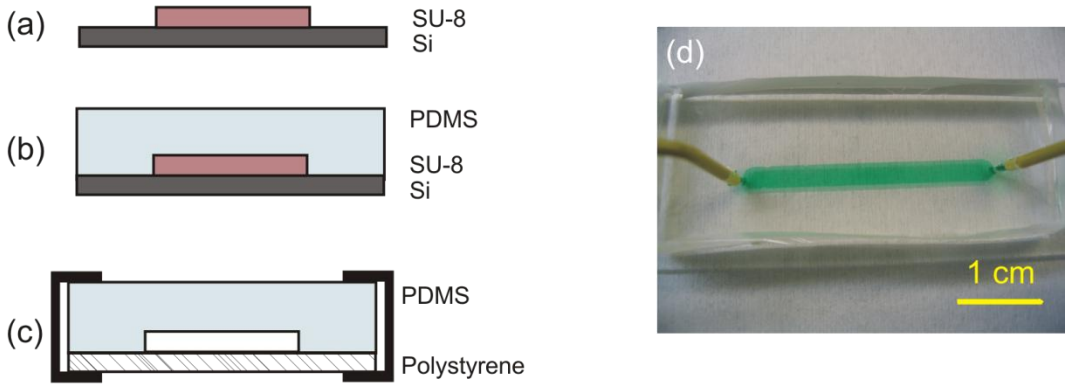

Figure 2.1: Fabrication of a PDMS microfluidic channel using a pre-existing SU-8 mold. (a) Pre-existing SU-8 mold on silicon contains the negative of the desired microfluidic channel shape. (b) Liquid PDMS base and hardener are mixed, poured onto the mold, and cured. (c) The cured PDMS upper piece containing the patterned microfluidic channels is clamped to a tissue-culture polystyrene substrate. (d) Photograph of single-channel microfluidic device used in this chapter. Green food coloring has been used to illustrate the microfluidic channel. Note: (a-c) not to scale. Typical PDMS thickness ~7 mm, typical SU-8 thickness ~85 μm.

PDMS is a clear silicone elastomer especially suitable for creating biological microfluidic devices: it is non-cytotoxic[69], autoclavable, gas permeable, can reproduce features on the order of microns using soft lithography, is widely available, and has been used successfully in many cell-based microfluidic applications[31, 42, 45, 46, 58]. Since PDMS is gas permeable, thin PDMS membranes (thickness ~ 100 μm) can be used as gas exchange surfaces in microfluidic perfusion culture systems to support cell culture[43]. From a fabrication standpoint, the flexible nature of PDMS allows the creation of integrated mechanical valves and pumps[70, 71]. Finally, PDMS has appealing properties for microscopy; it has low autofluorescence when compared with many plastics used in microfabrication[72], making it suitable for fluorescence imaging applications.

Despite the advantages to using PDMS, the material's permeability may affect its function in some cases. Water vapor and organic solvents can readily permeate PDMS, potentially causing unwanted evaporation and changes in osmolality[73, 74] that may be detrimental to cell culture. Heo *et al.* observed evaporation-mediated changes in osmolality when culturing cells in PDMS devices[73]. I have observed that water or ethanol entrained in PDMS can decrease its clarity; the PDMS can appear cloudy, as though micron-scaled particulates are included throughout the bulk material. This cloudiness disappears upon drying. Water transport into PDMS can also cause unwanted permeation-driven flows, which can be eliminated by pre-soaking the PDMS to supersaturate it prior to an experiment or by coating the PDMS with parylene to prevent water permeation[73, 75]. I addressed these issues by saturating the PDMS microfluidics by perfusing the system with culture media for 24 hours prior to cell seeding.

To pattern the PDMS (Figure 2.1(b)), I mixed liquid PDMS (Sylgard 184, Dow Corning, Midland, MI) in a ratio of 10:1 (by mass), base to curing agent, degassed the mixture in vacuum for 30 minutes, and poured a 7-mm-thick layer onto the SU-8 mold wafer. After allowing the PDMS to degas for ~30 minutes I cured it for 2 hours in a 65°C oven. After curing I removed the PDMS from the mold, cut out individual devices, and punched access holes into the PDMS using a 16-gauge blunt-end needle. Figure 2.1(c) shows device assembly, where the patterned PDMS upper piece is clamped to a polystyrene substrate using binder clips.

2.1.3 Optics

To gather image data I used an inverted microscope (Zeiss Axiovert 200, Thornwood, NY) with a SPOT RT Color 2.2.1 camera (Diagnostic Instruments, Sterling Heights, MI).

2.1.4 Experimental setup for fibroblast culture/coculture

This section describes the fluidic setup used to interface to the microfluidic channel during initial perfusion experiments involving fibroblasts and fibroblast/mESC coculture. The setup is shown in Figure 2.2(a). I connected the single-channel microfluidic device to off-chip fluidics using HPLC connectors, valves, and tubing from Upchurch (Oak Harbor, WA) which have the advantage of low dead volumes and autoclavability. I used a syringe pump (KD Scientific 200, Holliston, MA) as a constant flow source for the fluidics. I placed the syringe pump outside the incubator (Steri-cycle, Thermo Forma, Philadelphia, PA) and positioned the device and bubble trap inside the incubator to maintain the device in a 37°C, humidified, 5% CO_2 environment. I connected a plastic syringe (Becton Dickinson, Franklin Lakes, NJ) outside the incubator to ~2 feet of flexible Teflon tubing (1536, Upchurch Scientific, Oak Harbor, WA) that was threaded through an existing access port in the incubator. Inside the incubator, I attached the tubing to a Luertight connector system (P-837, Upchurch, Oak Harbor, WA) which I connected to a large bubble trap (6115, Varian, Torrance, CA) with a ~1-mL total volume using flexible Tygon tubing. The large bubble trap allowed the device and fluidics setup to be disconnected and removed from the incubator for microscopy without introducing bubbles. The large bubble trap was then connected using flexible Tygon tubing to PEEK tubing from Upchurch, which fed into the microfluidic device.

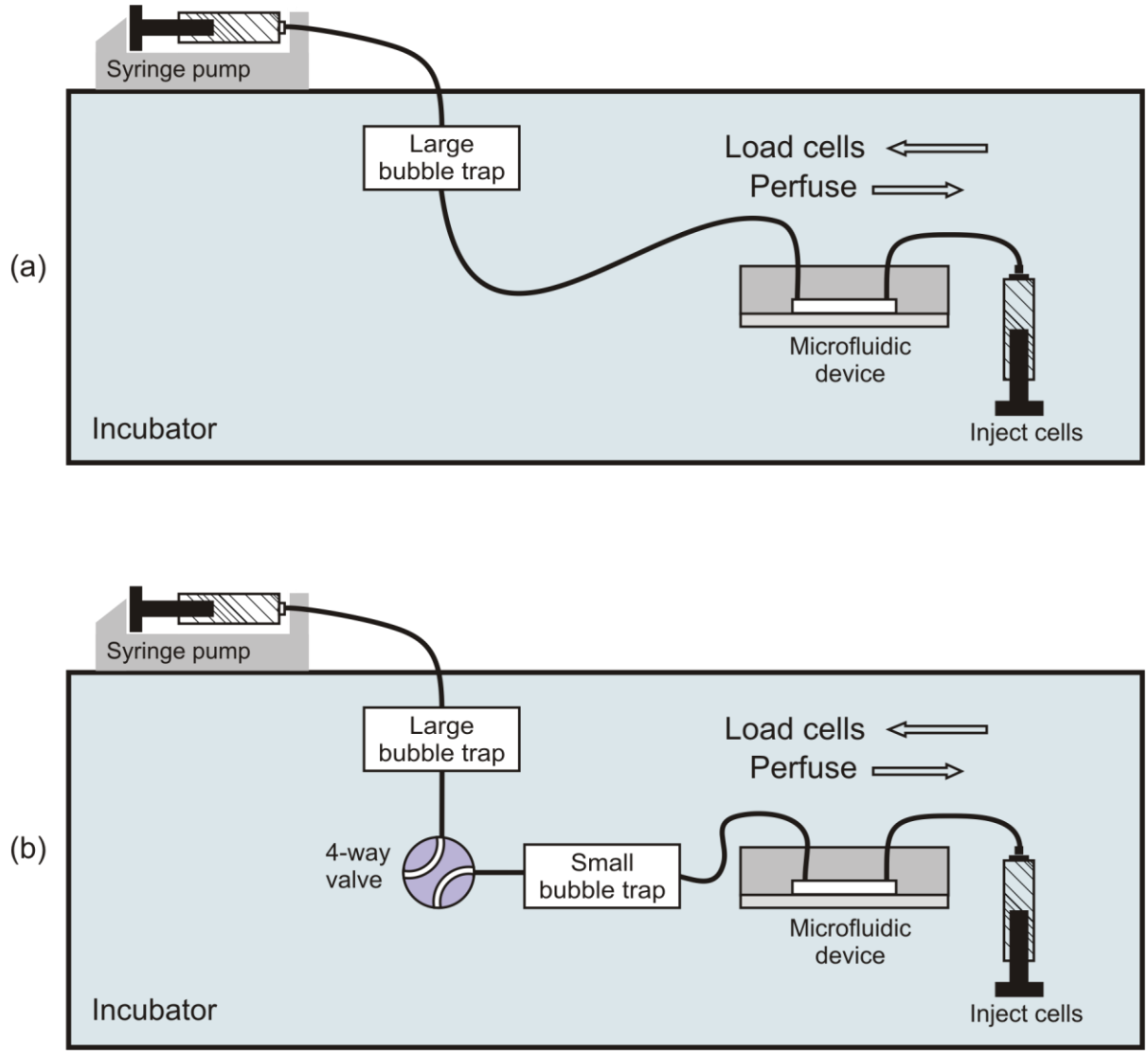

Figure 2.2: Experimental setup evolution. a) Setup with large upstream bubble trap was successful in achieving viable perfused culture of fibroblasts and fibroblasts cocultured with mESCs. To achieve viable mESC monoculture in the device, the setup was modified as shown in configuration b) to incorporate a 4-way valve and small bubble trap that improved isolation of the microfluidic device during attachment. Note: figure not to scale.

2.1.5 Experimental setup for mESC monoculture

Although the setup in Figure 2.2(a) resulted in viable fibroblast cultures and viable fibroblast and mESC cocultures, using the same setup and protocols did not result in viable microfluidic mESC monocultures. To improve results with mESCs I modified the experimental setup to be as shown in Figure 2.2(b). One hypothesis for the poor growth of mESCs was a failure to attach due to mechanical disturbances by the fluid. Since the large bubble trap contained a large amount of fluid (~1 mL) and was mounted above the level of the device, there was some concern that, although the system was closed, the fluid in the bubble trap may have caused unwanted flow. Therefore, to fluidically isolate the microfluidic device from the upstream large debubbler and

large lengths of tubing, I inserted a 4-way valve between the large bubble trap and the microfluidic device to allow fluidic isolation of the microfluidic device during cell attachment. To trap any bubbles generated in the 4-way valve, I incorporated an additional bubble trap (Figure 2.3) with a smaller trap; even with the larger, upstream bubble trap at the input, I still often observed new air bubbles in the device a few days after starting perfusion. The smaller volume of the custom bubble trap also enabled loading cells upstream of the small bubble trap if desired. I fabricated the smaller, downstream bubble trap by carving a ~200 μL cavity in a ~2 cm × 2 cm × 0.7 cm slab of PDMS, punching two access holes in the bubble trapping chamber and irreversibly bonding the PDMS slab to a ~2 cm × 2 cm piece of glass slide (48300-025, VWR, West Chester, PA) or to another piece of PDMS, creating a microfluidic chamber. The protocol for plasma bonding involved cleaning the PDMS surfaces with adhesive tape and exposing the surfaces to be bonded to air plasma for one minute (PDC-001, Harrick Plasma, Ithaca, NY). Then I immediately bonded the PDMS and glass (or PDMS and PDMS) to form a completed device, shown in Figure 2.3. To strengthen the bond, I placed the bonded device in a 65°C oven overnight. I oriented the small bubble-trap cavity side up with press-fit input and output tubes pointed downward so that any passing bubbles would collect in the chamber. Figure 2.3(b) shows the fabricated bubble trap in practice, with a trapped air bubble.

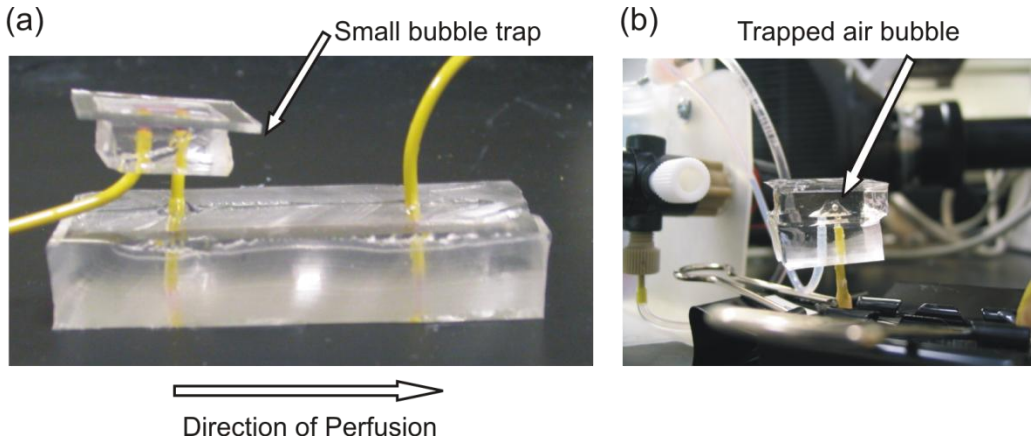

Figure 2.3: Small custom bubble trap is fabricated by carving out a bubble trapping chamber into PDMS and bonding the PDMS to glass (a) or another piece of PDMS to seal the chamber. (b) A trapped air bubble shown in (b). Note on scale: The small bubble traps in both photos are ~1.5 cm.

2.2 Results

2.2.1 Microfluidic perfusion culture of 3T3 fibroblasts

On the day before loading cells, I prepared a microfluidic chamber as described above, assembled the setup and flushed the system with ethanol to sterilize. Using the experimental setup described in Section 2.1.4, I then connected appropriate tubing (also flushed with ethanol), and set up the chamber inside the incubator. To purge residual bubbles from the system before loading cells, I connected high-resistance tubing to the end of chamber (5 inches of 1/16" PEEK tubing with inner diameter 0.0025", Upchurch) and perfused the chamber at 3 μL/min overnight with 3T3 media to drive bubbles out of the device. This pressurization method (also known as "blind filling" or "dead end filling"[70]) works by creating a high pressure > 5 psi in the microfluidic channel, quickly driving gas out through the permeable PDMS within an hour.

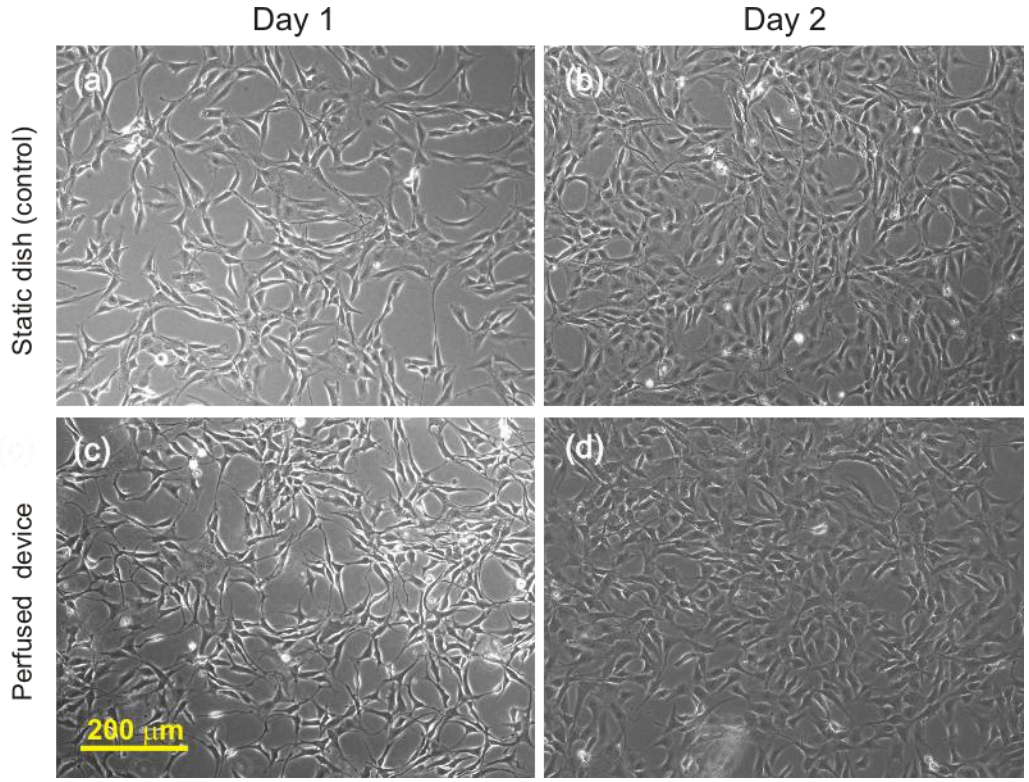

Figure 2.4: (a-b) 3T3 fibroblast culture in a static Petri dish. (c-d) Microfluidic perfusion culture of 3T3 fibroblasts. Cells in both static and perfusion culture exhibit good attachment and typical 3T3 morphology, as well as increased density on day 2, implying conditions that support proliferation. All photos were taken at the same scale.

On day 0 I loaded 3T3 fibroblasts into the device. All actions were performed inside a sterile tissue-culture hood. I trypsinized the cells, spun them down, and resuspended them in 3T3 media at a concentration of ~ 3×10^6 cells/mL. After loading a 3 mL plastic syringe (Beckton Dickinson) with the cell suspension, I let the syringe rest for a few minutes to reduce bubbles. I then loaded cells into the output of the device as shown in Figure 2.2(a). To attach the syringe without introducing air bubbles, I used a droplet merging technique[76], first perfusing forward with 3T3 media to produce a droplet at the device output, then connecting the syringe by merging the droplet at the end of the syringe to the droplet at the device outlet. As a control, I plated cells from the same cell suspension at a comparable areal density onto a conventional polystyrene tissue-culture dish. On day 1 I fed the static dish with 3T3 media and began perfusing the device with 3T3 media at 50 μL/hr and continued perfusion to day 2. Non-CO_2-equilibrated 3T3 media was used throughout the experiment.

The results shown in Figure 2.4 compare 3T3 fibroblast morphology on days 1-2 in a standard dish (Figure 2.4(a-b) vs. in the perfused microfluidic device (Figure 2.4(c-d)). Cells in both conditions show good attachment, typical morphology, and proliferation from day 1 to day 2. In general, almost all trials performed with 3T3 fibroblasts resulted in a successful culture, with no observable problems with attachment or proliferation. These results were in keeping with the fact

that fibroblast culture generally robust, and indeed Brian Taff in our lab had already demonstrated the ability to culture 3T3s in these same microfluidic chambers in static culture for a couple days. Adding perfusion to this device did not cause problems, and encouraged further trials with mESCs.

2.2.2 Microfluidic perfusion culture of mESCs + 3T3 fibroblasts

After successfully culturing fibroblasts, I demonstrated microfluidic perfusion culture with a mixture of 3T3 fibroblasts and mESCs. Although 3T3 fibroblasts and mESCs are not normally cultured together, the purpose here for coculturing them was to use the 3T3 cells as a control, since I had previously demonstrated successful culture of 3T3 fibroblasts using similar protocols. If the mESCs died while the 3T3s survived, this would indicated that the mESC death was not due to a general problem with the perfusion culture protocol, but due to a specific requirement of the mESCs, which are generally more difficult to maintain in culture, even using traditional methods. In these experiments the PDMS microchannel was clamped to a tissue-culture polystyrene layer, which formed the base of the flow chamber to which cells would attach. I prepared the device and microfluidic setup as described in 2.2.1, but using ES media instead of 3T3 media during the overnight blind filling process.

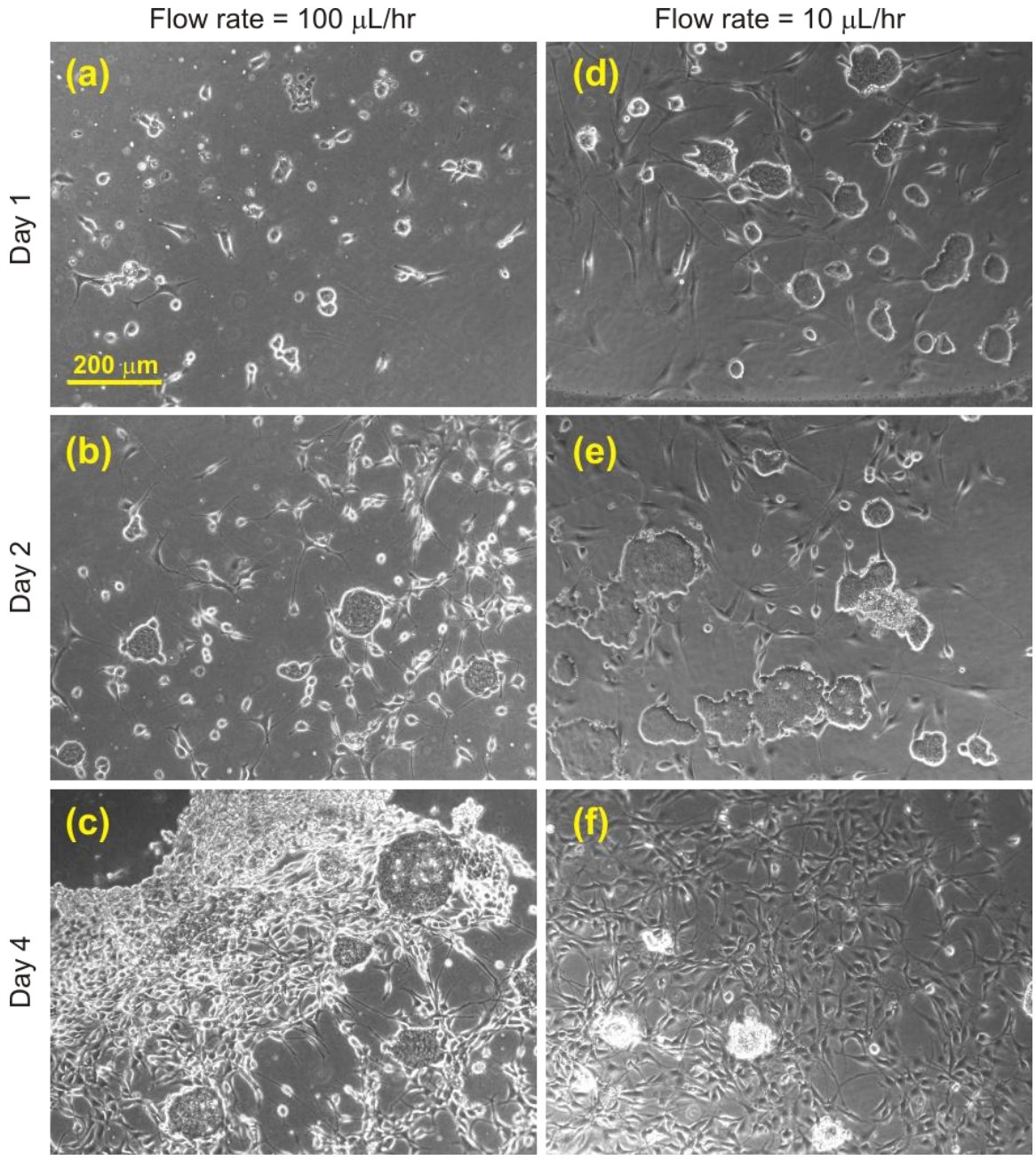

Figure 2.5: Microfluidic perfused coculture of mESCs and 3T3 fibroblasts on days 1-4 at a flow rate of 100 μL/hr (a,b,c) and 10 μL/hr (d,e,f). The spread-out, flattened morphology seen on day 2 indicates good attachment of both fibroblasts and mESCs. Because the seeding density of mESCs was higher in the 10 μL/hr experiment, early colonies are already seen on day 1 (round shapes with bright borders). Comparable cocultures are seen at both flow rates on day 2. Day 4 results show significant fibroblast proliferation at both flow rates, whereas mESC colonies have grown larger at the higher flow rate (c), but have actually decreased in size at the lower flow rate (f). All photos were taken at the same scale.

On day 0, I loaded a cell suspension of 3T3 fibroblasts and ABJ1 mESCs in non-equilibrated ES media through the back end of the device as shown in Figure 2.2(a) using the droplet-merging technique and allowed them to attach overnight. I started perfusion of non-equilibrated ES media at a flow rate of 100 μL/hr. I repeated the experiment but used a flow rate of 10 μL/hr to

compare effects. Perfusion was maintained continuously until day 4 at the respective flow rates, except for ~15 minutes each day when the microfluidic device was disconnected from the media input for microscopy, then reconnected to the perfusion source afterwards. The device was disconnected upstream of the large bubble trap to avoid air bubbles in the microfluidic culture channel.

Figure 2.5 shows the results of the perfused coculture at both flow rates. Although the results look similar on day 2, by day 4 the fibroblasts exhibit good proliferation at both flow rates, but the mESC show larger colonies only at the higher flow rate. Although there was considerable fibroblast proliferation at the higher flow rate by day 4, the fibroblast morphology looked atypical. Although the colony morphologies were not the same in perfusion as in typical static culture, the fact that both the mESCs and fibroblasts attached and proliferated at the higher flow rate was significant, and encouraged further experiments involving monoculture of mESCs.

2.2.3 Monoculture of mESCs: Day 1 survival study in static culture

Although culture involving 3T3 fibroblasts was relatively straightforward, developing a successful protocol for monoculture of mESCs in microfluidic perfusion culture was significantly more challenging and involved many attempts over the course of several months. In the first several attempts, the mESCs did not survive and attach overnight as the fibroblasts or the fibroblast/mESC coculture had.

There were several hypotheses about why the mESCs failed to attach and proliferate in the failed trials. An initial hypothesis was that the cells failed to attach due to poor handling of the cells (rough conditions during trypsinization and trituration to single cells) prior to loading into the device. Another hypothesis was that the cells were nutrient deprived 1) during the initial static attachment period and/or 2) during the perfusion period (i.e., the perfusion rate was too low). Although it is known that similar areal densities of cells could survive in conventional culture for > 24 hrs, the media layer height in the device was > 10× smaller than in conventional static culture. Other hypotheses surrounded cell attachment: 1) the surface was not conducive to attachment 2) mechanical forces were disturbing cell attachment 3) chemicals in the microfluidic setup disturbed cell attachment 4) the static attachment period was too short to allow cells to attach.

To test these hypotheses an effort was made to repeat the failed protocols with controlled variations. However, even when I attempted to repeat a protocol the exact same way without apparently introducing changes, it was common for unaccounted-for variations to cause variable results. Another challenge was that, due to the complexity of the experiment, it was possible that there were multiple failure modes. Using these methods I was able to rule out or control some of the failure mode hypotheses: 1) Cell handling prior to the microfluidic seeding was not a major cause of failure, as evidenced by almost 100% success when using the same cell suspension loaded into the device to seed standard Petri dish controls (see Figure 2.6). 2) To remove any doubts about the suitability of the cell-culture substrate, I moved from using glass substrates (which enabled more convenient fabrication with PDMS) to using tissue-culture polystyrene. 3) A harsh chemical environment related to the microfluidic device was not a problem – this was

demonstrated by successful culturing of mESCs in a Petri dish on glass and tissue-culture polystyrene substrates in the presence of immersed PDMS (data not shown).

To illustrate a typical experiment used during the process of refining the protocols, here I describe an experiment designed to test the following hypotheses about cell attachment A) whether cell handling prior to cell seeding was a problem B) whether some properties of the microfluidic device itself caused failure C) whether the connection of the microfluidic device to the off-chip fluidic components affected cell attachment. In this experiment I was looking solely at attachment before any flow had been applied. I cultured ABJ1 mESCs taken from the same original culture dish in three conditions: static Petri dish, static isolated microfluidic device, and static microfluidic device connected to the full set-up (Figure 2.2(a)). In this experiment, glass substrates were used as the cell-culture substrate in the microfluidic device. To encourage a cell-culture-friendly pH, I equilibrated the mESC culture media by incubating the media overnight in a 10-cm cell-culture dish in a humidified 37°C environment with 7.5% CO_2. I then prepared an isolated microfluidic device and a microfluidic device in the experimental setup of Figure 2.2(a), prepared on the day before loading using the same techniques described in section 2.2.2.

I loaded the same cell suspension into both devices and plated cells from the same suspension into the dish at a comparable density per area as seen in Figure 2.6(a). By day 1, the cells in the Petri dish attached with good colony morphology, but the cells in the devices did not appear to attach. This implied that the problems with cell attachment involved the microfluidic device setup and procedures, not the preparation of the cell suspension which was the same in all three conditions. When I repeated this experiment, I found that cells in the isolated microfluidic device had comparable attachment on day 1 to the static dish. While I could not explain the different results, the fact that both the static dish control cells and the cells in the isolated microfluidic device were able to attach overnight ruled out hypotheses A, but unfortunately leaving hypotheses B and C. In addition, because there dish control was performed on polystyrene, whereas the device has a glass cell-culture substrate, another possible explanation for the results was poor adhesion to glass.

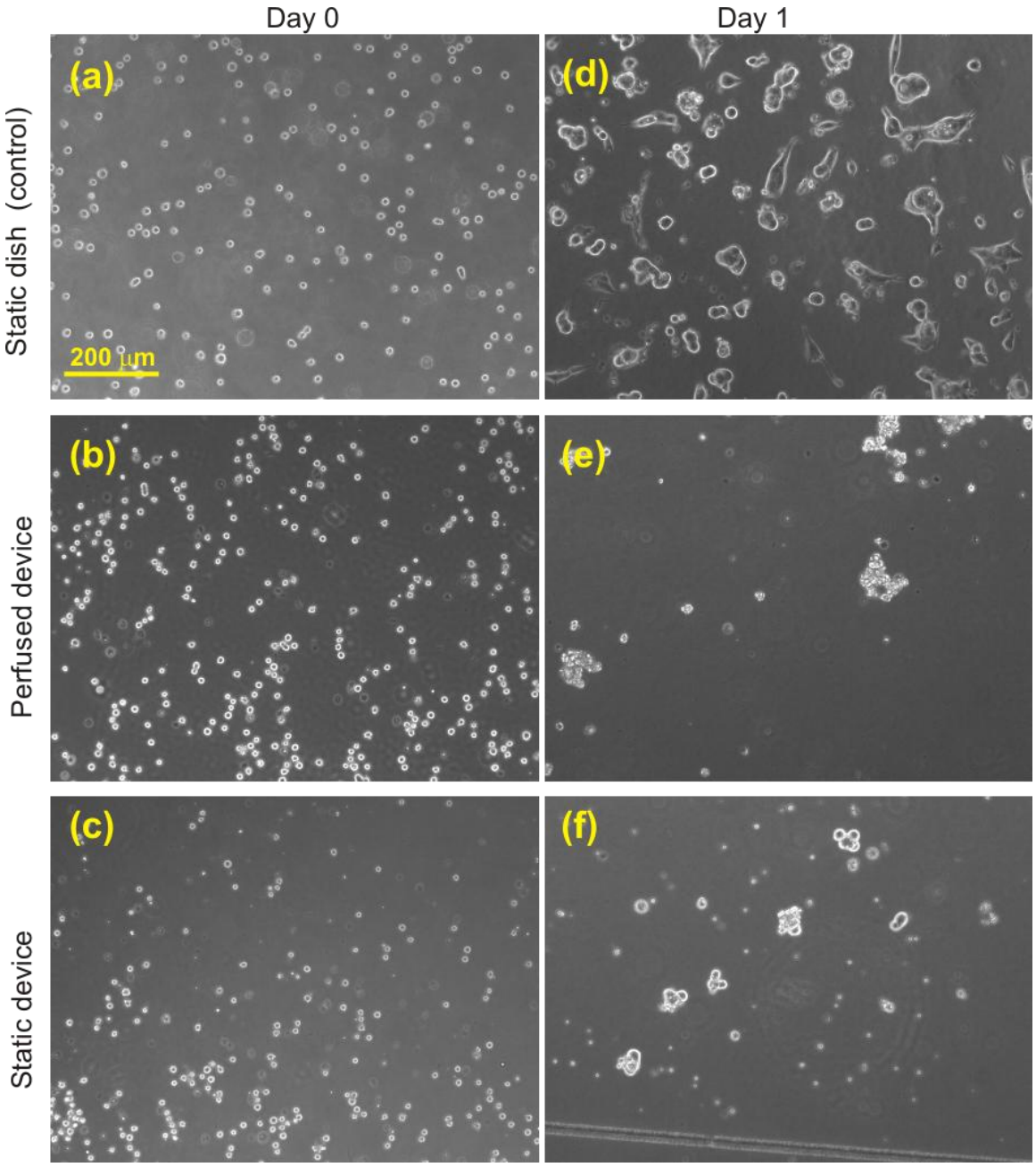

Figure 2.6: Control for mESC attachment in microfluidic device vs. static Petri dish. Day 0 results (a-c) show representative initial seeding densities. After overnight incubation, cells in the Petri dish (c) formed typical healthy colonies with compact round morphology and bright borders, while cells did not seem to attach well in either the isolated microfluidic device or in the microfluidic device connected to the full external fluidic setup. All photos were taken at the same scale.

2.2.4 Monoculture of mESCs in microfluidic perfusion

After many iterations and modifications to the experimental setup and protocol, I succeeded in demonstrating repeatable, viable monoculture of mESCs in microfluidic perfusion. The significant changes were: 1) I modified the base of the device to be polystyrene instead of glass 2) I allowed the cells to attach for 4 hours before starting perfusion (instead of waiting overnight) 3) I increased perfusion to a rate of 200 μL/hr (vs. 50 -100 μL/hr used previously) 4) I modified the experimental setup to add a 4-way valve and a small bubble trap, described in section 2.1.5. At the time, it was not clear exactly which of these changes were critical to success. However, with hindsight, it is likely that the change to the polystyrene base as well as the introduction of the 4-way valves were significant. The reason for this is that later it was shown that flow rates > 15 μL/hr for this chip geometry were sufficient to culture mESCs on glass in Chapter 3.

As in the attachment study, I prepared equilibrated ES media by incubating the media overnight in a 15-cm cell-culture dish in a humidified 37°C environment with 7.5% CO_2. On the day before loading cells I assembled the rest of the fluidic setup as shown in Figure 2.2(b), flushed it with ethanol, attached high-resistance tubing (5 inches of 1/16" PEEK tubing with inner diameter 0.0025", Upchurch Scientific) to the output of the microfluidic device, and perfused the system overnight with ES media at 3 μL/min.

On day 0 I gelatinized the device to promote cell attachment. I flushed the microfluidic device with an ES-qualified 0.1% gelatin solution (0.1% Specialty Media #ES-006-B) and left the gelatin in the device at room temperature for > 30 minutes to allow time for the gelatin to coat the surface. To remove the gelatin solution, I flushed the device forwards (in the perfusion direction) with ES media. I then loaded a suspension of 2×10^6 cells/mL mESCs in equilibrated ES media into the back end of the device. This experiment was repeated with ABJ1 mESCs and D3 mESCs in separate runs. I turned the 4-way valve to fluidically isolate the microfluidic device from the upstream fluidics and large bubble trap, and plugged the end of the 4-way valve connected to the device as well as the output tubing from the device. I allowed the cells to attach for four hours (instead of overnight as in previous experiments) before turning the 4-way valve to connect the microfluidic device to the upstream syringe and started perfusion at 200 μL/hr. As in previously described experiments, perfusion was maintained continuously until day 6 except for ~15 minutes each day when the microfluidic device was disconnected from the media input for microscopy, then reconnected to the perfusion source afterwards.

As shown in Figure 2.7, this protocol resulted in perfused cultures that proliferated over several days with large, round colonies at day 5, for both D3 and ABJ1 mESC lines. The ABJ1 cells have an incorporated GFP reported for the transcription factor Oct-4. Oct-4 expression is correlated with pluripotency of mESCs and begins to be downregulated at day 4 in differentiating cultures. The presence of the Oct-4 GFP signal in the ABJ1 colonies (Figure 2.7(f-inset)) suggests that the protocols used here preserve the pluripotent condition of mESCs. If essential secreted factors were swept away during perfusion culture, their function was replaced by factors in the serum-containing ES media. Although the results in Figure 2.7 go to day 5, I continued perfusing to day 6 with similar results (data not shown).

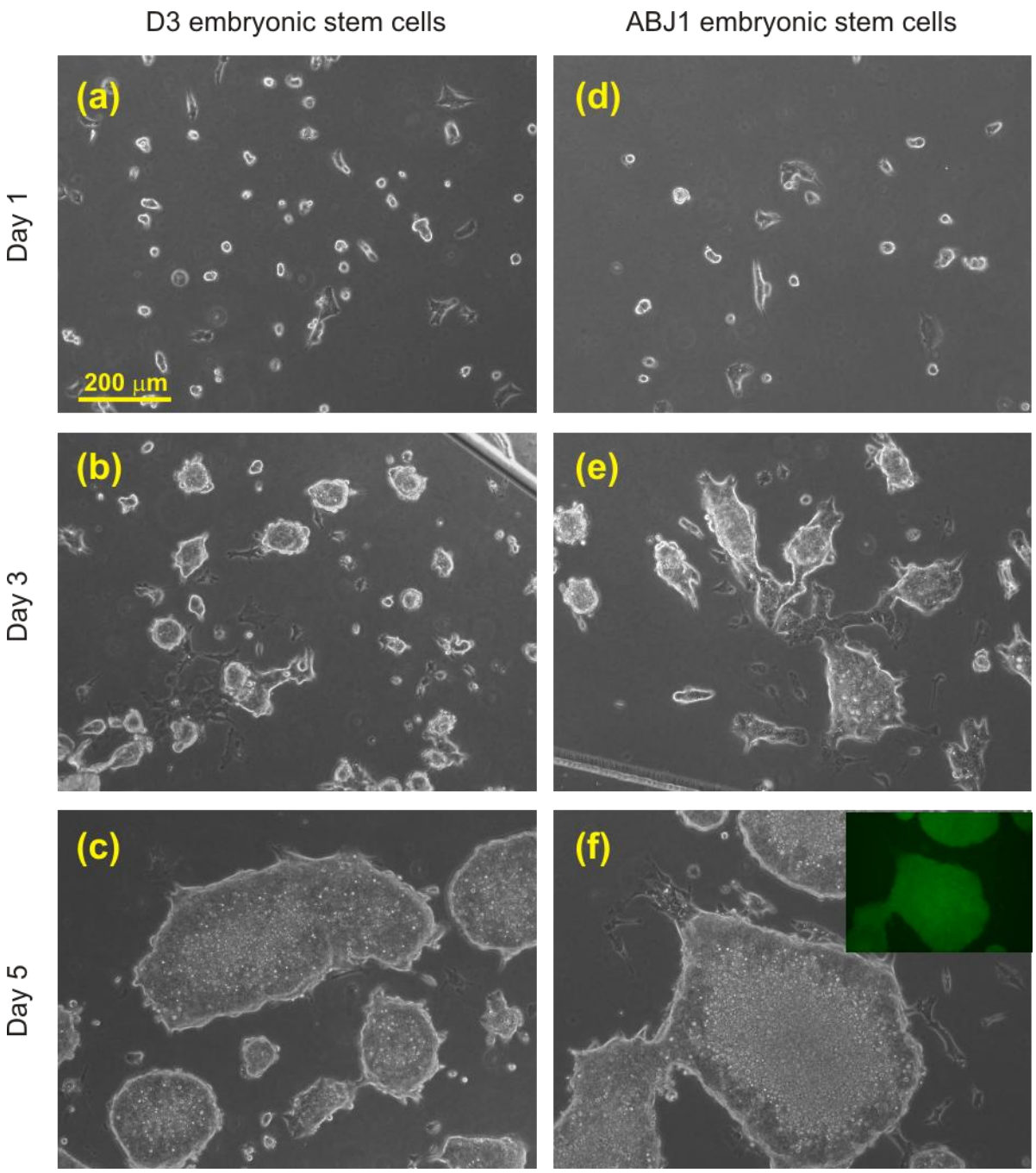

Figure 2.7: Microfluidic perfusion monoculture mESCs over 5 days at 200 μL/hr. D3 line of mESCs (a-c). ABJ1 line of mESCs (d-g). Both experimental runs demonstrate increasing colony size over time and compact, round morphology typical of mESCs. The ABJ1 line of mESCs contains a GFP reporter for the transcription factor Oct-4. The inset in (f) shows same area as the main photo of (f), but was taken using fluorescence imaging and shows the Oct-4 GFP signal. The expression of Oct-4 suggests that the colonies cultured in microfluidic perfusion remain pluripotent. These results are representative of results from three repeated experiments. All photos were taken at the same scale (scale bar shown in (a)).

2.3 Discussion

The goal of the work in this chapter was to establish basic conditions for a viable monoculture of mESCs in microfluidic perfusion. Initial experiments involving 3T3 fibroblasts alone or in combination with mESCs resulted in viable cultures fairly rapidly. However, achieving a successful monoculture of mESCs in the microfluidic device was more challenging, involving many permutations before leading to the final protocol described in section 2.2.4.

Why did the final protocol succeed, while previous attempts failed? When failure was due to air bubbles entering the system, it was usually observable because the bubbles would remain in the microfluidic device. However, there were several trials in which there were no observable bubbles throughout the process, yet the cell culture did not seem to attach or proliferate. In these cases, failure was likely due to poor initial attachment. These possibilities and strategies to combat them are discussed below. Strategies for uniform cell seeding are also discussed.

2.3.1 Eliminating air bubbles

Unwanted air bubbles are a significant practical challenge in microfluidic systems. Air bubbles are undesirable because they can obstruct fluid flow as well as kill cells at the gas-liquid interface. Eliminating bubbles is especially important in perfusion culture experiments, because a single bubble can cause failure of a week-long experiment, and because the continuous perfusion increases the chance that a bubble may be introduced from an upstream source. In the experiments in this chapter, air bubbles caused failure of > 50% of trials. Thus, there was great motivation to develop reliable methods for reducing bubble-related failure. Several methods were employed in this chapter which did reduce the appearance of air bubbles: 1) pressurization of the PDMS chamber before loading cells to drive out existing air bubbles in the microfluidic channel 2) techniques for avoiding introduction of air bubbles while loading cells into the microfluidic device 3) large and small bubble traps to prevent new bubbles from entering the device during perfusion culture. However, despite the fact that these methods did reduce bubble-related failure, there were still significant problems related to bubbles forming in the device after loading. Because the bubble traps were located off of the device, they fundamentally could not trap bubbles that formed within the device after loading.

The bubbles that appeared post-loading may have formed due to a couple reasons: 1) spontaneous generation from gas nuclei at hydrophobic defect sites, although this phenomenon is not well understood[77] 2)expansion of trapped micro (or nano-) bubbles that are not apparent at the time of loading, but that grow larger with changing conditions on chip, such as an increase temperature[78]. When working with PDMS microfluidics I have observed that the interface between the PDMS and inserted tubing is a common site of bubble generation. Considering that bubbles nucleate at defect sites, this may be due to surface defects in the punched PDMS hole acting as nucleation sites for bubbles. To create smoother interfaces, one can mold holes in PDMS (described in Chapter 3) or punch them using especially smooth tools. However, while these types of precautions may reduce bubble formation, even in molded-hole devices, I still observed that any slight motion of the PDMS tubing input to the device was correlated with bubble formation. The eventual solution adopted in Chapters 4 and 5 involves using a pneumatic, active bubble trap to continuously apply vacuum from the outside of the PDMS microchannel,

creating a pressure differential[78] that removes air from the fluidic system. This solution, as described in section 4.1, practically eliminated the appearance of bubbles during perfusion experiments

2.3.2 Cell seeding

Although uniform cell seeding is not required for achieving a viable perfusion culture, it is important for establishing repeatable densities. Cell seeding density affects cell-cell and cell-media interactions. The seeding flow rate must be relatively low so as not to compromise cell viability. However, low flow rates may cause cells to settle in the reservoir and fluidic connections, causing spatial non-uniformity in the final cell density. To improve uniformity of the cell density during loading, I minimized the distance between cell-suspension input and the microfluidic device. Since the cells begin settling after about a minute, I also took care to triturate the cell suspension immediately before loading into a syringe, and then immediately load this suspension into the device as quickly as possible.

2.3.3 Cell attachment

Once the cells are in the device, the cells must attach to the substrate so that they are not washed away upon media perfusion. Attachment depends on many factors, including cell-culture substrate material properties, fluid forces, time allowed for attachment, type of cell culture media, and the biological state of the cells. From the experiences in this chapter as well as throughout the entire thesis, the importance of achieving good initial cell attachment is critical to the success of the perfusion culture and cannot be emphasized enough. As mentioned in section 2.2.4, it is likely that improved attachment conditions were responsible for the success of the protocols described in that section.

The choice of cell substrate material is important because it affects not only attachment, but the biological outcomes. The cell substrate material allows cell attachment via adhesive proteins or peptides adsorbed from the cell culture media, or pre-immobilized cell-attachment proteins such as gelatin, collagen[44], laminin[31], or fibronectin[45]. For mESCs, the cell-culture substrate material is known to affect differentiation[10, 79], and indeed many of the cell-attachment proteins which encourage greater attachment also encourage high rates of differentiation and are therefore undesirable. In conventional cell culture, mESCs are typically grown on tissue-culture polystyrene substrates, which are used in this chapter. Although polystyrene is the ideal substrate since it is identical to that used in conventional culture, polystyrene cannot be bonded to PDMS. Glass, which can bond to PDMS, is not a typical substrate for ES culture. In this chapter I began by attempting to culture mESCs in microfluidic devices with glass substrates, but did not achieve success and switched to polystyrene, which produced better results comparable to culture in a static dish. Due to a more complex microfluidic design, in Chapter 3, I again attempted to culture mESCs on glass substrates, with some success, although with colony morphologies that differed from those in static culture on polystyrene, motivating a switch back to polystyrene (and more complicated device fabrication) in Chapter 4 and 5.

It is notable that successful fibroblast/mESC coculture was achieved early on under more tolerant conditions than the mESC monoculture. It is possible that the fibroblasts, which attach more readily than mESCs, formed an initial "sticky" substrate to which the mESCs attached easily. Therefore, the success of the cocultures may have been due to better attachment, whereas mESC monocultures using the same setup and protocol did not attach and required more refined methods.

Mechanical forces can be detrimental to cells if they are disturbed during the attachment process. For example, I have observed that in conventional static dish culture, if mESCs are mechanically disturbed during the first hour of attachment, their subsequent level of attachment is noticeably less when compared with undisturbed cells. Thus most perfusion culture protocols incorporate an initial static attachment period before perfusion is started. However, even if a static culture is the goal, non-idealities of the experimental setup and protocol may lead to undesirable motion during the attachment period. The change in experimental setup from Figure 2.1(a) to Figure 2.1(b) allowed the microfluidic device and small bubble trap to be fluidically isolated from the upstream fluidics, reducing mechanical disturbance due to fluid flow. In addition, protocols used in section 2.2.4 plugged the input and outputs of the device after loading to prevent fluid movement. It is not known which specific modification to the protocols from section 1.2.3 to 1.2.3 enabled successful culture. However, evidence from later experiments (Chapters 3-6) is consistent with the idea that minimizing fluid motion during seeding improves attachment.

There is also a time window for allowing sufficient cell attachment without nutrient and oxygen depletion. The duration of this static attachment time may vary from 2 hours[44, 47] to overnight[42], depending on cell type, cell density, cell substrate properties, effective culture volume, and choice of culture medium used during seeding. In the series of experiments in this chapter, I tried attachment times of 1.5 hours, 4 hours, and overnight, and achieved successful cultures using all but the 1.5-hour time. Chen *et al.* describe a similar time frame for attachment, observing that monkey ESCs readily attach to collagen and matrigel substrates within 2 hours of seeding[79].

The content of the cell-culture media and the biological state of the cells can significantly affect how well the cells attach. Chapters 2-4 use standard serum-containing media, which is favorable for mESC attachment. However in Chapter 5 I explore the use of perfusion culture with serum-free media. Even when using conventional techniques, serum-free media is known to be more challenging for attachment. Culturing mESC in microfluidic serum-free cultures requires more attention to substrate, attachment time, and minimizing fluid movement.

2.3.4 Cell proliferation: sufficient feeding

Once the cells have attached, the last requirement is to provide a sufficient growth environment using microfluidic perfusion. In the fibroblast/mESC coculture, both the 10 μL/hr and 100 μL/hr cultures proliferated by day 2, but the mESCs did not proliferate as well by day 3 in the 10 μL/hr condition. Chapter 3 explores effects across a wide range of flow rates, including those performed in this chapter. When results from Chapter 2 are compared against the results of Chapter 3, the 10 μL/hr flow rate falls below the flow-rate range needed for good culture. It is true that the successful results of section 2.2.4 had the highest flow rate used (200 μL/hr)

amongst all the trials conducted in this chapter. While it was initially thought that this was the main cause for success, subsequent data from Chapter 3 cast doubt on this idea. Many trials in this chapter failed despite flow rates of 50-100 μL/hr which should have been sufficient for nutrition according to the results in Chapter 3. Therefore, while sufficient feeding is critical to maintaining a viable mESC culture in microfluidic perfusion, it was not the chief obstacle to success in these trials.

2.4 Chapter Summary

In this chapter I established sufficient requirements for successful microfluidic perfusion culture of 3T3 fibroblasts, coculture of fibroblasts and mESCs, and culture of mESCs (D3 and ABJ1 lines). I demonstrated for the first time perfusion culture of mESCs in a microfluidic environment. Results showed that while fibroblasts are easily cultured under a wide variety of conditions, mESCs, especially monocultured mESCs, required more specific protocols to achieve successful culture in microfluidic perfusion. I developed experimental setups and methods that enabled cell seeding, attachment, and proliferation for up to six days in culture without disruption due to bubbles. While later chapters discuss improvements to these methods, the basic concepts remain the same.

Chapter 3. Logarithmically scaled perfusion culture

After establishing conditions for mESC culture in a single microfluidic channel, the next goal was to develop microfluidic devices that would enable simultaneous investigation of mESC growth across a broad range of conditions. Microfluidics offers the potential for massively parallel cell-culture systems; incorporating logarithmic scales, both in perfusion and in reagent concentration, extends the range of parameterized control of the soluble microenvironment. Although logarithmic ranges are often used in biology to explore a large parameter space, to-date they have not been commonly applied to microfluidic perfusion culture. In the area of logarithmic gradients, Pihl *et al*.[80] have developed a device to generate logarithmic concentration gradients for pharmacological testing on a patch-clamped cell. Gu *et al*.[45] have developed a microfluidic device that can apply a logarithmic range of flow rates using on-chip peristaltic pumps that recirculate media from a large reservoir. Instead, this work focused on developing a system for applying logarithmic flow rates across a single chip using non-recirculating perfusion.

With this goal, I designed a microfluidic device for culturing adherent cells over a logarithmic range of flow rates. The device sets flow rates through four separate cell-culture chambers using syringe-driven flow and a network of fluidic resistances. The design is easy to fabricate with no on-chip valves and is scalable both in the number of culture chambers as well as in the range of applied flow rates. Using particle velocimetry, I characterized the flow-rate range using particle velocimetry. In this device I demonstrated for the first time culture of mESCs (mESCs) in continuous, logarithmically scaled perfusion for 4 days, with flow rates varying >300× across the array. Cells grown in the slowest and fastest flow rates did not proliferate, while colonies grown in a mid-range of flow rates proliferated and exhibited compact round morphology. I also demonstrated logarithmically scaled continuous perfusion culture of 3T3 fibroblasts for 3 days, with proliferation at all flow rates except the slowest rate.

To demonstrate how the logarithmic flow-rate device can be combined with other microfluidic functions, such as a logarithmic concentration gradient, I also designed an extension of the design that combines the logarithmic flow-rate functionality with a logarithmic concentration gradient across the array. Using fluorescence measurements it was verified that a logarithmic concentration gradient was established in the extended device.

This chapter describes the design, fabrication, and evaluation of this logarithmically perfused cell-culture system. This chapter is adapted from "Microfluidic arrays for logarithmically perfused embryonic stem cell culture" (*Lab on a Chip* 2007)[68]. Michael Vahey and Hsu-Yi Lee assisted with the experimental characterization of logarithmic flow rates and concentration gradient.

3.1 Theory

Pressure-driven flow through rectangular channels is a well-known phenomenon. The devices described here operate by connecting a constant flow source to a network of geometrically set fluidic resistances. These conditions determine flow rates through each part of the microfluidic network. To determine the geometry corresponding to these fluidic resistances, I calculated the

fluidic resistances, *R*, using the formula for steady-state pressure-driven flow in a rectangular channel[81]:

$$\Delta P = QR \tag{3.1}$$

$$R = \frac{12\mu L}{h^3 w\left(1 - \frac{192h}{\pi^5 w}\sum_{n=0}^{\infty}\frac{\tanh\frac{\pi w}{2h}(2n+1)}{(2n+1)^5}\right)} \tag{3.2}$$

where *P* is the pressure, *x* is the length along channel, *Q* is the fluid flow rate, *L* is the channel length, *w* is the channel width, *h* is the channel height, and μ is the fluid viscosity. This calculation assumes that the direction of flow is along the channel length and that *w*>*h*.

I assumed the flow profile in the middle of the culture chambers would be well-approximated by parallel-plate Poiseuille flow[62]:

$$v_x(y) = 1.5U\left(1 - \left(\frac{y - 0.5h}{0.5h}\right)^2\right) \tag{3.3}$$

where *y* is the distance in the vertical direction (*y=0, h* at the walls), v_x is the velocity in the *x* direction, and *U* is the mean channel velocity.

I modeled the fluid shear on the cells by assuming that it would equal the shear stress (τ) at the wall between parallel plates under parabolic flow and using equation (1.1) to estimate shear stress, as is common for microfluidics. This estimate does not account for changes in flow due to the presence of the attached cells, but since the goal was to ensure that the shear stress is low enough to have little physiological effect, I was interested in order-of-magnitude estimates, and thus used equation (1.1) to calculate shear stress. Equation (1.1) is also used by other researchers exploring the effects of shear on mESC culture in laminar flow, and thus makes a good basis for comparison[65].

However, if one is interested in obtaining a more detailed estimated of the actual shear experienced by the cells, it may be necessary to take into account the exact conformation of the cells and how that affects the flow. For example, Gaver and Kute estimated the shear stress on a single cell adhered to a channel wall (no neighboring cells) to be ~3 times greater than the shear stress calculated for an empty channel when *k/h=0.1*, where *k* is the height of the adhered cell[82]. Since in our case, *k/h*~0.1, a more conservative estimate for the shear experienced by the cells is:

$$\tau_{singlecell} = 3\tau \tag{3.4}$$

3.2 Experimental

3.2.1 Cell culture

Culture of 3T3 fibroblasts and ABJ1 and D3 mESCs was performed as described in Chapter 2.

3.2.2 Microfluidic fabrication: 1×4 logarithmic flow-rate device

The 1×4 logarithmic flow-rate device consists of a single-layer network of channels molded in PDMS (Sylgard 184, Dow Corning, Midland, MI) and bonded to glass using standard procedures[83] as shown in Figure 3.1. Because the operation of the devices in this chapter relied on maintaining a good seal between the PDMS and substrate to maintain the desired fluidic resistance ratios, I chose to fabricate the devices using glass substrates which could be irreversibly plasma-bonded to PDMS.

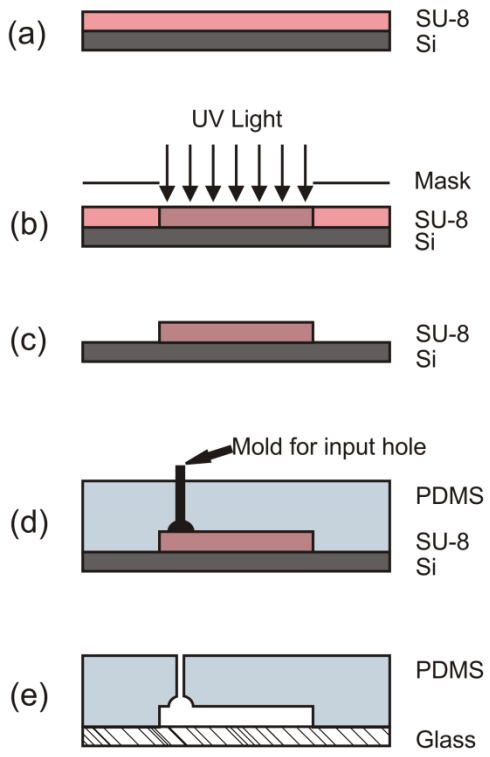

Figure 3.1: Fabrication of 1×4 logarithmic flow-rate device: a) Spin on SU-8 photoresist, softbake. b) Expose SU-8. c) Postbake, develop SU-8, and coat wafer with HMDS. d) Add mold for input hole, pour PDMS upper layer onto mold, cure. e) Remove PDMS from mold, cut out individual devices, punch output holes in PDMS and bond to glass. Note: figure not to scale.

I created the microfluidic channel layout using AutoCAD (Autodesk, San Rafael, CA), printed the design onto high-resolution transparencies and transferred it to a chrome photomask (Fineline Imaging, Colorado Springs, CO). To create the mold, I prepared a silicon wafer (dehydration baked at 130°C for 10 minutes, then cooled to room temperature and cleaned with pressurized N_2

to remove any stray dust particles on the surface. I poured SU-8 2050 negative photoresist (Microchem, Newton, MA) onto the stationary wafer and then spun (10 sec at 500 rpm, 10 sec ramp, 25 sec at 1100 rpm) as shown in Figure 3.1(a). Next I soft-baked the wafer (95°C hotplate ~ 7 minutes), exposed the wafer using the photomask (Hoya UV-36 filter, 2.5 minutes) (Figure 3.1(b)) and post-baked the wafer on a hotplate (65°C, 1 minute, then 95°C, 6 minutes). After the post-bake I turned off the heating element and cooled the wafer on the hotplate to 65°C before developing to avoid sudden temperature changes and reduce stress in the SU-8 layer. I spin-developed the SU-8-coated wafer in poly-mono-acetate (PM-acetate, Air Products and Chemicals, Allentown, PA) for 5 minutes. Finally, to minimize PDMS adhesion I coated the wafer with hexamethyldisilizane (HMDS, Arch Chemicals, Norwalk, CT) in a vacuum chamber for 30 minutes, thus completing the SU-8 mold wafer.

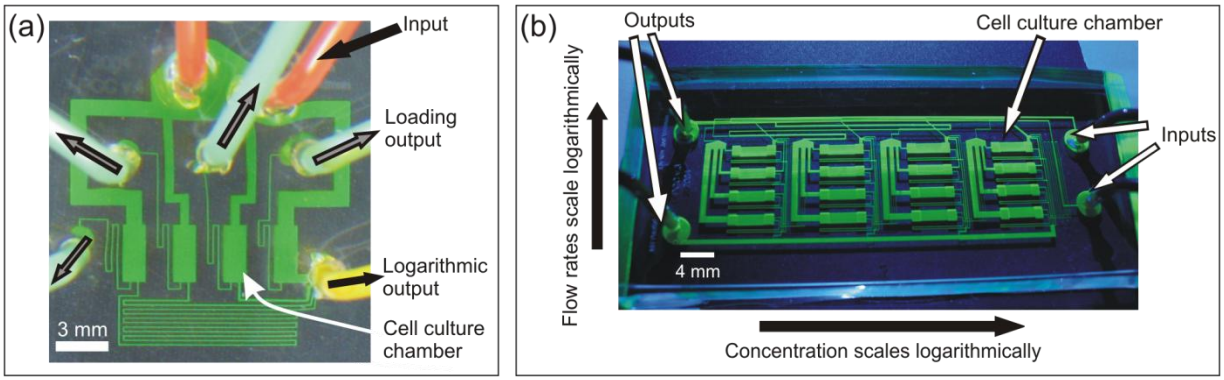

Figure 3.2: a) Photograph of 1×4 device filled with fluorescein to illustrate channels. The four gray arrows illustrate the four loading outputs. This chip has two orange input tubes (one for loading cells, one for perfusion). b) Photograph of multi-layer 4×4 device, filled with fluorescein to illustrate channels. The diluter is the network of channels at the upper end of the device.

I mixed PDMS in a ratio of 10:1, base to curing agent, degassed the mixture in vacuum for 30 minutes, and poured a 7-mm-thick layer onto the SU-8 mold wafer with HMDS-coated steel wires resting on the wafer to mold input holes, shown in Figure 3.1(c). The purpose of molding the input holes was to minimize generating PDMS particles that might clog narrow channels. After allowing the PDMS to degas for ~5 minutes I cured it for 2 hours in a 65°C oven. After curing I removed the PDMS from the mold wafer and removed the steel posts, cut out individual devices, and punched output access holes into the PDMS using a 16-gauge blunt-end needle. Since fluid flow was always unidirectional from input to output, the more convenient punching method could be used for the output holes, since any PDMS particles at the output would not be swept back into the device. Meanwhile, I cleaned standard 25 mm × 75 mm glass slides (48300-025, VWR, West Chester, PA) with 70% ethanol, immersed the slides in Nanostrip (Cyantek Corp., Fremont, CA) for 10-15 minutes, then rinsed them in de-ionized (DI) water, dried them with compressed N_2 and placed them in a 65°C oven for 5 minutes to dehydrate. I cleaned the PDMS surfaces with adhesive tape and exposed the PDMS and glass slide to air plasma for one minute (PDC-001, Harrick Plasma, Ithaca, NY). Then I immediately bonded the PDMS and glass to form a completed device, shown in Figure 3.1(d). To strengthen the bond, I placed the bonded device in a 65°C oven overnight. A photograph of the completed device is shown in Figure 3.2(a).

3.2.3 Microfluidic fabrication: 4×4 flow-rate and gradient device

Fabricating the upper and lower PDMS molds

As shown in Figure 3.3(g), the finished 4×4 flow rate and concentration gradient device consisted of four interconnected microfluidic layers: a 30-μm-high mixer layer, a 100-μm-high delivery layer, a 100-μm-high via layer, and a 100-μm-high chamber layer. An upper PDMS slab contained the mixer and delivery layers, while a lower PDMS slab contained the via and chamber layers. To pattern the upper and lower PDMS slabs, I fabricated two 2-layer SU-8 molds[84]. Figure 3.3(a-d) summarizes the fabrication of a 2-layer SU-8 mold—I used similar procedures[85] to make the upper and lower molds, the only difference being the heights and masks used for individual layers. To fabricate the mold wafer for the lower PDMS slab, I patterned the 100-μm chamber layer onto a Si wafer using the same procedure described for the 1×4 device, except that the SU-8 layer was not developed (Figure 3.3(a-b)). I then repeated the procedure, coating a second 100-μm layer on top of the patterned but undeveloped layer and aligning the photomask for this via layer with the visible (but undeveloped) pattern, exposing both layers (Figure 3.3(c)). Finally, I spin developed both layers simultaneously for 7-10 minutes (Figure 3.3(d)). I repeated this process for the "upper" wafer, substituting a thinner 30-μm second layer using SU-8 2015 (Microchem, Newton, MA. 5 sec spread at 500 rpm, 5 sec acceleration, 30 sec at 1300 rpm), with shorter softbake (95°C, ~2 min), exposure (1 min) and postbake (95°C, ~1 min) routines. I coated both upper and lower mold wafers in HMDS for 30 minutes to prevent PDMS adhesion.

Molding the PDMS and assembling the device

I mixed PDMS in a ratio of 10:1, base to curing agent, degassed it in vacuum for 30 minutes, and poured a small volume (<5 mL) onto the lower mold wafer. Next I sandwiched the PDMS-coated wafer between two sheets of transparency film, placed a blank 4" Si wafer on top of the transparency layer that touched the PDMS, and sandwiched the stack between two 1-cm-thick aluminum plates. I placed the entire sandwich, including aluminum plates, on a room temperature hotplate and compressed it using a large C-clamp, creating a ~200-μm-thick layer of PDMS, illustrated in Figure 3.3(f). I set the hotplate temperature to 65° C and cured the PDMS in this setup for 2 hours. After curing I removed the transparency+PDMS+wafer sandwich from the hotplate and peeled away the transparencies, leaving the PDMS on the wafer mold. At this time I inspected the patterned PDMS layer and manually cleared any unopened vias.

Meanwhile we patterned the upper PDMS slab using HMDS-coated 19-gauge steel wire posts to mold input and output holes. I poured PDMS onto the upper mold wafer to a thickness of ~7 mm and cured the PDMS in an oven at 65° C for 2 hours, shown in Figure 3.3(e). I then peeled the cured PDMS off of the mold and cut apart individual devices. Without removing the lower PDMS layer from the mold wafer, I exposed the lower and upper PDMS layers to air plasma for one minute, then aligned by hand and bonded the two PDMS layers. Next I removed the two bonded PDMS layers from the lower mold wafer, cut apart individual devices, and plasma bonded them in the same manner to a standard 25 mm × 75 mm glass slide (48300-025, VWR, West Chester, PA), shown in Figure 3.3(g). I placed the entire device in a 65° C oven overnight under compression to improve bond strength. The completed device is shown in Figure 3.2(b).

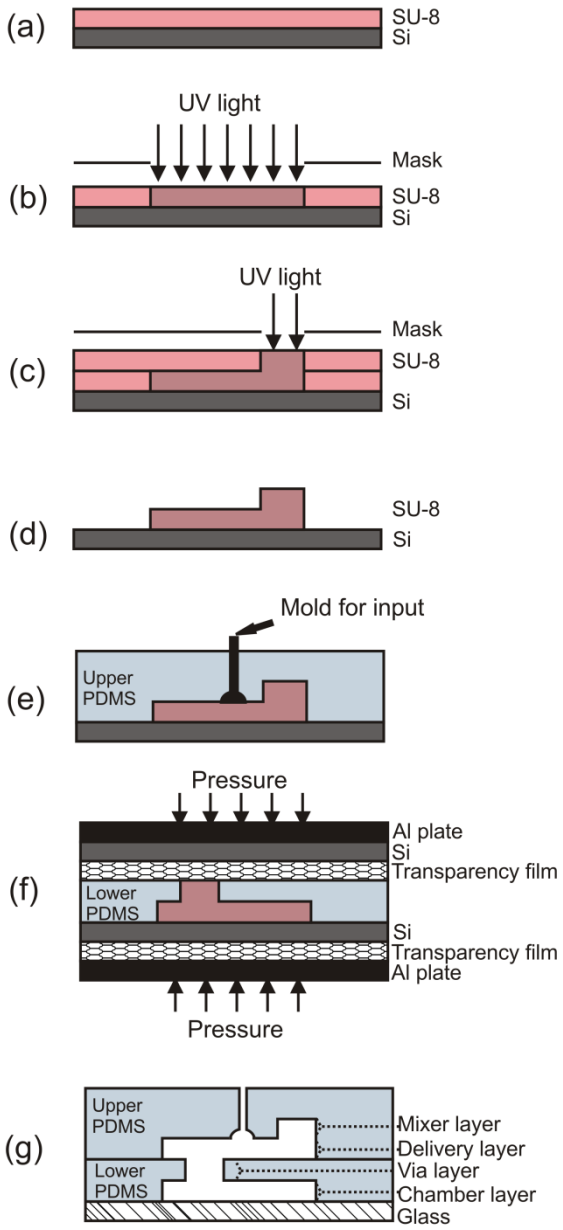

Figure 3.3: Fabrication of 4×4 device. Create mold for upper PDMS layer: a) Spin-on SU-8 photoresist b) Expose SU-8 without developing c) Spin-on and expose 2nd layer of SU-8 d) Develop both SU-8 layers and coat surface with HMDS. Repeat steps a-d to create mold for lower PDMS layer, using a different set of masks. e) Pattern upper PDMS layer by pouring PDMS onto mold (including input hold molds) and curing. f) Form lower PDMS layer by squeezing PDMS between flat plates to form via holes. g) Remove upper PDMS layer from mold, punch output holes, plasma bond to lower PDMS layer. Plasma bond lower layer to glass. Note: figure not to scale.

3.2.4 Optics

As in Chapter 2 I used an inverted microscope (Zeiss Axiovert 200, Thornwood, NY) with a SPOT RT Color 2.2.1 camera (Diagnostic Instruments, Sterling Heights, MI). An automated

upright microscope (Zeiss Axioplan 2 Imaging, Thornwood, NY) with an LA Vision ImagerQE camera was used in the particle velocimetry and concentration gradient experiments, and also for measuring the PDMS layer heights using a 20× Mireau interferometric objective (Nikon).

3.2.5 Measuring microfluidic channel heights

To measure the chamber heights for both the 1×4 and 4×4 devices I used a 20× Mireau interferometric objective (Nikon) to locate planes within the PDMS by visualizing interference fringes. I made measurements on unbonded PDMS pieces patterned from the same molds used to make the devices I characterized. I measured the distance between planes by recording the microscope stage height at each plane. I repeated this at several locations across the device. Channel heights typically varied by ~10% across each chip. For the 1×4 device the mean channel height was 83.1 μm with a standard deviation of 3.6 μm over 20 measurements. For the 4×4 device the mean height of the chamber layer was 102.9 μm ±3.3 μm (±1 S.D., n=16 measurements). The mean height of the delivery layer was 97.5 μm ±2.5 μm (n=19). The mean height of the mixer layer was 32.7 μm ±1.4 μm (n=10), and the mean height of the via layer was 116.5 μm ± 5.9 μm (n=16).

3.2.6 Characterization of logarithmically scaled flow rates

To characterize the flow rates in the 1×4 logarithmic flow-rate device I worked with Hsu-yi Lee, who designed and carried out measurements using a particle velocimetry approach. To access the microfluidic channels we press-fit PEEK tubing (1532, Upchurch, Oak Harbor, WA) into the input, four loading outputs, and logarithmic output. We plugged the four loading outputs closed using unions (P-702, Upchurch, Oak Harbor, WA) and Teflon plugs (P-316, Upchurch, Oak Harbor, WA). To remove air bubbles in the device, we filled the chip with deionized (DI) water using a syringe at high pressure (>5 psi) for ~15 minutes (this standard procedure is also referred to as "blind filling" or "dead-end filling"[70]). We suspended 2-μm-diameter red-fluorescent polystyrene beads (19508, Polysciences, Warrington, PA) in DI water with 0.1% Triton X-100 (Sigma, St. Louis, MO) at a concentration such that the areal density at one focal plane was ~1.5×10^{-3} beads/μm^2. We loaded this suspension into a 250-μL glass syringe (Hamilton, Reno, NV) that was mounted into a syringe pump (KD Scientific 200, Holliston, MA). Taking care not to introduce new bubbles, we connected the syringe to the device to inject the bead suspension.

We measured the bead velocities one chamber at a time, starting with the slowest chamber. For each chamber, we set the syringe pump flow rate and allowed the system to reach equilibrium for ~5-10 minutes. Then we focused the microscope halfway through the depth of the chamber and took snapshots of the bead suspension at 5-second intervals, repeating this at three locations along the length of the culture chamber. After taking measurements for each chamber, we flipped the device upside-down to minimize bead settling. Because of the wide range of flow rates across the device, we used different total-chip flow rates to measure each chamber. This scaling ensured that the bead velocities remained within a practically measureable range. We set the total perfusion rates to 0.1 μL/min, 0.1 μL/min, 3 μL/min, and 5 μL/min (slowest chamber to fastest chamber). To calculate the velocities, we used Matlab (Mathworks, Natick, MA) to measure the distances traveled by beads in the 5-second intervals. For each sample, we chose the fastest bead velocity, as it represented the centerline flow velocity.

3.2.7 Measurement of logarithmic concentration gradient

To characterize operation of the logarithmic diluter in the 4×4 device, I worked with together with Mike Vahey, who developed and implemented a quantitative fluorescence microscopy method to measure the concentration gradient. We first blind-filled the device with DI water to remove any air bubbles. We then filled one 1-mL plastic syringe (Becton Dickinson, Franklin Lakes, NJ) with 1 mM fluorescein sodium salt (Sigma, St. Louis, MO) and a second with DI water. We selected the fluorescein concentration to enable imaging over a large range of dilutions without requiring excessive exposure times. We then established a concentration gradient with the device in the "loading" mode by setting a flow rate of 5.00 μL/min for the fluorescein solution and 13.02 μL/min for the DI water. After a steady gradient was established throughout the array, we imaged each chamber. We selected exposure times such that fluorescent intensity varied linearly with exposure time at the concentrations of interest (as determined by calibration measurements), allowing us to compensate for differences in exposure times across the 4×4 array by linearly scaling the results. For each chamber, we imaged the chamber's center, fully occupying the field of view. We waited 2 minutes after each exposure before obtaining the next image, allowing the contents of each chamber to turn over ~5 times to minimize the effects of photobleaching. (With the device in "loading" mode, all chambers had equal flow rates.) We used a calibration curve (created via a dilution series of the 1 mM fluorescein solution) to convert fluorescence intensity to concentration.

3.2.8 Logarithmically scaled perfusion culture: fluidic setup

This section describes the fluidic setup used for culturing cells in the 1×4 logarithmic flow-rate device. I connected the 1×4 logarithmic flow-rate device to off-chip fluidics as shown in Figure 3.4(b) using connectors, valves, and tubing from Upchurch (Oak Harbor, WA). I used a syringe pump (KD Scientific 200, Holliston, MA) as a constant flow source for the fluidics. I placed the syringe pump outside the incubator (Steri-cycle, Thermo Forma, Philadelphia, PA) and positioned the device and accompanying valves inside the incubator to maintain the device in a 37°C, humidified, 5% CO_2 environment. I connected a plastic syringe (Becton Dickinson, Franklin Lakes, NJ) outside the incubator to ~2 feet of flexible Teflon tubing (1536, Upchurch Scientific, Oak Harbor, WA) that was threaded through an existing access port in the incubator. Inside the incubator, I attached the tubing to a Luertight connector system (P-837, Upchurch, Oak Harbor, WA) which I connected to a large bubble trap (6115, Varian, Torrance, CA) with a ~1-mL total volume. The bubble trap allowed the device and fluidic setup to be disconnected and removed from the incubator for microscopy without introducing bubbles. As shown in Figure 3.4(b), the fluidics setup inside the incubator consisted of two main paths to the device: a loading path and a feeding path, connected by various Upchurch valves (V-101D, V-101T, Upchurch Scientific, Oak Harbor, WA). Using separate loading and feeding tubes reduced the amount of "backlog" cell suspension fed to the cells after starting perfusion. For this reason I also minimized the length of the tube joining the T-connector to the device. I also included an additional, smaller bubble trap and 2-μm filter (P-272X, Upchurch, Oak Harbor, WA) in the feeding path to guard against bubbles during perfusion; even with the larger, upstream bubble trap at the input, I still occasionally observed new air bubbles in the device a few days after starting perfusion. I fabricated the smaller, downstream bubble trap by carving a ~200 μL cavity in a ~2 cm x 2 cm x 0.7 cm slab of PDMS, punching two access holes in the cavity, and bonding

the PDMS slab to a glass slide, creating a microfluidic chamber. I oriented the small bubble trap slide-side up with press-fit input and output tubes pointed downward so that any passing bubbles would collect in the chamber. I connected the output of the small bubble trap to a 2-μm filter (P-272X, Upchurch, Oak Harbor, WA) to prevent large particles from clogging the smaller channels in the device. Except for the tubing connecting to the small bubble trap chamber, all other fluidic routing used flexible clear Teflon tubing (1529, Upchurch Scientific, Oak Harbor, WA and 10-15-00214 Optimize Technologies).

3.2.9 Logarithmically scaled perfusion culture: general procedure

Each perfusion experiment used the following protocol: I prepared equilibrated media by incubating the media overnight in a 10-cm or 15-cm cell-culture dish in a humidified 37°C environment with 7.5% CO_2; this media was used throughout the experiment (blind filling and perfusion culture). Next I assembled the entire fluidics system as shown in Figure 3.4(b) and flushed the fluidics and chip with 70% ethanol for >30 minutes to sterilize the system. To remove air bubbles from the device and flush the ethanol out of the system, I plugged the loading outputs shut, connected 2" of 1/16"-OD/0.0024"-ID tubing (1560, Upchurch, Oak Harbor, WA) to the logarithmic output, and perfused the system overnight with equilibrated media at 10 μL/min, creating pressures >5 psi within the channels to drive air out through the PDMS walls[29]. I set the 3-way valves so that all parts of the system were fluidically connected as shown in Figure 3.4(a.1).

The next day (designated day 0) I loaded the cells into the microfluidic device. I made a cells-in-media suspension by trypsinizing cells with TrypLE Express (12605-010, Invitrogen, Carlsbad, CA), quenching trypsin with serum-containing media, then counting cells on a hemacytometer. To make the appropriate concentrations I centrifuged the initial cell suspension for 5 minutes at 1000 rpm, aspirated the supernatant, resuspended the cells in equilibrated media, and triturated to produce a single cell suspension at a density of 0.5×10^6 cells/mL for the 3T3 cells and 2.2×10^6 cells/mL for the mESCs. All cells used were passage 21 or lower. After placing the fluidics and device in a sterile biosafety cabinet, I turned the upstream 3-way valve such that the cell suspension would flow only through the loading input tube and the feeding tube was bypassed (no flow through the feeding tube), shown in Figure 3.4(a.2). I then plugged the logarithmic output shut and unplugged the four loading outputs. I loaded the cell suspension (described below) into a 1-mL syringe (Becton Dickinson, Franklin Lakes, NJ) and attached it to the 4-way valve as shown in Figure 3.4(b). To monitor loading I placed the device on a phase microscope (Zeiss Axiovert) and slowly injected the cell suspension by hand. When sufficient cells were loaded into each chamber, I plugged the loading outputs and removed the syringe containing the cell suspension. I then turned the upstream 3-way valve so that the device was fluidically isolated from the syringe input, leaving the logarithmic inputs plugged. (Thus, all inputs/outputs to the device were blocked to minimize fluid movement during cell attachment.) To flush out any extra cells in suspension in the tubing I flushed the rest of the system with new media. Figure 3.4(a.3) shows the valve/plug settings for this step.

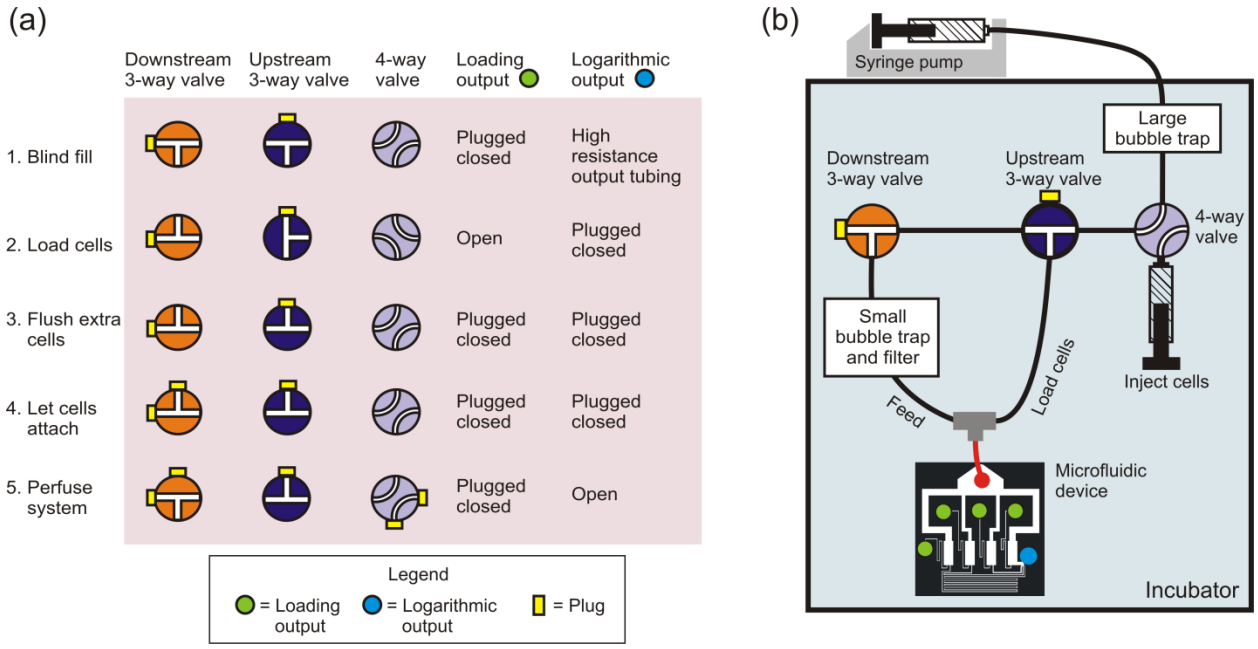

Figure 3.4: Off-chip fluidic setup for perfusion culture experiments using the 1×4 flow-rate device. a) Table showing valve and plug settings for each step of cell perfusion culture experiment. a.1) During the "blind fill" step the chip was filled with liquid and any remaining bubbles were driven out through the PDMS. a.2) Next a suspension of cells in media was loaded into the chip through the "loading" input tube—the loading outputs were temporarily plugged shut while the logarithmic output was open. a.3) After cells were loaded, extra cells in the tubing were flushed out to waste. a.4) To minimize fluid movement during cell attachment, all outputs were plugged closed and the valves were turned to fluidically isolate the device. a.5) After 4 hours of static culture, perfusion was started. Media was delivered to the device via the feed tube. Unused outputs on the valves were plugged closed to prevent leaks. b) Schematic diagram of macrofluidic setup, showing "feed" tube and "load cells" tube.

I allowed the cells to attach for 4 hours in static culture (no perfusion) by placing the setup in the humidified incubator at 37°C and 5% CO_2, with valve/plug settings as shown in Figure 3.4(a.4). For both 3T3 and mESC culture I observed that minimizing fluid movement during the attachment period was helpful for cell attachment. After cell attachment I re-connected the setup to the syringe outside of the incubator. I removed the logarithmic output plug (placing the device in logarithmic mode) and switched the downstream 3-way valve so that media could flow from the syringe through the feeding tube to the device, as shown in Figure 3.4(a.5). I set the syringe pump outside of the incubator to a fixed flow rate. Each day perfusion was interrupted for a brief time (<30 min) while I removed the setup from the incubator to take images at the microscope. After imaging I replaced the setup inside the incubator and resumed perfusion.

3.3 Results

3.3.1 Design of 1×4 logarithmic flow-rate device

The design of the 1×4 logarithmic flow-rate device is easy to fabricate, with no on-chip valves, and operates as a simple, single-layer fluidic resistance network. An off-chip syringe pump feeds constant-current flow to the fluidic resistance network in the device, creating a logarithmic range

of flow rates through separate cell-culture chambers. The device layout is shown in Figure 3.5(a) and contains four cell-culture chambers, each 1.25 mm × 3.2 mm × 80 μm for a culture area of 4 mm^2 and chamber volume of 0.32 μL. The chambers are connected to a joint input via low-resistance channels designed to have the same fluidic resistance.

Each chamber has two output channels, a "loading" output and a "logarithmic" output. The loading output channels have the same geometry and fluidic resistance, whereas the logarithmic output channels have logarithmically varying fluidic resistances. The device operates either in "loading mode", where the logarithmic output is temporarily plugged, or in "logarithmic mode", where the loading output channels are plugged (Figure 3.5). In "loading mode" the flow rates through each channel were designed to be the same, whereas in "logarithmic mode" the flow rates through each channel were designed to span a logarithmic range across the device. The logarithmic output channels all connect to the same tube off of the chip, whereas the loading output channels each lead to a separate tube off of the chip.

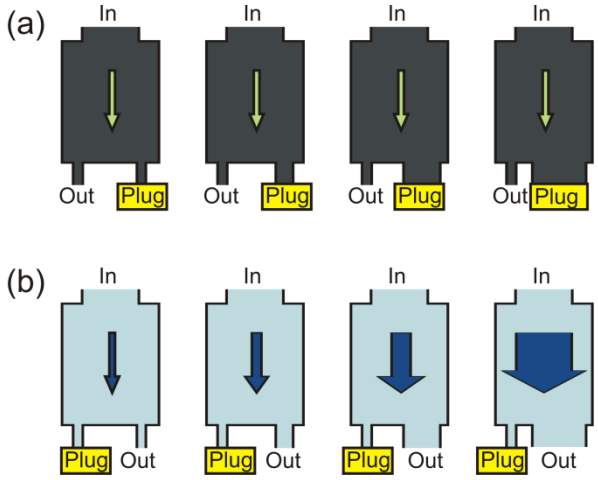

Figure 3.5: Schematic of the fluidic resistance network for the 1×4 flow-rate device in two modes of operation. In both a) and b) all of the "In" points are joined to a single constant flow source, yielding an equal pressure drop from each "In" to "Out". a) In loading mode each culture chamber flow path has the same resistance, creating the same flow rate in all chambers. Outputs with a "Plug" are temporarily plugged. b) In logarithmic mode the fluidic resistances are scaled logarithmically, causing the flow rate to increase logarithmically from one chamber to the next. Note: channel/chamber sizes not to scale.

I set the logarithmic flow rates by choosing the appropriate fluidic resistance for each logarithmic-mode output channel (R_i, where $i=1,2,3,4$ in Figure 3.6(a)). To illustrate, consider a hypothetical isolated Y-shaped tubing junction, with a constant input flow rate from the bottom tube of the "Y". If the fluidic resistances of the left and rights branches are the same, there will be equal flow through each branch. However, if the fluidic resistance of the right branch is 6× larger than that of the left branch, the flow rate through the right branch will be 6× smaller than the flow through the left branch according to equation (3.1) and Kirchhoff's current and voltage laws. Using these principles, we designed a logarithmic range of flow rates across four parallel "branches", where the flow rate of each branch, Q_i is determined by equation (3.5).

$$Q_i = Q_{total}\left(\frac{1}{(R_{ch}+R_i)\sum_j \frac{1}{R_{ch}+R_j}}\right) \tag{3.5}$$

where i is the branch index, j is a dummy index over all branches, and Q_i, Q_{total}, R_{ch}, R_i, and R_j refer to flow rates and fluidic resistances as shown in Figure 3.6(a). I assume that in logarithmic mode, $R_L \rightarrow \infty$ and there is no flow through the R_L branches.

For both devices presented here, I designed the flow rates to vary by a factor of 6 from one chamber to the next when in logarithmic mode. I chose the factor of 6 to allow the entire device to be of a size that it could be extended to a 4×4 array that would fit on a standard microscope slide. In addition, I designed the smallest channel dimension to be >40 μm to reduce channel clogging during operation. To avoid bulging of the PDMS or bursting the PDMS/glass bond, I designed the channel geometries so that the pressure drop in the device was small (<<1 psi) under normal operation. To allow easy connection to off-chip fluidics, I designed large areas for input/output tubing.

To choose the device geometry, I first started with the desired flow rates, Q_i, and worked back to calculate the necessary channel geometries using equations (3.1)-(3.2) and basic circuit theory. I show a schematic of the design process for the 1×4 device in Figure 3.6(a) along with an image of the completed device in Figure 3.6(a). I designed the layout of the device as follows:

1. Choose logarithmic mode flow rates Q_1-Q_4.
2. Determine all fluidic resistances R_{ch}, R_L, and $R_{i,}$, where $i=1,2,3,4$:
    a. Choose R_{ch}, R_L.
    b. Choose an arbitrary, low pressure difference P_{in}-P_{out}.
    c. Assume $Q_{L1}=Q_{L2}=Q_{L3}=Q_{L4}=0$ in logarithmic mode. (Loading outputs plugged closed.)
    d. Using Kirchhoff's current law: $Q_{ch1}=Q_1$, $Q_{ch2}=Q_2$, $Q_{ch3}=Q_3$, $Q_{ch4}=Q_4$.
    e. Calculate $P_i=P_{in}-Q_iR_{ch}$, where i=1, 2, 3, 4.
    f. Calculate $R_i=(P_i-P_{out})/R_i$ where i=1, 2, 3, 4.
3. Draw an initial network layout of lines to determine L_i=channel length for each resistor R_i.
4. Given R_i, L_i, and h_i=channel height, calculate w_i=channel width using equation (3.2). (I used the "fsolve" nonlinear solver in Matlab with n=2.)
5. "Fill out" the network layout using w_i's calculated in step 4.

6. Repeat steps 3-6, adjusting the network layout until channels fit, with acceptable spacing between channels. Also iteratively adjust P_{in}-P_{out} as necessary to create practical fluidic resistances.

Although I designed the device to experience constant flow through the chambers during culture, in some cases the flow might be so slow that diffusion could become important. This was a concern since the four cell-culture chambers were interconnected through the inputs and the logarithmic outputs. To ensure that diffusion would not be relevant, I designed the interconnections between the channels to be much longer than the ~1.5-mm that a typical 20-kDa molecule would diffuse in 4 days in static conditions.

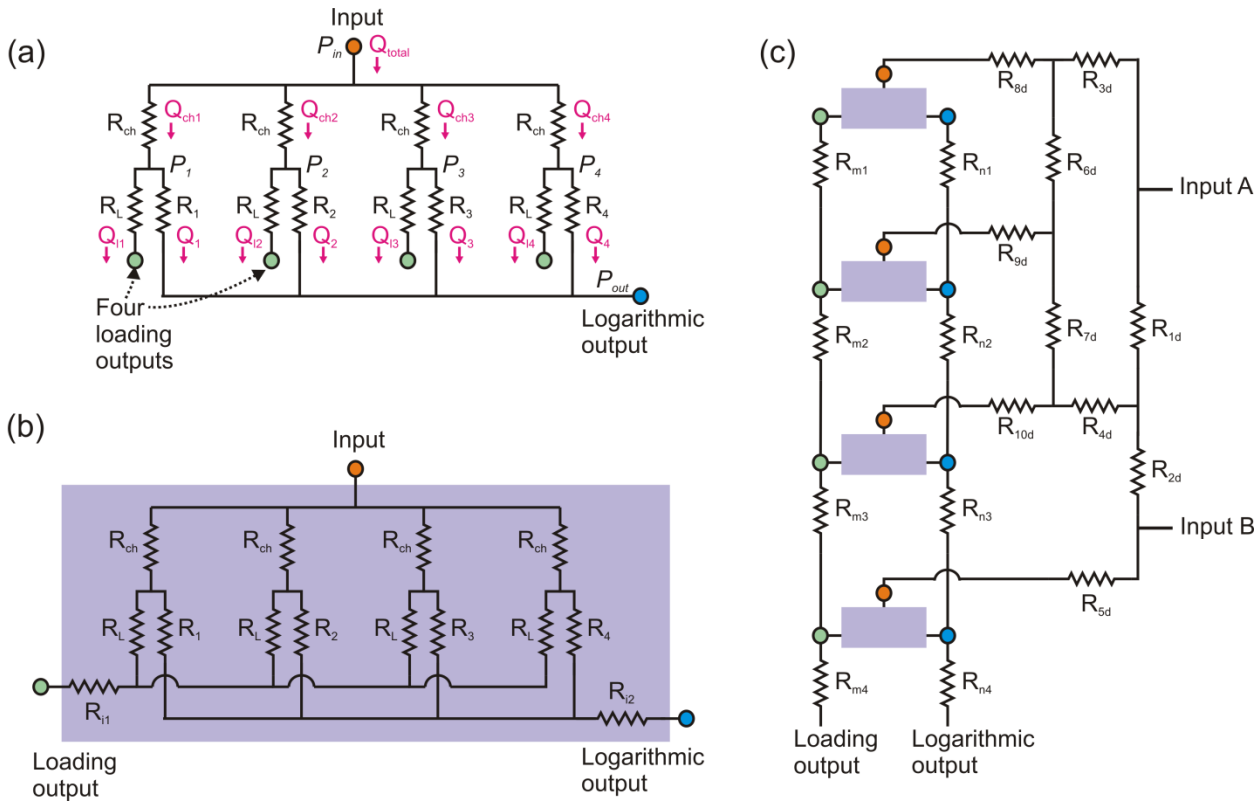

Figure 3.6: Schematic fluidic resistor network diagram for logarithmic flow-rate device (a) and flow rate/concentration gradient device (b-c). a) Fluidic resistor network for 1×4 device shows four loading mode resistors (R_L) with the same resistance, four culture chambers with the same resistance (R_{ch}), and four logarithmically scaled resistors (R_1-R_4). b) Fluidic resistor network for one row of 4×4 device. This is identical to the network in a), however the loading mode output resistors are joined into a single output. c) Fluidic resistor network for 4×4 flow-rate/concentration-gradient device. An on-chip diluter (R_{1d}-R_{10d}) mixes inputs A and B in logarithmic ratios and sends four different concentrations to each row (blue box). The blue boxes represent the flow rate resistor network in b). All of the logarithmic outputs are combined into a single output, and all of the loading mode outputs are also combined into a single output.

3.3.2 Flow rate measurements vs. modeling

Since the goal was to develop a device that could easily create a large range of flow rates from a single input, it was important to ensure that the flow rate ratios across the chambers corresponded to predictions. Since the microfluidic channels have rectangular cross-sections and thus a known parabolic flow profile (equation (3.3)), I used a simplified version of particle velocimetry to measure the actual flow rates in each of the chambers. I assumed that the highest fluid velocity was at the midpoint of the chamber height, and that combining this velocity with the chamber dimensions would allow me to back-calculate the volumetric flow rate. Thus, I measured the centerline flow velocity by finding the velocity of a set of beads in two imaged fields (separated in time) and then used the highest velocity as the centerline.

Figure 3.7(a) shows a comparison between measured vs. predicted maximum velocities for each channel in logarithmic mode. I calculated the predicted velocities using a combination of Matlab and COMSOL modeling of as-fabricated fluidic resistances. This shows that the device indeed generates logarithmically varying flow rates across the device. Although the actual range of velocities/flow rates (>300×) was larger than designed for (216×), this is due to a modest (~43%) difference in the lowest measured flow rate; the resulting range is extremely sensitive to variations in the smallest flow rate. This difference is likely due to a combination of experimental error, differences between designed-for and fabricated geometries, and simplifying assumptions in the model.

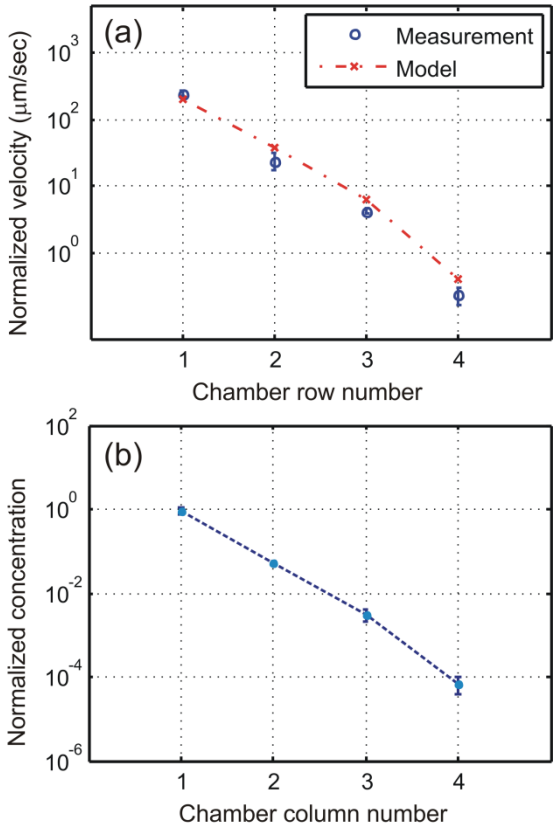

Figure 3.7: Characterization of logarithmic flow rates and logarithmic concentration gradient. a) Normalized measured channel velocities compared with model predictions. Error bars show +/- one standard deviation over four measurements. b) Measured, normalized concentration. Each data point represents the average concentration for a row of culture chambers across all columns, and error bars show the standard deviation across the 4 rows.

3.3.3 3T3 perfusion culture

To demonstrate the use of the 1×4 logarithmic flow-rate device with cells, I performed perfusion culture of murine 3T3 fibroblasts for 3 days in the device at a total flow rate of Q_{total}=10 μL/hr ($Q_{total} = Q_1 + Q_2 + Q_3 + Q_4$). I estimated the flow rates applied to the four individual cell-culture chambers to be 1.6×10^{-4}, 2.9×10^{-3}, 1.7×10^{-2}, and 0.17 μL/min using the particle velocimetry data. During cell loading I achieved a roughly uniform seeding of cells throughout the chamber. Figure 3.8 shows qualitative results on days 1 and 3 at each of the four flow rates. Over several days of culture, cells exhibited a well-adhered, healthy morphology comparable to static culture. Cells proliferated in the fastest 3 chambers but not in the chamber with the slowest flow rate. In the chamber with the fastest flow rates, cells proliferated more than in the other chambers and were more densely packed on day 3, while for the middle two flow rates, the proliferation was qualitatively similar. After day 3 I stopped the experiment because the cultures were confluent. These results are consistent with several 3T3 perfusion culture experiments I have run at various cell seeding densities and flow rates on multiple devices.

Although the device was designed for one-time use, I have observed the ability to remove all adhered 3T3 cells from the device by flowing trypsin through the device. I was also able to successfully reseed the surface with new 3T3 cells (data not shown).

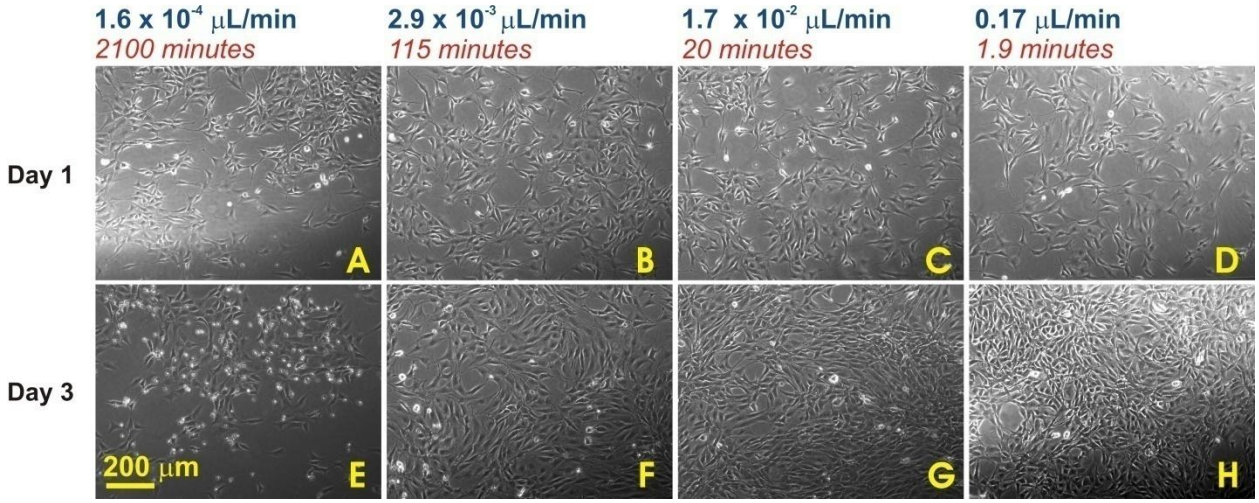

Figure 3.8: Perfusion culture of 3T3 mouse fibroblast cells over logarithmically scaled flow rates. A-D show cell cultures after one day of perfusion at various rates. E-F show resulting cultures after 3 days of perfusion at various rates. Each column (A/E, B/F, etc.) displays results for a different flow rate. Calculated flow rates for each column are shown above in bold. The average time to replace one culture-chamber volume is shown in italics. Cultures in all four conditions were seeded at the same initial density, however, by day 3 cells in the slowest flow condition (E) show poor proliferation, whereas the culture in the highest flow condition is nearly confluent. All photos are at the same scale.

3.3.4 mESC perfusion culture

Unlike 3T3 fibroblasts which can tolerate a wide variety of culture conditions, mESCs are known to have more specific culture requirements. For example, while fibroblasts readily attach to uncoated glass substrates, uncoated glass normally does not support the culture of mESCs, although mESCs grow well on uncoated tissue-culture polystyrene. By pre-incubating glass with serum-containing media or gelatin for 1 hour, mESCs showed enhanced attachment, permitting them to be cultured in microfluidic perfusion systems (Figure 3.9). Thus, surface modification of cell substrates to facilitate cell attachment can be critical in microfluidic perfusion culture. In fact, surface modification of cell substrate is more important in microfluidic perfusion culture systems than in static systems because one typically has a limited time to allow for cell attachment under static conditions before media perfusion must be initiated to replenish depleted nutrients.

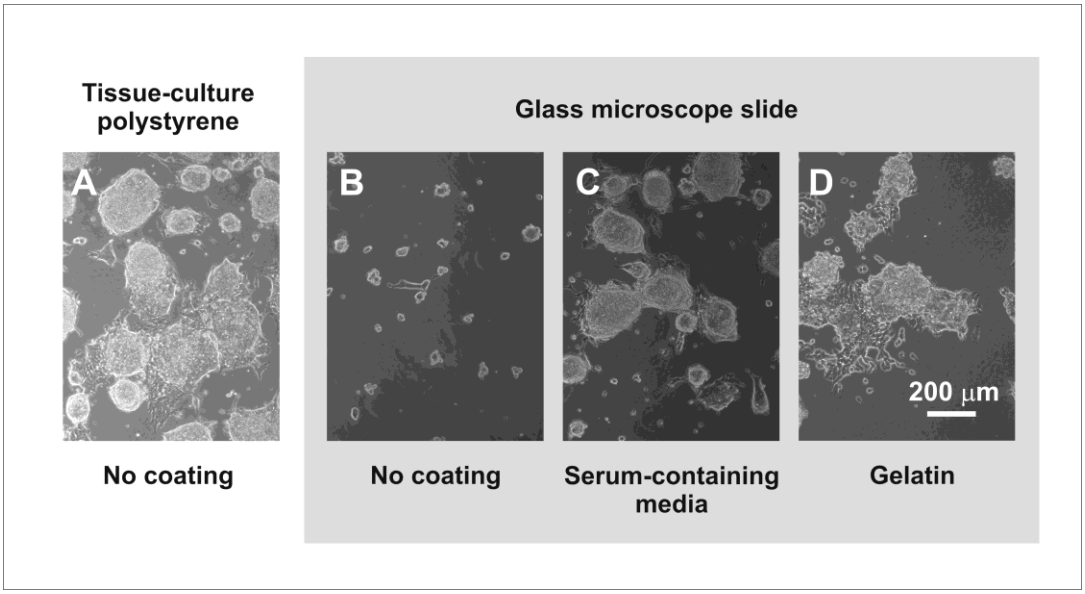

Figure 3.9: Surface modification of cell substrates with cell attachment molecules can be used to improve their biocompatibility. Murine embryonic stem cells exhibit different adhesion and morphology on different substrates. (A)-(C) show ABJ1 mESC colonies on day 3 of static culture. (A) mESC colonies on uncoated tissue culture polystyrene exhibited good attachment with typical round, compact colonies. (B) Although ES cells will initially attach to untreated glass microscope slides, by day 3 of static culture, there are few cells remaining. (C) ES growth on glass slide coated with serum-containing media for 1 hour. (D) A separate plating of ABJ1 murine ES showing growth on a glass slide coated with 0.1% gelatin. Figure taken from Kim *et al.*[86]

To demonstrate the capability of 1×4 logarithmic flow-rate device for culturing more demanding cell lines, I performed 4-day perfusion culture of mESCs in the logarithmic flow-rate device. I applied a total flow rate Q_{total}=65 μL/hr to the entire device, and the flow rates through each chamber were estimated using the particle velocimetry data to be 1.0×10^{-3}, 1.9×10^{-2}, 0.11, 1.1 μL/min. Figure 3.10 shows the results on days 1 and 4 at the four applied flow rates. The faster flow rates produced larger but fewer colonies.

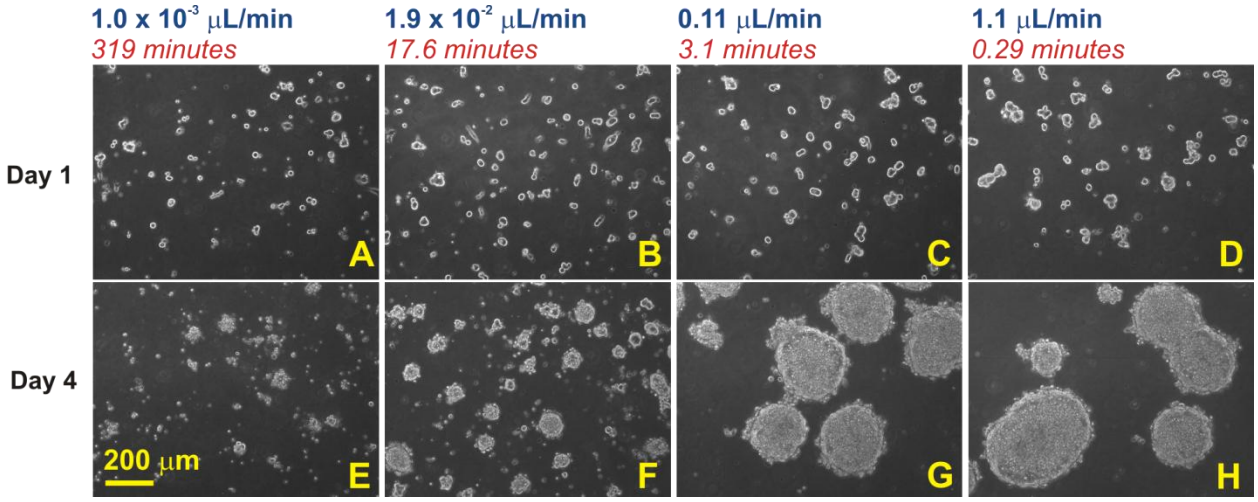

Figure 3.10: Perfusion culture of ABJ1 mouse ESCs over logarithmically scaled flow rates. A-D show cell cultures after one day of perfusion at various rates. E-F show resulting cultures after 4 days of perfusion at various rates. Each column (A/E, B/F, etc.) displays results for a different flow rate. Calculated flow rates for each column are shown above in bold. The average time to replace one culture-chamber volume is shown in italics. By day 4, chambers with high flow rates (G-H) display large, round colonies, suggesting a favorable growth environment, however, the chamber in E with the lowest flow rate has poor proliferation. All photos are at the same scale.

I then repeated this experiment, but applied a total flow rate Q_{total}=650 μL/hr to the entire device, such that the flow rates through each chamber were estimated using the particle velocimetry data to be 1.0×10^{-2}, 1.9×10^{-1}, 1.1, 11 μL/min. Figure 3.10 shows the results on days 1-3 at the four applied flow rates. The faster flow rates produced larger but fewer colonies. I used MATLAB image processing tools to threshold the images (three image fields per flow condition) and segment colonies from both experiments (at 65 and 650 μL/hr). Once colonies were identified and data was collected from all three image fields, the largest colony was discarded, as were colonies that were smaller than 0.1 times the second-largest colony. The mean of the remaining colony areas was found for each flow condition and is shown in Figure 3.11(m), plotted against flow rate and shear stress estimated using the particle velocimetry data and equation (3.4). Colony size varied with flow rate and was greatest at a mid-range of flow rates, between 0.01 and 0.1 μL/hr.

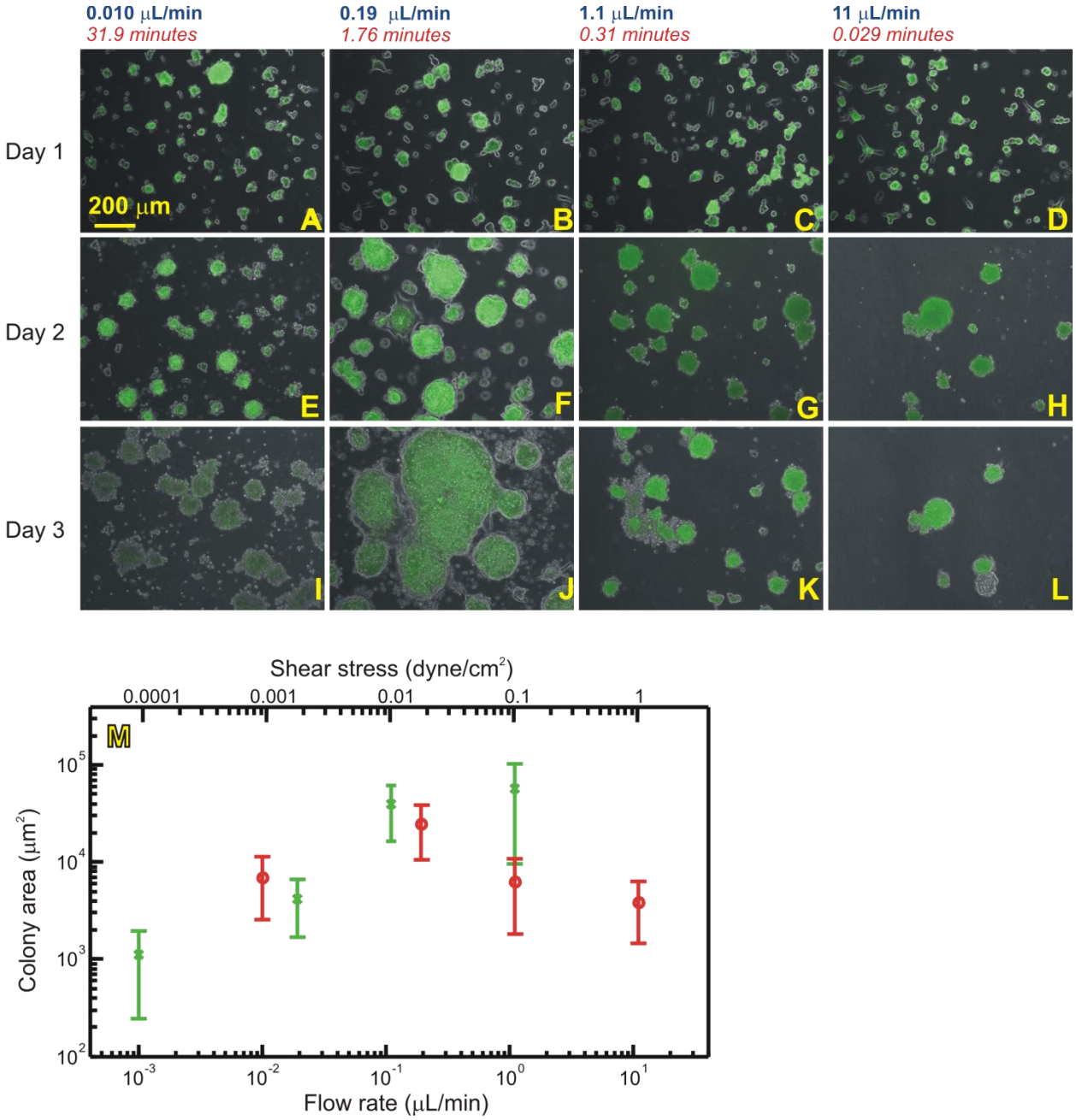

Figure 3.11: Perfusion culture of ABJ1 mouse ESCs over logarithmically scaled flow rates. A-D show cell cultures after one day of perfusion at various rates. E-F show resulting cultures after 2 days of perfusion at various rates. I-L show culture at day 3. Each column (A/E, B/F, etc.) displays results for a different flow rate. Calculated flow rates for each column are shown above in bold. The average time to replace one culture-chamber volume is shown in italics. By day 3, chambers at the mid-range flow rate (J) displays large, round colonies, suggesting a favorable growth environment, however, the chambers with lowest and highest flow rates (I, K, L) exhibit poor proliferation. All photos are at the same scale. M) Mean colony area vs. flow rate and estimated shear stress for ABJ1 mouse ESCs grown under continuous perfusion (merged data from day 4 of Figure 3.10 (green data points) and day 3 of conditions I-L in the current figure (red data points). The mean colony areas are larger at a mid-range flow rates (0.1-1.0 μL/min) while the mean colony area is smaller at the lowest flow rate. Each data point shows the mean value and standard deviation over all colonies from three images at each flow condition.

Additionally, mESC colonies had an unusually round appearance, suggesting a possible spherical shape and significant 3-dimensional growth (in contrast with conventional mESC colony morphology, which is only a few cell layers thick). To assess the 3-dimensional shape of the colonies, I perfused an ABJ1 mESC culture on the 1×4 device using the same procedures, but at a total flow rate of 250 μL/hr. On day 3 I perfused the culture with 2-μm fluorescent beads, occasionally turning the device upside down to help counter effects of bead settling. Once the sample had been well perfused with beads, I measured distances by focusing on beads at different heights and using the automated microscope to record the heights. Using this method I measured the height of typical colonies at three culture-condition flow rates (Figure 3.12). To measure the colony height, I focused on the beads directly above the colonies, then focused on the chamber floor where the majority of beads had settled. The colony height was the difference of these heights. For comparison, I also focused on the highest beads I could find in the chamber that were not overlapping colonies and used these measurements to record "Chamber" heights, although, due to bead settling, it is likely that the measured chamber heights were smaller than the chamber height of ~85 μm measured using the interferometric objective. From the height measurements, I found that the mESC colonies had a 3-dimensional aspect, and were much taller in height than conventional colonies. At the fastest flow rate, the colony heights were almost the same as the previously measured 85 μm chamber height, indicating that the colonies had been growing almost as high as the chamber ceiling, and may have been pillar-shaped. Attempts at nuclear staining using a Hoechst stain and standard 10-minute incubation time agreed with these observations (data not shown). Bright staining around the circumference, but no staining on the interior of the colonies, suggested that the stain had difficulty penetrating to the center of the colony, consistent with a pillar-shaped colony.

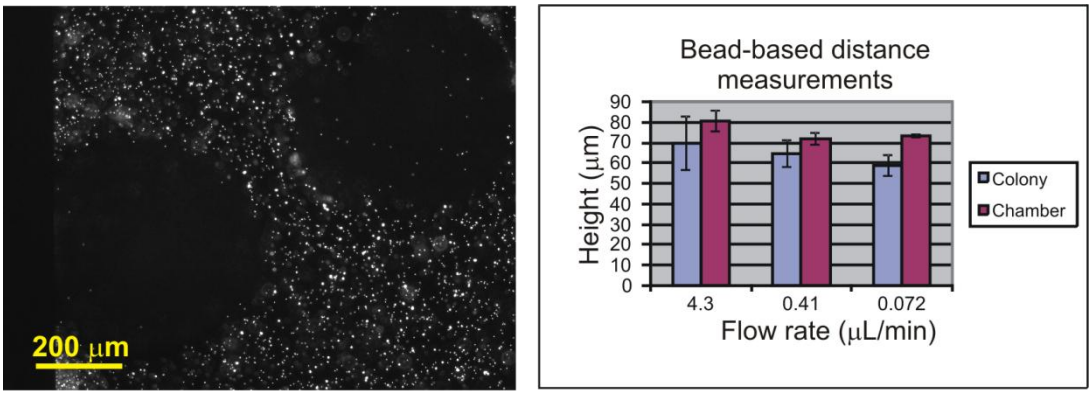

Figure 3.12: (Left) Photograph of fluorescent beads in liquid surrounding two mESC colonies on day 3. Note how few beads overlap the black round areas where the colonies are, suggesting that the colonies have significant 3-dimensional structure that obstructs the flow. (Right) Bead-based measurements of the colony heights, compared with the measured overall chamber height. Error bars represent the standard deviation of three measurements from distinct beads.

3.3.5 Extension to 4×4 array with logarithmic concentration gradient

In addition to characterizing the logarithmic flow-rate device, I was also interested in exploring how logarithmic flow rates could be integrated with other microfluidic functions. To demonstrate, I designed and fabricated a microfluidic device to combine the logarithmic flow-

rate functionality with a logarithmic concentration gradient in a 4×4 array. As shown in Figure 3.2(b), a logarithmic concentration gradient is applied along one axis of the device while logarithmic flow rates are applied along the other axis. Each column of the device is a replica of the 1×4 logarithmic flow-rate device, however, each column receives a different reagent concentration from an on-chip logarithmic diluter. Thus, each cell-culture chamber can experience a unique combination of perfusion and reagent concentration. Like the 1×4 logarithmic device, the 4×4 concentration/flow-rate device operates in "loading mode" and "logarithmic mode" so that cells may be seeded at uniform flow rates across the chip. The diluter design also enables a logarithmic cell density gradient across the device. During loading, it is possible to flow low and high density cell suspensions into the two diluter inputs—these cell suspensions would be mixed in logarithmic ratios, generating a logarithmic cell density gradient across the device. However, a uniform seeding density across the device can also be easily achieved by perfusing the same density cell suspension into both inputs of the diluter. This design allows the user to flexibly and independently choose uniform or logarithmic operation for cell seeding density, reagent concentration, and flow rates.

To implement the logarithmic concentration gradient, I designed an on-chip diluter to produce dilutions of 0:1:10:100. To conserve space on the chip, this diluter uses 9:1 mixes at each junction (instead of 1:1 mixes as are commonly used in linear diluters). A schematic diagram of the diluter is included in Figure 3.6(c), where resistors R_{1d}-R_{10d} comprise the diluter.

I designed the diluter using a similar method to that used for the 1×4 flow-rate device, again using the fluidic resistance calculation for rectangular channels in equation (3.2) with n=2. To conserve space, I incorporated staggered herringbone mixers into the diluter design to promote faster mixing for a given channel length[87] for channels R_{4d} and R_{9d} (Figure 3.6(c)). I followed published design rules and designed the mixer to have a fluid rotation per channel length comparable to published devices[87]. Then using empirical data I estimated the number of mixer cycles necessary for thorough mixing at typical flow rates used in this device.

To combine the logarithmic concentration gradient with the diluter, I attached slightly modified copies (Figure 3.6(b)) of the 1×4 flow-rate device to each of the four diluter outputs. Thus, each created reagent concentration led to four cell-culture chambers that spanned a logarithmic range of flow rates. The difference between the flow-rate block in the 4×4 system (Figure 3.6(b)) compared with the 1×4 device (Figure 3.6(a)) is that the four loading resistances R_L are joined.

I then combined all the loading outputs from each 1×4 flow-rate-block (Figure 3.6(b)) into one joined output off of the chip, connecting them with fluidic resistances $R_{m1\text{-}m4}$. Using a design method similar to that used for the 1×4 flow-rate device, I chose each R_{i1} (where i=1,2,3,4) and $R_{m1\text{-}m4}$ such that the pressure at the node between R_{i1} and R_L would be the same for each block. I similarly joined the logarithmic outputs from each 1×4 flow-rate-block to form a single joint logarithmic output off of the chip. Because this 4×4 design contains 16 culture chambers, having 16 separate loading outputs would have been unwieldy. This joint-loading-output design eliminates the necessity of plugging each output individually, and also eliminates the hardware needed for 16 loading outputs. However, the flexibility of being able to control the individual loading outputs is lost—cells cannot be extracted separately from separate chambers in this design. Finally, merging the loading outputs to a common loading output and the logarithmic

outputs to a common logarithmic output made it topologically necessary to use two layers of interconnected microfluidics.

I assumed that each logarithmic flow rate block would operate identically (but with a different reagent concentration). Because this 4×4 system contained many interconnected cell-culture chambers, I modeled the system as a resistor network in SPICE in both loading and logarithmic modes to ensure that there was no undesired backflow due to communication between chambers. In addition the fluidic resistance of the loading outputs had to be high enough so that in logarithmic mode the proper flow rates were still generated (to prevent the fluid from taking a lower resistance path through the loading output resistor). I estimated the fluidic resistance of individual resistors using equation (3.2) with n=2.

Because this device spanned several centimeters, the PDMS thermal shrinkage was ~500 μm over the length of the device. After curing at 65°C, I cooled both upper and lower PDMS pieces to room temperature and removed the upper layer of PDMS completely off the mold, leaving the lower PDMS layer on the mold wafer. The lower layer remained the same dimensions as the mold, whereas the upper layer shrunk ~1% (linear coefficient of thermal expansion=310 μm/(m-ºC), Dow Corning product information sheet for Sylgard 184). I compensated for this shrinkage by expanding all features in the upper layer by ~1%.

3.3.6 Extension to 4×4 device: Concentration measurements

Since I had already measured the flow rates on the 1×4 flow-rate device, I assumed that flow-rates in the 4×4 device would be similar and instead concentrated on characterizing the operation of the logarithmic diluter. DI water was fed into diluter Input A and a fluorescein solution into diluter Input B (Figure 3.6(c)) and measured the fluorescence intensity for each diluter output. To calibrate the intensities with concentration, we measured the fluorescent intensities of known concentrations of fluorescein. These calibration intensities were used to convert intensities to normalized concentration, shown in Figure 3.7(b). These results demonstrate that we successfully attained logarithmic concentration dilution across the array.

Although measurements of the concentration gradient verified the logarithmic operation of the on-chip diluter, these results differed from the designed normalized concentrations of 0, 0.01, 0.1, and 1. Instead of the designed dilution factor of 10 between columns one and two and between columns two and three, dilution factors of ~18 were measured. These differences are likely due to errors in estimating the fluidic resistances, since the resistances at channel intersections were not taken into account, and the heights of the as-fabricated channel layers were not exactly the same as designed and varied over the device.

3.4 Discussion

These perfusion culture experiments have shown the ability to culture mESCs and 3T3 fibroblasts on chip under a wide range of flow rates for several days, and shown that these conditions have significant effects on mESC colony morphology. I also demonstrated the design, fabrication, and testing of a 4×4 array which simultaneously applies a logarithmic flow rate

gradient and logarithmic concentration gradient. In contrast with previous work on perfused cultures, these devices exploit logarithmic scales to explore a large range of biological conditions simultaneously. These devices also offer new levels of control over the soluble microenvironment as well as the potential for massively parallel experiments combined with automated microscopy; such tools may enable biologists to explore a wider range of more precisely defined conditions during cell culture.

3.4.1 1×4 logarithmic flow-rate device design and characterization

The simplicity of design of the 1×4 logarithmic culture device offers many advantages for perfusion experiments. First, the simple SU-8/PDMS fabrication enables the design layout to be easily tailored for specific experiments—customizing the culture chamber size, flow-rate range, etc. The design itself is also simple, with no on-chip valves, and could easily accommodate other procedures such as staining on chip or culture of ESCs on a layer of feeder cells. Second, because the culture chamber volumes are small—0.32 μL each—the total fluid consumed is minimal. Even a 7-day experiment running at 65 μL/hr would only consume ~11 ml, while a similar experiment in even a 384-well plate would consume ~683 ml (assuming a well volume of 20 μl), never mind that changing the media every ~17 sec (as in Figure 3.10) in such a system would be tedious.

This design is also scalable both in the *range* of applied flow rates as well as the *number* of different flow rates applied. First, this design could easily accommodate a much larger range of flow rates simply by changing the resistor dimensions. This is in contrast to the programmable flow-rate device of Gu *et al*.[45] that generates flow by pumping fluid on-chip using piezoelectric pins on a Braille display. While it can also generate a logarithmic range of flow rates (500×)[45], the dynamic range is limited by hardware issues such as pumping frequency, elastomeric/fluidic mechanical time constants, and pump design—for example, the large pump design reaches a plateau in flow rate as pumping frequency increases[71]. We can also easily scale up the number of flow rates that we apply by increasing the number of chambers in our devices. A 1×*n* device could easily be fabricated by adding more channels to the layout, only limited by space.

The device controls flow rates by setting the fluidic resistance of individual channels in the microfluidic network. One potential challenge is that if any one element of the network changes its resistance (gets clogged with particles), the operation of the entire device will change. This can be minimized by using off-chip filters, by molding inlets to the PDMS device, and by limiting the smallest channel dimension to prevent clogging, as I have demonstrated in experiments. In practice I rarely observed clogging, and I observed no clogging in the experiments presented here. Because we are applying a logarithmic range of flow rates, slight alterations in the individual flow rates due to the presence of cells/colonies in the culture chambers should not have a large effect on the biological outcome when compared with the overall logarithmic flow rate scaling.

3.4.2 4×4 device design and characterization

The 4×4 logarithmic flow rate and concentration gradient device demonstrates the ability to apply a wide variety of conditions simultaneously. While this design shares many aspects of the

1×4 device, there are important differences. Because the loading outputs are joined into a single loading output tube off of the chip, the design is more scalable. Although the 4×4 design is multi-layered and more challenging to fabricate, it offers greater options for controlling experimental conditions. The user can independently choose uniform or logarithmic operation for the initial cell density, flow rates during culture, and reagent concentration during culture. These options allow increased flexibility in experimental design.

Although the 4×4 device design has advantages, there were practical issues related to creating open vias between the layers. Because the SU-8 layers were rarely completely planar, clamping the PDMS and mold during curing often created imperfect vias, reducing device yield. Creating a more planar mold might reduce this problem, but such fabrication difficulties call into question the original design motivation. The original motivation to create a valve-less design was to minimize design and fabrication complexity. To create a 2D valve-less array, interconnected multi-level microfluidics were required, making fabrication complex. Thus, if future devices of this type are pursued, it may be worthwhile to consider alternate designs incorporating valves.

3.4.3 mESC culture across a logarithmic range of flow rates

Our results show a dramatic difference in cell culture when perfused over a wide range of flow rates, especially for mESCs. In the fibroblast culture, qualitative observations of the proliferation implied increasing proliferation with flow rate. This is consistent with previous studies on C2C12 myoblasts in perfusion culture[45]. This is also consistent with previous results that show that perfused cultures grow poorly at lower flow rates[46, 61]. The 3T3 fibroblasts required lower flow rates than the mESCs to maintain a proliferating culture, which is consistent with the static culture requirements of the two cell types since typical 3T3 fibroblasts require feeding once every few days, whereas mESCs require daily feeding.

However, this does not explain why the colony sizes and shapes varied so much in the mESC cultures at different flow rates. At the lowest flow rates, there were many small colonies. At the mid-high range of flow rates, not only were the colony areas larger, but there were fewer colonies. At the highest flow rates, there were few, small colonies. I repeated this experiment several times (data not shown) with similar results. Possible mechanisms behind the flow-rate dependent effects include altered cell attachment, nutrient delivery, waste removal, and concentration of secreted factors. Although shear stress is a possible explanation, it is unlikely. Using equation (1.1) and a velocity estimate based on particle velocimetry measurements described below, I calculated shear stresses corresponding to the mid-range flow rates in Figure 3.11(m) where good proliferation was observed. These shear stresses of 0.01-0.1 dyn/cm^2 are well within the acceptable range for shear stresses discussed in section 1.4.4. Even our highest applied shear stress of ~ 1 dyn/cm^2 was several times lower than the shears used in Fok *et al.*[19], suggesting that shear stress should have minimal effect on the cell cultures

Since shear was probably not the explanation, I looked at other evidence for clues. The data in Figure 3.10 and Figure 3.11 was taken from the culture chamber area of the device only. However, because there was no way to selectively seed cells only in the culture chambers, cells were seeded throughout the upstream delivery channels as well. When these areas were imaged

in a typical experiment, I found that healthy colonies were in fact growing upstream, even in the slowest flow rate condition (data not shown). This evidence supports the idea that larger colony areas at higher flow rates could have been due to increased nutrient delivery, increased waste removal, and increased removal of proliferation-inhibiting secreted factors. Fewer, smaller colonies at the highest flow rates could have been due to attachment problems (perhaps there was flow during the attachment period in lower-resistance paths). Uneven attachment before perfusion was started was observed in at least one case, with the slower flow-rate channel having the best attachment, and the highest flow-rate channel having the worst attachment. It is also possible that cells in the fastest flow-rate condition were dividing but were swept away during mitosis.

Although these experiments did not fully explain why colony sizes varied with flow rate, the mESC results did lend further insight to the results in Chapter 2. For example, the 30 mm × 3 mm × 0.085 mm single chamber perfused at 200 µL/hr corresponds to an average flow velocity of 784 mm/hr. In Figure 3.10, the fastest flow-rate condition corresponds to an average velocity of ~621 mm/hr. Therefore the successful culture from Chapter 2 falls well above the flow rate threshold found here. However, the Chapter 2 device perfused at 50 µL/hr also was above the flow rate threshold for good proliferation and should have resulted in large colonies. Close inspection of the results at 50 µL/hr vs. 200 µL/hr shows that the cells in the 200 µL/hr run were better attached, displaying a more spread-out morphology on day 1, suggesting that initial degree of attachment may have a significant effect on colony proliferation and morphology.

3.5 Chapter Summary

In this chapter I expanded upon the work in Chapter 2. I developed a microfluidic device for culturing adherent cells over a logarithmic range of flow rates and demonstrated an extended version of the device that integrates a logarithmic concentration gradient capability. These devices set the stage for studying the effects of continuous media exchange on the soluble microenvironment. To demonstrate operation of the flow-rate device with cells, I cultured mESCs and 3T3 fibroblasts in continuous perfusion over logarithmically-scaled flow rates and observed qualitative perfusion-dependent differences in proliferation and morphology which agree with experiments from Chapter 2. The flexible design enables easy customization, scalability, and potential integration with other devices so that a wide range of conditions may be tested in one experiment. The microfluidic implementation consumes minimal reagents while enabling culture in non-recirculating perfusion over several days. The dramatic difference seen in mESC culture over a wide range of flow rates in Figure 3.10 provided motivation to further explore this phenomenon and possible mechanisms behind it. These further studies are described in Chapter 4.

Chapter 4. Role of glucose depletion in perfused mESC culture

In section 3.4.3 I noted that colony size depended not only on flow rate, but also on the upstream-vs.-downstream position of a colony within a single flow-rate channel (p. 66). The goal of Chapter 4 was to further explore this by

1) Verifying and quantifying the phenomenon of colony sizes decreasing along the length of the channel at low flow rates, but maintaining a large size throughout the entire channel length at high flow rates.

2) Exploring the mechanism behind this phenomenon by looking at the role of glucose depletion.

To address the first goal, I designed a new 1×6 logarithmic flow-rate device which incorporated several improvements in design over the 1×4 device of Chapter 3. The 1×6 device incorporates longer chambers to enable observation of how colony size varies along the length of the channels, taller chambers to remove any vertical restriction to colony growth, valves to ensure cell seeding only in the culture chambers, and an on-chip active debubbler to reduce the incidence of bubbles. These design choices are explained and summarized in section 4.1.1.

I used the newly designed device to address the first goal and repeatedly observed flow-rate and location-dependent colony area patterns similar to those in Chapter 3. These results are consistent with the literature on general cell culture, mESC culture, and microfluidic perfusion culture. It is well known that cell culture conditions such as cell density, amount of serum in media, and feeding times affect proliferation in cell culture[88]. When culturing C2C12 myoblasts in microfluidic perfusion, Tourovskaia and Folch observed poor proliferation at low flow rates[46], and Takayama observed increased cell numbers at upstream locations when culturing C2C12 myoblasts in recirculating microfluidic systems[45]. Fong *et al.* working with Andre Choo have observed that human ESCs grown in macroscale perfused bioreactors exhibit 70% higher cell numbers than those in static culture[18]. The patterns of flow-rate dependent proliferation observed in this chapter are suggestive of a) proliferation-enhancing molecules being depleted downstream at low flow rates or b) proliferation-inhibiting molecules accumulating downstream at low flow rates. These molecules may be large signaling molecules (such as growth factors), or small molecules, such as glucose (nutrient) or lactate (waste product). Any or all of these possibilities may contribute to the dependence of colony size on flow rate and distance along the axis of flow.

After confirming repeatable flow-rate- and location- dependent proliferation patterns, I investigated whether glucose may be involved in the mechanism behind these patterns. Glucose is a prime candidate because it is the main energy source for mammalian cells and is particularly important for mESCs which undergo rapid cell division [89, 90]. Glucose concentrations affect not only proliferation, but also differentiation of mESCs; culturing mESCs in low-glucose (5mM) conditions causes a delay in differentiation[89]. There is also evidence that mESCs regulate glucose transporter (GLUT) isoform expression during the differentiation process to manage glucose uptake[89]. Kim *et al.* cultured mESCs in various concentrations of glucose and found that cell proliferation increased at high glucose levels, and that high glucose increased levels of cell-cycle regulatory proteins acting in G1-S phase[90].

Experimentally, I explored the role of glucose in three ways: 1) by comparing differences in proliferation in perfused high-glucose media vs. perfused low-glucose media, 2) by modeling glucose consumption and proliferation to assess whether glucose depletion was a likely contributor to the proliferation patterns seen experimentally, and 3) by measuring glucose at the output of a perfused system to detect potential glucose depletion. These studies are described in this chapter.

4.1 Microfluidic device design

4.1.1 Design of the 1×6 logarithmic flow-rate device

The improved logarithmic flow-rate device incorporated a number of improvements that specifically address issues that arose when using the 1×4 logarithmic flow-rate device of Chapter 3. These improvements are summarized in **Table 4.1**. These improvements increased the complexity of the design, both in terms of fabricating the device as well as using it. However, the improvements enabled experiments that could not be carried out in the previous, simpler design.

Table 4.1: Improvements incorporated into 1×6 logarithmic flow-rate device.

Issue	***Solution***
Low culture chamber height (85 μm) restricted 3D growth	Increased culture chamber heights (250 μm)
Short culture chambers (3.2 mm) did not capture location-dependent proliferation	Increase culture chamber lengths (30 mm)
4 flow rates (limited resolution in flow rate)	6 flow rates (improved resolution in flow rate)
Poor colony morphology	Reintroduced polystyrene cell-culture substrate
Cells seeded upstream of culture chambers prevented precise control over media content at culture chamber input	Valves restricted cell seeding to culture chambers
Low experimental success rate due to air bubbles	On-chip active debubbler

Changes to the number and geometry of culture chambers

In my initial observations of location-dependent proliferation in the 1×4 device, I noticed that at the lowest applied flow rate, colonies downstream inside the culture chamber were small, whereas colonies upstream of the culture chamber, yet still within the low-flow-rate delivery channel were large. However, because the delivery channels and culture chambers had different cross-sections, even though they experienced the same flow rate, they experienced different velocities. To investigate depletion/accumulation of proliferation enhancing/inhibiting factors in

a more controlled manner where all cells at a single flow-rate condition experienced the same fluidic velocity, I lengthened the culture channels from 3.2 mm to 30 mm. To reduce concerns about the culture chamber ceiling height restricting the colony growth, I increased the height of the culture chambers to 250 μm. Finally, to improve the resolution of the measurement in flow, I increased the number of chambers to 6.

Change to the cell culture substrate
To improve attachment and colony morphology, I returned to using a tissue-culture polystyrene substrate (as in Chapter 2) instead of glass (as in Chapter 3), which greatly improved colony morphology. However, since PDMS cannot bond to polystyrene, this necessitated use of an adjustable clamp to hold the device to the substrate. This added complexity to the device fabrication as well as device use, but the advantages gained from having a superior cell-culture substrate were important enough to outweigh these drawbacks.

Changes incorporating valve technology
To selectively seed cells only in the culture chamber areas but not upstream, I incorporated a system of pneumatically actuated PDMS valves. To increase the flow rate resolution, I increased the number of channels from 4 to 6. Finally, to reduce the chance of failure due to bubbles, I incorporated an on-chip active debubbler developed by Alison Skelley in our lab.

Although the experimental setup in Chapter 3 included both a large and small bubble trap, bubbles still reached the device, causing a high percentage of failures. The ability to seed cells only in the culture chambers, with no upstream cells, is particularly important when investigating how cells may deplete or condition media, since it establishes a clean upstream boundary condition. These benefits outweighed the additional fabrication complexity of the 1×6 design. The Smooth-Cast molds enabled parallel fabrication of many devices at once, also reducing concerns about fabrication complexity.

Principle of operation
As with the 1×4 device, the 1×6 device operates in "loading mode" and "logarithmic mode". The flow-rate-setting resistors were designed in the same manner as in Chapter 3 for the 1×4 device, however here I chose the flow rates to vary by a factor of 4× from one chamber to the next while in logarithmic mode, for a total range spanning 1024×. Figure 4.1 shows the device design and operation in loading and logarithmic modes. The gray channels illustrate the 250 μm-high fluidic network which is joined to the 100 μm-high fluidic network in red that represents the flow-rate-setting resistors. The purple and orange channels are separate pneumatic networks for valve actuation. In loading mode, the purple, logarithmic-mode pneumatic lines are pressurized and vacuum is applied to the orange, loading-mode pneumatic lines, forming the fluidic network shown in green in Figure 4.1(b). This configuration enables a cell suspension to be loaded simultaneously and specifically throughout the culture chamber areas only. During cell attachment, neither vacuum nor pressure is applied to any of the pneumatic lines, leaving all valves normally closed to discourage fluid movement in the device.

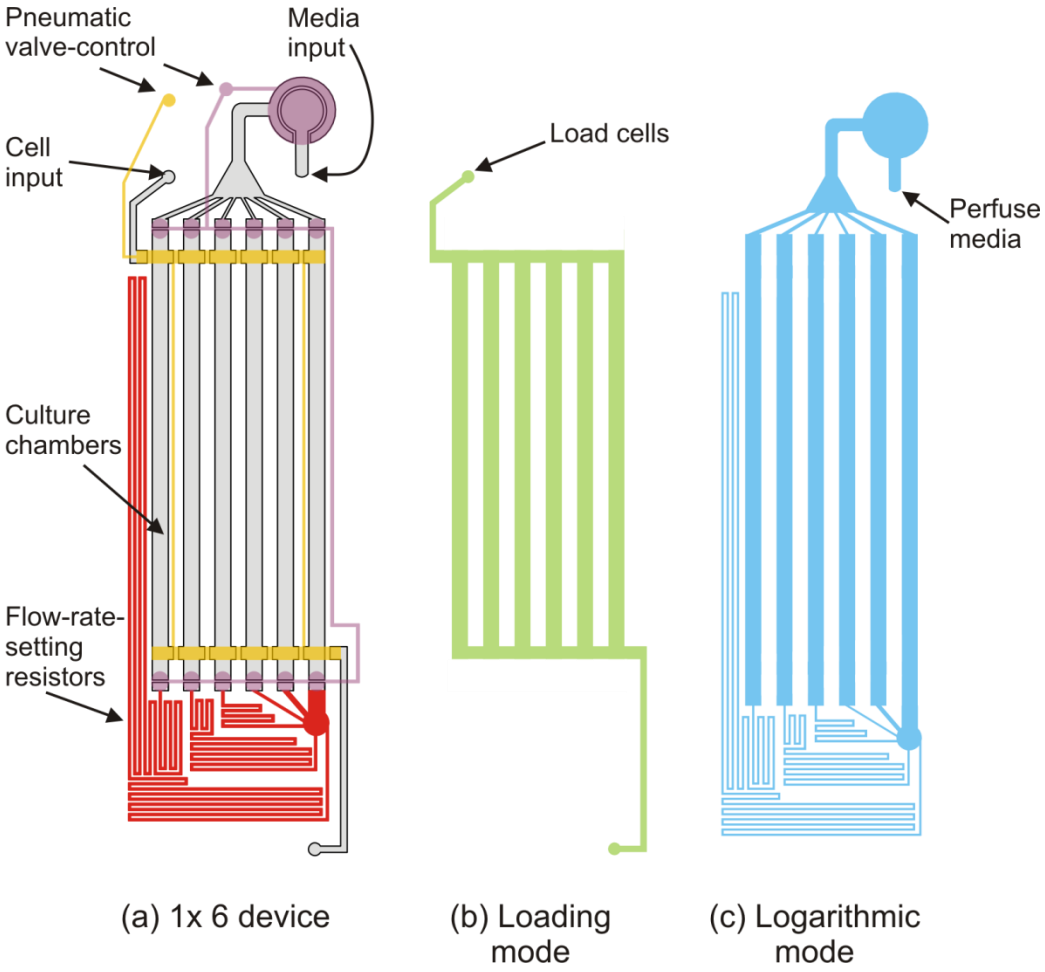

Figure 4.1: Design and operation of 1×6 valved logarithmic flow-rate device. (a) To-scale diagram of device design. (b) Loading mode. The green network shows the resulting fluidic network during cell loading. The green network results when the purple, logarithmic-mode valves are closed and the orange, loading-mode valves are opened by the application of vacuum. This enabled seeding of the culture chamber areas only, while preventing cells from seeding in upstream or downstream locations. (c) Logarithmic mode. The blue network shows the resulting fluidic network during perfusion culture. Here, the blue network results when vacuum is applied to the orange, loading-mode pneumatic line.

Figure 4.2 shows the principle of operation for the valves and debubbler. The valves incorporated in this device were based on designs developed and optimized by Alison Skelley in our lab (personal communication). The basic valve, shown in Figure 4.2(a) consists of a PDMS valve seal (a discontinuity in the fluidic channel) above which lies a pneumatic displacement chamber. In the relaxed state, when no pressure or vacuum is applied to the pneumatic chamber, the valve seal blocks off the fluidic channel, and the valve is normally closed. When vacuum is applied to the pneumatic channel, the valve seal lifts off of the polystyrene substrate, opening the valve. This type of normally closed valve is similar to the valve used by Irimia *et al.*[91], except that in this design, the PDMS device is clamped, not bonded to the substrate. The clamping pressure is crucial to successful operation of the device – too loose and the fluidic channels leak, too tight and the valves do not open. I based the valve geometries here on designs optimized by Alison Skelley (personal communication). Since the device was operated in logarithmic mode

for the majority of the time, I wanted to ensure that the loading-mode valves would stay closed during perfusion, even when no pressure was applied. Accordingly, I designed the logarithmic-mode valve seal to have 200-μm-thick walls whereas the valve seals for the loading-mode valves had 400-μm-thick walls. This difference in geometry made it more difficult to open the loading-mode valves than the logarithmic-mode valves.

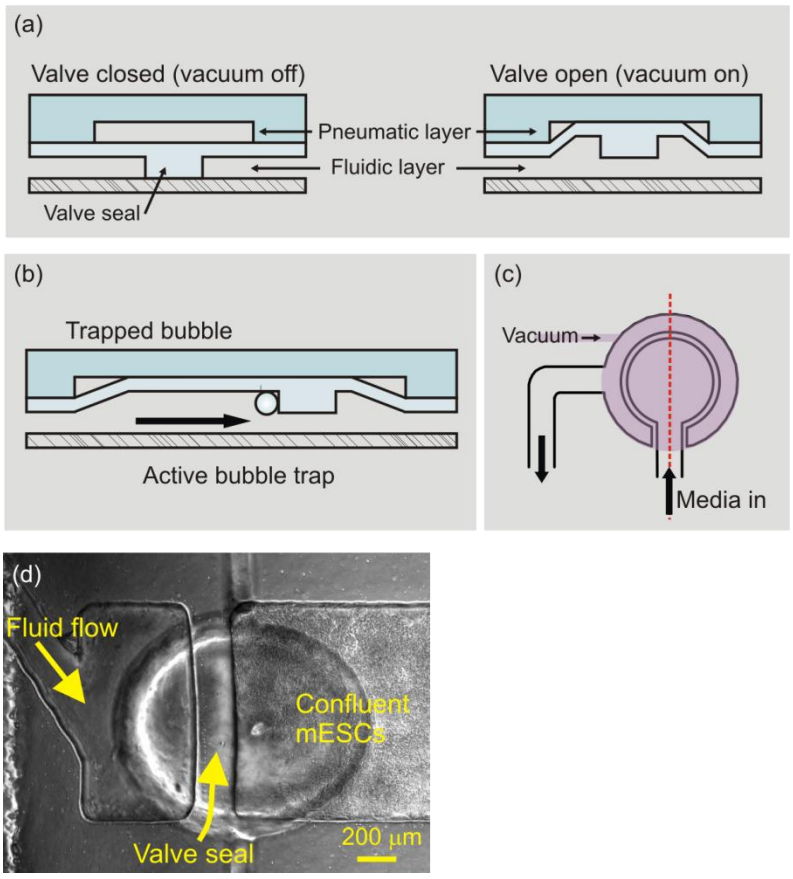

Figure 4.2: Operation of valves and active debubbler. (a) Left: Normally closed valve with no vacuum in the pneumatic channel. Right: When vacuum is applied to the pneumatic channel, the flexible PDMS valve lifts up, opening the valve and allow fluid to pass. (b) Active debubbler in operation is a widened valve. Cross-section in (b) corresponds to red dotted line in (c), which shows the overhead view of a typical debubbler. In (c), the purple area represents the pneumatic channels where vacuum is applied to keep the valve open and to shrink trapped bubbles. Finally, (d) shows a close-up of day 3 cell culture around a logarithmic-mode valve (closed during cell loading, open during perfusion culture). This valve is located at the input of the culture channel, and demonstrates the effectiveness of the valves in preventing cell seeding upstream of the valve. The blurred oval shape is the pneumatic channel above the valve.

The active debubbler, also designed by Alison Skelley and shown in Figure 4.2(b)-(c) is essentially a large valve. During perfusion culture, vacuum is constantly applied to the debubbler (part of the logarithmic-mode, pneumatic-channel network), keeping the valve open. In the open position, bubbles rise to the ceiling as they traverse the debubbler and are trapped by the edge of the valve seal. The applied vacuum then actively shrinks trapped bubbles by pulling air through the gas-permeable PDMS layer. In fact, all the valves function as debubblers, albeit smaller ones.

Therefore if a bubble manages to get past the initial large debubbler during perfusion, there is a second line of defense immediately downstream in the form of the logarithmic-mode valves, which remain open during the course of perfusion.

4.1.2 Measuring glucose concentration: 1×3 single-flow-rate device

For the experiments measuring glucose concentration, I needed a device able to culture a quantity of mESCs at a single flow rate such that it would be feasible to measure the glucose concentration at the device output, even at low flow rates. For this purpose I designed a device with three culture chambers of the same dimensions as those in the 1×6 device. These three chambers were joined together using equal fluidic resistances, so that they all experienced the same flow rate. Initially I designed this device using a single-layer microfluidic network, as was used for the 1×4 device in Chapter 3. However, because of problems with bubbles, I modified the device design to incorporate and upstream debubbler identical to that in the 1×6 device. To fabricate this redesigned device, I used the same fabrication process described in section 4.2.3. (d) shows a photograph of the 3-chamber device in the original, single-layer design.

4.2 Experimental

4.2.1 Cell culture

D3 mESCs were used for the experiments in this chapter, and were cultured using the same protocols described in Chapter 3 For glucose experiments, the low-glucose media formulation was the same as the ES media from Chapter 2, but with DMEM replaced with low- or high-glucose DMEM. The high-glucose ES media formulation here is essentially the same as the one from Chapters 2-3, but with a different brand of DMEM.

Low-glucose ES media: Low-glucose DMEM with 1000 mg/L glucose (D5921, Sigma, St. Louis, MO) supplemented with 15% ES-qualified fetal bovine serum (16141079, Invitrogen, Carlsbad, CA), 4 mM L-glutamine (25030081, Invitrogen, Carlsbad, CA), 1 mM non-essential amino acids, 50 U/mL penicillin, 50 μg/mL streptomycin (15140122, Invitrogen, Carlsbad, CA), 100 μM β-mercaptoethanol (M7522, Sigma,St. Louis, MO), and 500 pM leukemia inhibitory factor (LIF, ESGRO, Chemicon, Temecula, CA).

High-glucose ES media: High-glucose DMEM with 4500 mg/L glucose (D1145, Sigma, St. Louis, MO). supplemented with 15% ES-qualified fetal bovine serum (16141079, Invitrogen, Carlsbad, CA), 4 mM L-glutamine (25030081, Invitrogen, Carlsbad, CA), 1 mM non-essential amino acids, 50 U/mL penicillin, 50 μg/mL streptomycin (15140122, Invitrogen, Carlsbad, CA), 100 μM β-mercaptoethanol (M7522, Sigma,St. Louis, MO), and 500 pM leukemia inhibitory factor (LIF, ESGRO, Chemicon, Temecula, CA). (This media is essentially the same as the standard ES Media in Chapter 2, the only difference being a different brand of DMEM.)

4.2.2 Microfluidic fabrication and device packaging

Two new devices were developed in this chapter: a 6-channel, valved logarithmic flow-rate device, and a 3-channel single-flow-rate device. Although the devices had different designs, both

devices incorporated pneumatically actuated PDMS valves and were fabricated using the same process.

4.2.3 Fabrication of pneumatically actuated valved devices

The 1×6 logarithmic flow-rate device consists of a single, interconnected, multi-height fluidic network of channels molded in PDMS (Sylgard 184, Dow Corning, Midland, MI) and a single, multi-height pneumatic network also molded in PDMS as shown in Figure 4.3. The fluidic and pneumatic channels do not join and are separated from each other by a thin, 250-μm layer of PDMS. The reason the fluidic network contained two-level channels is that the Viper Hi-Res process used to make the molds requires minimum wall thickness of ~100 μm. Since the culture chamber height was increased to 250 μm, in order to achieve a wide range of flow rates in the logarithmic scaling, some of the fluidic resistance output channels were 100-μm high in order to reach the necessary fluidic resistances while maintaining a channel width of 100 μm. The reason the pneumatic network contained two different channel heights was that there were concerns about the pneumatic communication channels collapsing in test devices under too high clamping pressures. Thus, although the height of the pneumatic actuation chamber was fixed to maintain characterized valve geometries, the pneumatic connections running between valves were increased in height prevent them from collapse under high clamping pressures.

Fabricating the pneumatic-layer and fluidic-layer PDMS molds
As in the 4×4 flow-rate device from Chapter Chapter 3, the 1×6 logarithmic flow-rate device also consisted of two bonded layers of PDMS, the pneumatic and fluidic PDMS layers, shown in Figure 4.3. The fluidic PDMS layer contained the fluidic network, which was composed of a 250-μm-high culture-channel layer joined to a 100-μm-high flow-rate-setting layer. A 250-μm PDMS membrane (part of the fluidic PDMS layer) separated the fluidic layer from the pneumatic PDMS layer, which consisted of 250-μm-high pneumatic channels connecting 150-μm-high pneumatically actuated displacement chambers.

Instead of using SU-8 molds to fabricate the PDMS slabs (as in Chapters 2-3), I used plastic molds fabricated using stereolithography prototyping. I designed the device layout in AutoCAD (Autodesk, San Rafael, CA) and submitted an extruded design to Fineline Prototyping (Raleigh, NC), where the molds were generated using a stereolithography rapid-prototyping process (Viper Hi-Res). The molds were composed of Prototherm 12120 plastic material. To prevent sticking of PDMS to the molds, I coated the molds with a silane ((Tridecafluor-1,1,2,2-Tetrahydrooctyl)-1-Trichlorosilane, #T2492, United Chemical Technologies, Horsham, PA) for 1 hour in a vacuum chamber. This coating initially produced a slightly milky appearance on the surface of the PDMS, which I cleaned off by curing PDMS on the surface of the mold (and then discarding the PDMS) a few times.

To enable parallel fabrication of several devices at once, I made copies of the Prototherm molds using a technique developed by Salil Desai in our lab (personal communication). This method uses Smooth-Cast plastics (Smooth-On, Inc., Easton, PA) to create new plastic molds from existing PDMS microfluidics that reproduce the microfluidic features. The fabrication process for making the Smooth-Cast molds is shown in Figure 4.4. The fabrication processes for the pneumatic-layer and fluidic-layer PDMS molds were slightly different, because of differences in

their final application of patterning PDMS. The pneumatic-layer PDMS mold is poured to the desired thickness (~6-7 mm), but achieving an exact thickness is not critical (Figure 4.3(b)). However, the fluidic-layer PDMS mold must have standoffs of an exact thickness (500 μm) such that when the fluidic-layer PDMS slab is fabricated in Figure 4.3(e), a 500-μm-thick PDMS layer is formed.

To create PDMS molds, I mixed PDMS in a 10:1 ratio by mass, base to curing agent, degassed it in vacuum for 30 minutes, poured it onto the silanized Prototherm molds, and cured at 65 °C for 2 hours (Figure 4.4(b),(g)). In the case of the pneumatic-layer PDMS mold, it was important to pour a thickness of PDMS that was the same or greater than that desired for the final PDMS layer (in this case, > 6 mm. Next I used the cured PDMS molds to pattern Smooth-Cast plastic. I agitated Smooth-Cast 310 White Plastic Part A and Part B each for 1 minute, then poured ~30 mL each of Part A and Part B into separate cups and degassed them in a vacuum chamber for 30 minutes. Meanwhile I cleaned the cured PDMS molds using adhesive tape and degassed them in a vacuum chamber for 30 minutes. After degassing, I combined Smooth-Cast 310 Part A and Part B together in a 1:1 ratio by volume, stirring until well-mixed, but not introducing new bubbles. I then poured the mixed Smooth-Cast 310 into the respective PDMS molds, as shown in (Figure 4.4 (d),(i)) removing any bubbles using a metal wire, and left the molds to cure at room temperature for >6 hours. For the fluidic-layer PDMS mold, I placed a silicone sheet (HT-6240, Rogers Corp., Carol Stream, IL) and pre-fixed plastic backing on top of the liquid Smooth-Cast, then placed a heavy, flat aluminum plate on the silicone/plastic sheets to ensure that the fluidic-layer mold would have a flat base and the same thickness as the original Prototherm mold. Finally, I removed the cured Smooth-Cast molds, which were ready to use without silanization (Figure 4.4 (e),(j)).

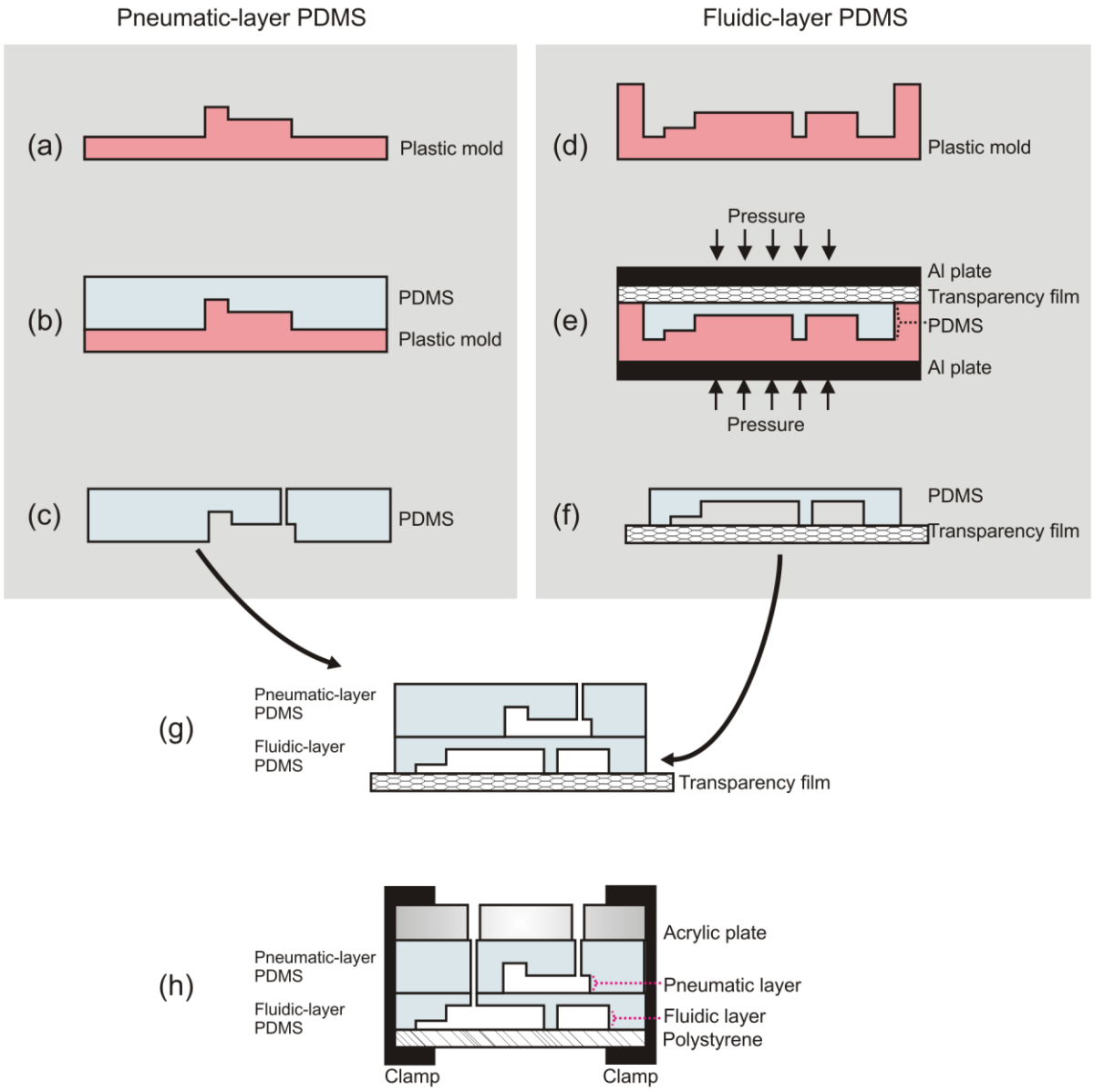

Figure 4.3: Fabrication process for the 1×6 logarithmic perfusion device and the 1×3 single-flow-rate device. (a),(d) show the starting plastic molds (either Prototherm or Smooth-Cast). Liquid PDMS is mixed and poured onto the molds in (b) and (e), with a transparency film and clamps applied in (e) to ensure a resulting PDMS layer with a defined thickness (500 µm). After curing, PDMS is removed from molds and cleaned (c),(f), and access holes to the pneumatic channels are punched (c). The two PDMS layers are plasma bonded in (g) and are heated overnight to strengthen the bond before access holes to the fluidic layer are punched. The PDMS device is autoclaved before attaching it to a sterile polystyrene base and clamping the PDMS and polystyrene together using a laser-cute acrylic plate and aluminum clamping setup, shown in (h).

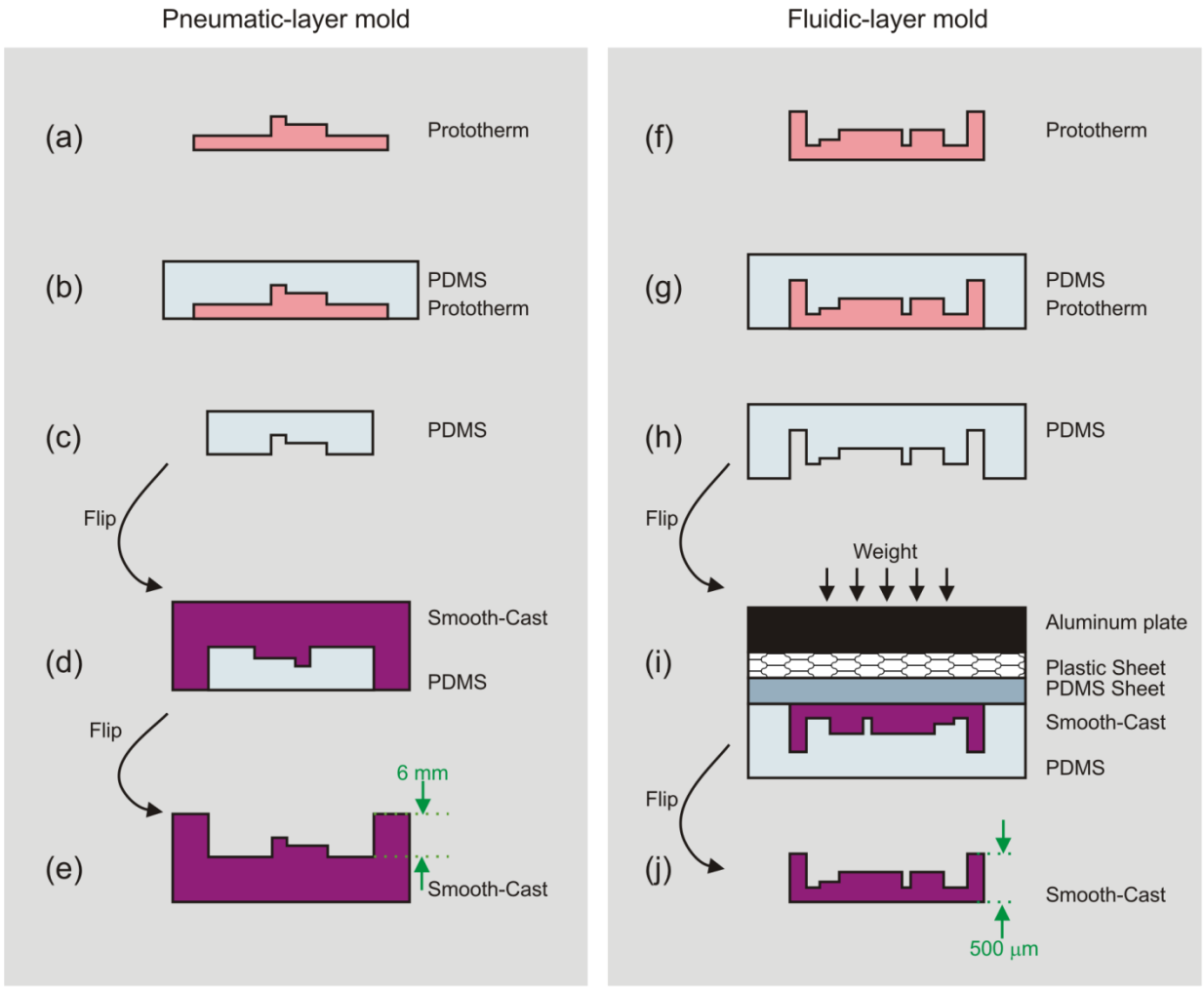

`

Figure 4.4: Fabrication process for making Smooth-Cast molds from Prototherm molds. (a)-(e) show the process for making the pneumatic-layer mold, while (f)-(j) show the process for making the fluidic-layer mold. (a) and (f) show the initial Prototherm mold. In (b) and (g), a thick (> 6 mm) layer of PDMS is patterned onto the Prototherm mold. In (c) and (h), the PDMS is removed from the Prototherm, and in the case of (c), the PDMS piece is cut out to have a slightly larger footprint than that of the finished device. In (d) the Smooth-Cast plastic is molded using the PDMS as a master. The same is true of (i), however, because the fluidic PDMS layer is fabricated using clamping (see Figure 4.3(e)), the Smooth-Cast master must be an exact copy of the original Prototherm master, with a flat base and no extraneously tall structures that prevent clamping in Figure 4.3(e). Finally, (e) and (j) depict the resulting Smooth-Cast plastic masters.

Molding the PDMS and assembling the device

The process for molding and assembling the device is similar to the fabrication process for the 4×4 device described in Chapter 3. To fabricate the fluidic PDMS layer, I mixed PDMS in a ratio (by mass) of 10:1, base to curing agent, degassed it in vacuum for 30 minutes, and poured a small volume (<5 mL) onto the fluidic-layer plastic mold and degassed it for 10 minutes. Next I placed a sheet of transparency film onto the liquid PDMS, taking care not to introduce bubbles. I placed the mold between two 1-cm-thick aluminum plates and screwed the plates together finger-tight to ensure that the transparency film would contact the 500-μm standoffs incorporated

into the mold design, thus forming a 500-μm-thick fluidic PDMS layer (Figure 4.3(e)). I placed the entire sandwich, including aluminum plates, into a 60°C oven for 4 hours to cure the PDMS. After curing, I removed the fluidic PDMS layer from the mold, placing it on a clean piece of transparency film (Figure 4.3(f)).

Meanwhile I fabricated the pneumatic PDMS layer. I poured PDMS onto the pneumatic-layer plastic mold to a thickness of ~6 mm and cured the PDMS in an oven at 65° C for 2 hours, shown in Figure 4.3(b). I then peeled the cured PDMS off of the mold, cut apart individual devices, and punched access ports to the pneumatic channels using thin-walled tubing (HTX-15X, Small Parts, Inc., Miami Lakes, FL), shown in Figure 4.3(c). To plasma bond the two PDMS layers, I exposed the fluidic and pneumatic PDMS layers to air plasma for one minute, then aligned by hand and bonded the two PDMS layers, shown in Figure 4.3(g). I placed the entire device in a 65°C oven overnight to improve bond strength. The next day I punched access holes to the fluidic channels and autoclaved the bonded PDMS layers to sterilize them. After waiting for the PDMS to dry (or actively drying it in a 65°C oven) to remove any water vapor introduced during autoclaving, the complete device was then assembled in a sterile biosafety cabinet immediately before use. Because the mESC colonies grown on glass in Chapter 3 did not seem to attach as well as colonies from Chapter 2 that were grown on polystyrene, for the 1×6 device I returned to using tissue-culture polystyrene to form the base of the device (Polystyrene Slide #260225, Ted Pella, Inc., Redding, CA). Because polystyrene cannot be plasma-bonded to PDMS, and because the valves in the device required an adjustable method for applying pressure to the device, I used an existing custom microscope stage (designed by Alison Skelley) to clamp the PDMS device to the polystyrene base, as shown Figure 4.5(c) and Figure 4.3(h). A schematic showing the layers of the completed device is shown in Figure 4.3(h).

4.2.4 Optics

As in Chapters 2 and 3 I used an inverted microscope (Zeiss Axiovert 200, Thornwood, NY) with a SPOT RT Color 2.2.1 camera (Diagnostic Instruments, Sterling Heights, MI). Here the inverted microscope was also updated with an automated stage (Ludl MAC 5000, Hawthorne, NY) and Metamorph imaging software (Molecular Devices, Downingtown, PA). Metamorph was used to acquire the raw images, which were later processed using Matlab (Mathworks, Natick, MA).

4.2.5 Characterization of logarithmically scaled flow rates

As in Chapter 3, I verified the flow rates of the 1×6 logarithmic flow-rate device using a simplified version of particle velocimetry. First I set up the device in logarithmic (Perfusion) mode, similar to the setup shown in Figure 4.5(b). However, I set up the device on the inverted microscope stage (not in an incubator), and I also did not include a syringe filter, since this would have prevented beads from reaching the device. To remove air bubbles in the device, I connected the vacuum line to the perfusion mode valves and filled the chip with deionized (DI) water using a syringe for ~30 minutes. The active vacuum applied removed air bubbles from the device. To facilitate applying vacuum and pressure to the pneumatic channels, I used a custom pneumatic switch box with lab vacuum and pressure lines connected to a pneumatic manifold with solenoid valves (#S070B5FGM3, SMC Corp., Indianapolis, IN), leading out to individually controllable vacuum and pressure lines.

I suspended 2-μm-diameter polystyrene beads (19508, Polysciences, Warrington, PA) in DI water with 0.1% Triton X-100 (Sigma, St. Louis, MO) at a concentration such that the areal density at one focal plane was a few hundred particles per 10× field. I loaded this suspension into a 5 mL plastic syringe (Becton Dickinson, Reno, NV) that was mounted into a syringe pump (KD Scientific 200, Holliston, MA). Taking care not to introduce new bubbles, I connected the syringe to the device to inject the bead suspension.

As in Chapter 3, I measured the bead velocities one chamber at a time, starting with the slowest chamber. For each chamber, after setting the syringe pump rate, I allowed the system to reach equilibrium for ~5-10 minutes before taking measurements. Then I focused the microscope halfway through the depth of the chamber and took a snapshot of the bead suspension, choosing an appropriate exposure time such that the paths of the beads were recorded as finite streaks. I repeated this at three locations along the length of the culture chamber. After taking measurements for each chamber, I inverted the device for a few minutes to minimize bead settling. Because of the wide range of flow rates across the device, I used different total-chip flow rates (Q_{total} from Chapter 3) for each chamber. This scaling ensured that the bead velocities remained within a practically measureable range. I set the total perfusion rates to 1 mL/hr, 1 mL/hr, 6 mL/hr, 9 mL/hr, 12 mL/hr, and 15 mL/hr, with respective exposure times of 50 msec, 200 msec, 200 msec, 150 msec, 300 msec, and 2000 msec (fastest to slowest chamber). I used image processing software ImageJ (National Institutes of Health, http://rsb.info.nih.gov/ij/) to measure the lengths of the 6 longest bead paths in each snapshot. I assumed that the longest bead paths in the snapshots corresponded to the centerline, highest fluid velocity. Using this assumption, as well as the exposure time and total flow rate, I calculated the volumetric flow rate and mean velocity for each chamber.

4.2.6 Perfusion culture protocols for 1×6 logarithmic device

On the day before loading cells, I set up and prepared the 1×6 logarithmic device by first assembling the entire fluidic system as shown in Figure 4.5(a), but with only the media syringe connected and the 4-way valve in the "plugged" setting. To prevent contamination I assembled the device inside a sterile biosafety hood, applied vacuum to all pneumatic channels to open all valves on chip, and then filled the system with the appropriate ES media (either low or high glucose). To remove air bubbles in the device, I connected vacuum to the perfusion mode valves and placed the device in the cell-culture incubator, letting the vacuum remove air bubbles overnight.

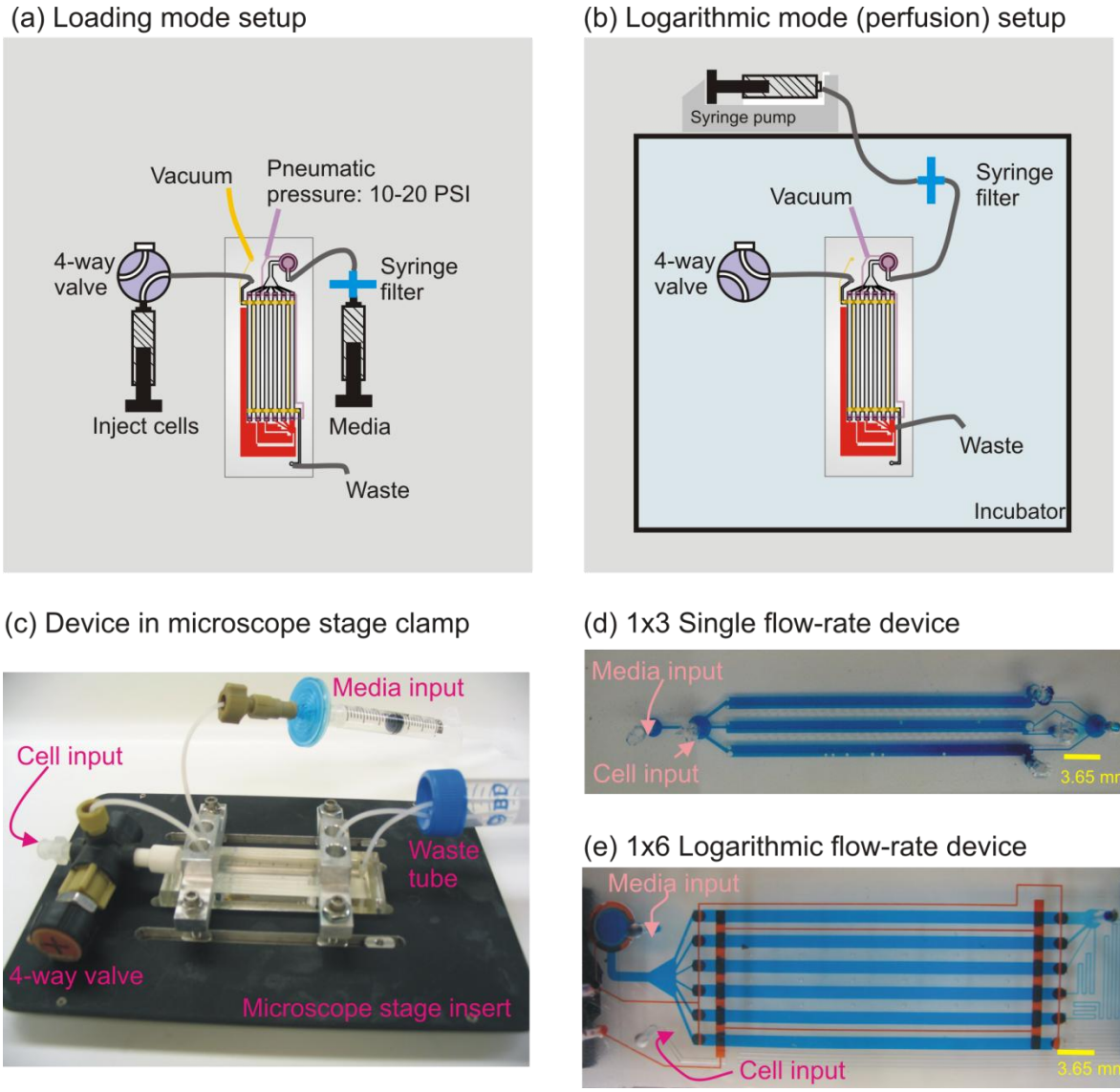

Figure 4.5: Experimental setup for perfusion culture in the 1×6 logarithmic flow-rate device and photographs of fabricated 1×3 and 1×6 devices. (a) In loading mode setup, vacuum is applied to the loading mode valves (orange) and pressure is applied to the logarithmic mode valves (purple) to allow all chambers to fill at the same rate, while preventing cells from seeding upstream of the culture chambers. (b) In logarithmic mode, vacuum is applied only to the logarithmic mode (purple) pneumatic newtork, activating the debubbler and setting up a logarithmic range of flow rates across the device. (c) Photograph of the experimental setup for a 1×6 device, showing the device clamped into an aluminum microscope stage insert using two adjustable aluminum clamps. (d) Photograph of original implementation of 1×3 device (without upstream debubbler) filled with dye to illustrate the three parallel channels with equal size fluidic resistance outputs, generating equal flow rates in all three channels when a current source is applied to the input. (e) Photograph of 1×6 device with blue dye illustrating the logarithmic mode fluidic path, and red dye showing both the loading-mode and logarithmic-mode pneumatic networks.

The next day (designated day 0) I loaded the cells into the microfluidic device. I made a cells-in-media suspension by trypsinizing cells with TrypLE Express (12605-010, Invitrogen, Carlsbad, CA), quenching the trypsin with serum-containing media, then counting cells on a Z2 Coulter

Counter (Beckman Coulter, Fullerton, CA). To make the appropriate concentrations I centrifuged the initial cell suspension for 5 minutes at 1000 rpm, aspirated the supernatant, resuspended the cells in either high- or low-glucose ES media (depending on experimental trial), and triturated to produce a single cell suspension at a density of 3 x 10^6 cells/mL. All cells used were passage 25 or lower. After placing the fluidics and device in a sterile biosafety hood, I connected a syringe filled with the cell suspension to the device as shown in Figure 4.5(b). To avoid bubbles while making this connection, I first opened all valves and used the media syringe to backflow media out of the opening in the 4-way valve where I would be attaching the cell-suspension-filled syringe. I then used droplet merging to attach the syringe to the 4-way valve[76]. Once the syringe was attached, I applied vacuum and pressure to the pneumatic networks as shown in Figure 4.5(a) to ensure that cells would not enter the upstream fluidics and would only be loaded into the culture chambers. Although the valves are in a normally closed position even when no pressure is applied, I applied pneumatic pressure during loading to prevent the valve seals from lifting up if too much pressure was applied by the manually operated cell-injection syringe. Applying pressures > ~2 PSI runs the risk of bubble generation if the PDMS membrane between fluidic and pneumatic channels is thin, therefore I limited the application of pressure to a few minutes (only during loading).

To monitor loading I placed the device on a phase microscope (Zeiss Axiovert 200M) and injected the cell suspension by hand. Cells begin settling quickly in suspension, within a couple minutes, so it is important to load the cells as quickly as possible to maintain the desired cell density. When sufficient cells were loaded into each chamber, I removed all pressure and vacuum lines and photographed samples across the device (10 images per flow channel, sampled every 3 mm). To avoid sampling cell areas that were exposed to flow entrance effects, I only sampled areas that were more than one channel width (1.25 mm) downstream of the beginning of the culture channel (same was true at the channel outlet). I allowed the cells to attach for 4 hours in static culture (no perfusion) by placing the setup in the humidified incubator at 37°C and 7.5% CO_2, with all pneumatic networks disconnected (all valves normally closed). After cell attachment I re-connected the setup to the syringe outside of the incubator and connected the logarithmic mode pneumatic networks to vacuum. I set the syringe pump outside of the incubator to a fixed flow rate of 0.2 mL/hr and continued perfusing to day 3. Each day I removed the setup from the incubator to take images at the microscope, interrupting perfusion for a brief time (<20 min). After imaging I replaced the setup inside the incubator and resumed perfusion.

Using cells from the same cell suspension, I plated a static control culture in three wells of a 6-well plate, maintaining the same areal density as on the device. I repeated this experiment three times for both the high- and low-glucose media conditions.

4.2.7 Glucose measurements and mESC perfusion culture: protocols

To measure glucose concentration at the output of mESC perfusion culture, I cultured D3 mESCs in a 1×3 single-flow-rate device with three parallel identical chambers (shown in Figure 4.5(d)). The goal was to compare the input vs. output glucose concentration for three experimental conditions: 1) high flow-rate cell culture 2) low flow-rate cell culture and 3) low-flow rate through a blank chip with no cells. From the modeling results, I chose a high flow rate of 0.153 mL/hr (equivalent to mean velocity of ~136 μm/sec) and a low flow rate of 8 μL/hr

(equivalent to a mean velocity of ~7.5 μm/sec). All experiments were performed using high-glucose ES media. I fabricated, assembled and prepared the 1×3 devices using the same methods as in section 4.2.6, filling the chambers with high-glucose ES media and incubating overnight to eliminate bubbles. I performed experiments for all conditions in two separate trials.

On day 0, I loaded a 3×10^6 cells/mL suspension of D3 mESCs in high-glucose ES media into the devices using the same methods of section 4.2.6. At the chip output I connected a tube to collect media. As in section 4.2.6 I allowed the cells to attach for 4 hours in static culture before starting perfusion culture, which continued to day 3. On each day I collected all tubes (measuring the new weight for the slow flow-rate conditions). I then measured the amount of glucose in the day 2-3 waste samples and compared them with the glucose concentration of the initial media mixture that was used to perfuse all three devices.

To measure glucose I used an enzymatic glucose assay kit from Sigma (#GAHK-20, Sigma-Aldrich) along with a spectrophotometer to measure absorbance (ND-1000, Nanodrop Technologies, Wilmington, DE). This kit functions by a series of reactions: 1) Using hexokinase, glucose is phosphorylated by ATP. 2) In the presence of NAD, the product of the previous reaction, glucose-6-phosphate, is oxidized to 6-phospho-gluconate by glucose-6-phosphate dehydrogenase. This step causes an equimolar amount of NAD is reduced to be reduced to NADH, causing a measurable increase in absorbance at 340 nm[92]. This kit was also used by Cochran *et al.* in studies investigating glucose consumption of mESCs[93].

4.3 Results

4.3.1 Flow-rate measurements in the 1×6 logarithmic device

Using a similar particle velocimetry technique as used in section 3.3.2, I measured the flow rates in the 1×6 logarithmic flow-rate device. The measured flow-rate range of the device was ~1390×, larger than the designed range of 1024×. As in Chapter 3, it is likely that the difference in range was due to discrepancies in measurements in the lowest flow-rate chamber, again probably due to a combination of experimental error, differences between designed-for and fabricated geometries, and simplifying assumptions in the model.

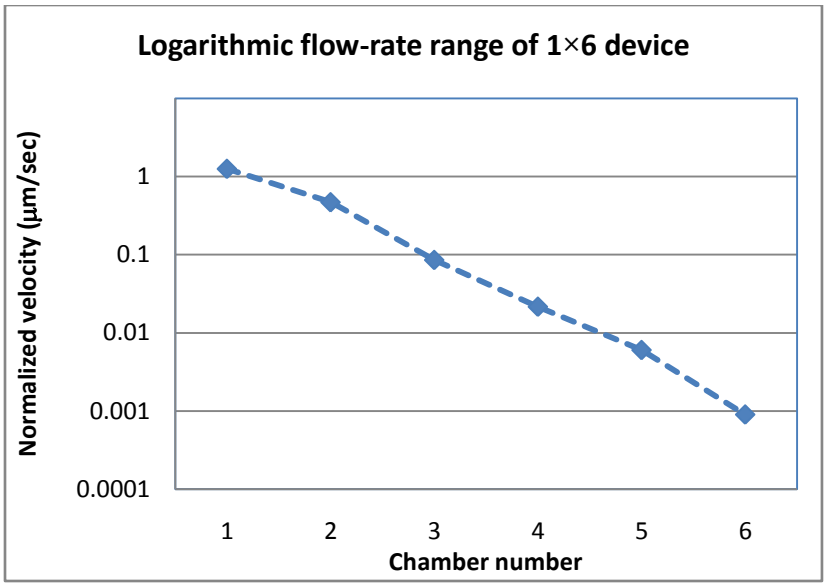

Figure 4.6: Experimentally measured maximum velocities in 1×6 logarithmic flow rate device.

4.3.2 mESC proliferation at high and low glucose levels

The first goal in this chapter was to verify the qualitative results from Chapter 3 using a device specifically designed to investigate the flow-rate and location-dependent proliferation patterns. I cultured D3 mESCs for three days across a logarithmic range of flow rates in standard (high glucose) ES media. Figure 4.7 shows typical cell seeding taken immediately after loading on day 0.

I continued to monitor the cell area every 24 hours after starting perfusion, and typical results from day 3 are shown in Figure 4.8. At low flow rates, upstream cell areas per photo were large, whereas downstream cell areas were small. At high flow rates, the total cell areas per photo were large throughout the culture chamber (both upstream and downstream). These results are consistent with the results from Chapter 3, which were essentially equivalent to looking at the downstream portion of each culture channel (blue boxed area in
Figure 4.9(b)). In addition, I observed that the colony morphologies appeared more flattened and spread-out compared to the colony morphologies seen in Chapter 3 where glass was used as the cell culture substrate. The colony morphologies seen in the 1×6 device at both high and low glucose levels were comparable to those in static controls, and similar to the colony morphologies from Chapter 2. These results are consistent with general knowledge that mESCs do not perform well on glass compared with polystyrene. It is known the cell attachment and adhesion are affected by surface properties such as hydrophobicity, and it is possible that differing hydrophobicities may have been the cause of the different cell morphologies observed on the different surfaces.

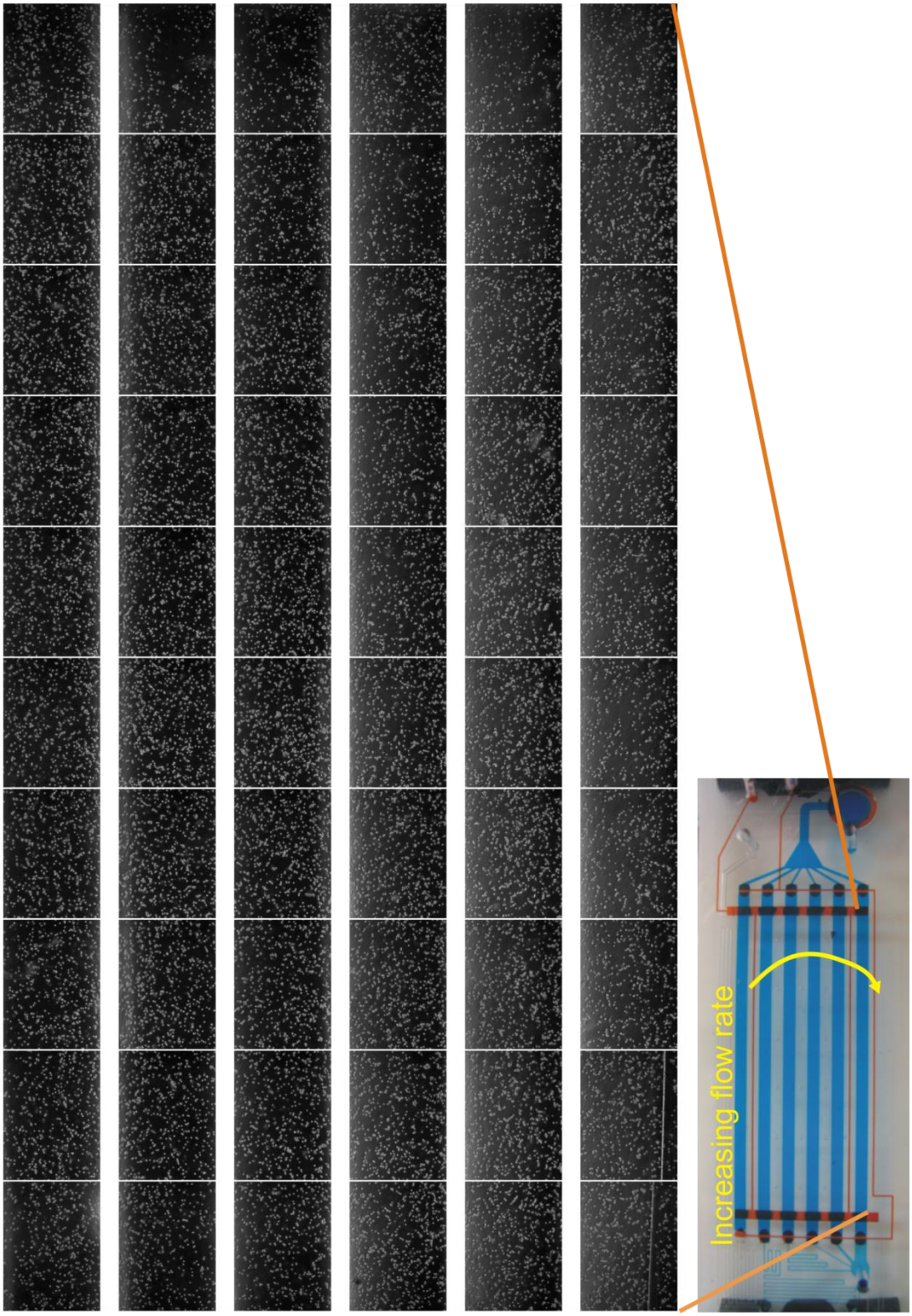

Figure 4.7: Typical cell seeding on day 0 in 1×6 logarithmic flow-rate device. Each column shows 10 photos sampled along the length of a single flow-rate channel at 3mm intervals. This data was used to normalize the colony areas on day 3 to compensate for slight variations in seeding density. Scale: each small photograph shows an area of 1.06 mm x 1.41 mm.

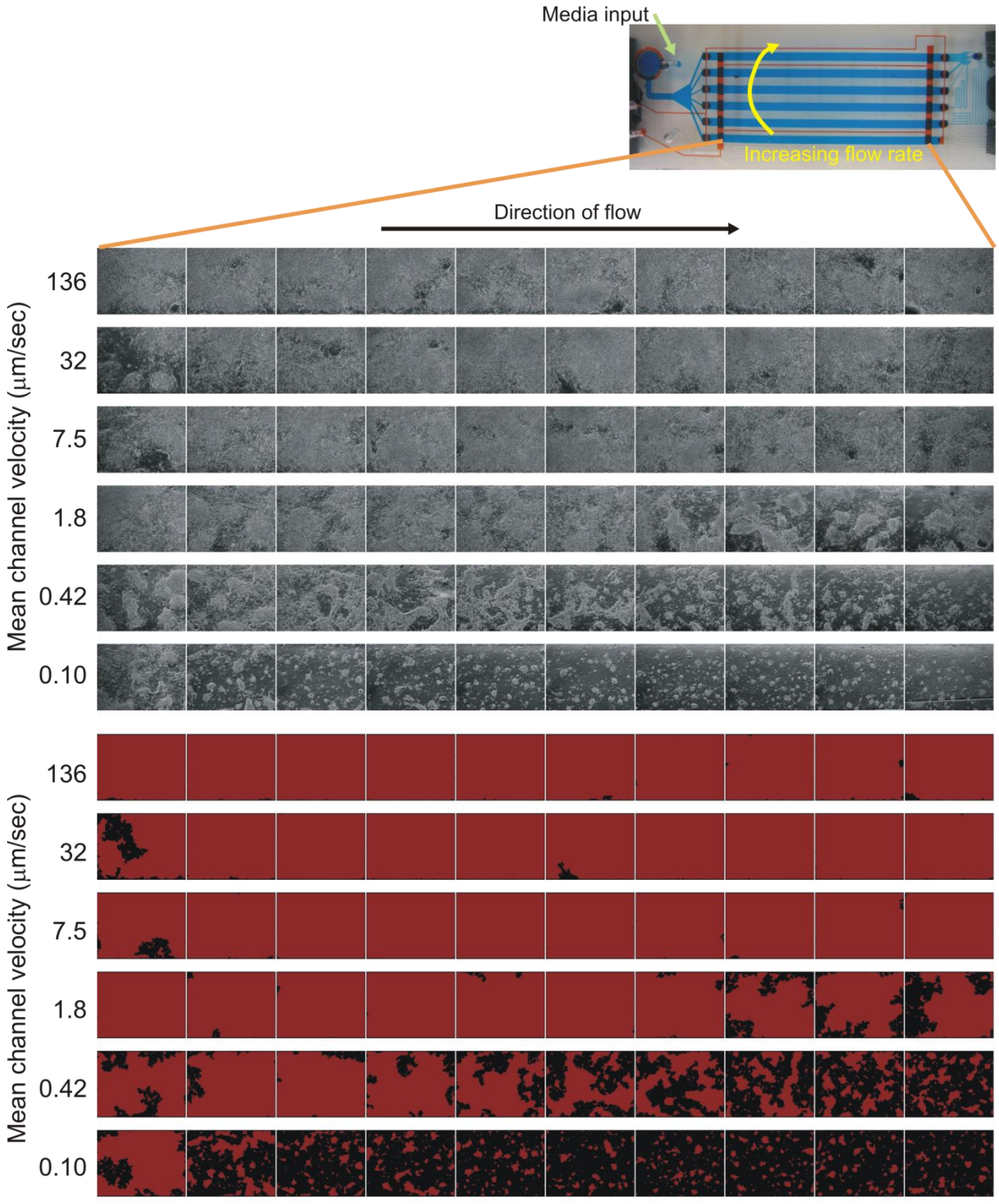

Figure 4.8: Typical day 3 high-glucose data. The upper set of images show the raw phase image data gathered from the device. Each row shows images from a single flow-rate culture channel, with the upstream samples

at the left and downstream samples to the right. Scaling: each small image shows an area of 1.06 mm x 1.41 mm.

To quantify the cell area results, I used the Matlab (Mathworks, Natick, MA) to process the phase images and extract a total cell area per photograph, as seen in the lower portion of Figure 4.8 (red area = extracted total cell area). Specifically, the following image processing steps were performed using standard Matlab image processing toolbox commands: 1) Adjust contrast using "imadjust()" 2) Threshold the gray image to become white in areas where there are cells, using "graythresh()" and "im2bw()" 3) Use fill and dilate operations to clean edges and to produce a more accurate black/white representation of the cell area and 4) Discard any areas that were smaller than the size of a cell. Here I chose to quantify total cell area rather than colony area (as in Chapter 3), because the cells were confluent in many of the images, and colony area was not as meaningful a measure of proliferation.

I then performed two more repeats of the high-glucose perfusion experiments and three repeats of the same experiments using low-glucose ES media instead. I interspersed these trials to attempt to avoid any unaccounted for bias in the state of the cells or culturing techniques over time. After quantifying cell areas, I normalized the cell areas by the initial day 0 cell area. Over time I noticed that variable amounts of cell attachment from one run to the next seemed to significantly affect cell area at later times. To compensate for varying amounts of attachment during different runs, I used a ratio of the day 1 to day 0 cell areas as a measure of attachment (larger ratio meant more spread-out cells on day 1, and implied better attachment). I normalized the final results by this attachment factor. The mean results at both high and low flow rates are shown in Figure 4.9. Since the colony areas at the channel outlets showed the greatest difference between flow rates, I averaged the colony areas from the three area samples closest to the channel outlets (blue boxes in Figure 4.9(b)). The averaged outlet areas for both high and low flow rates are shown in Figure 4.9(a). The next section describes the modeled results in Figure 4.9(c) that I compared against the experimental results of Figure 4.9(a).

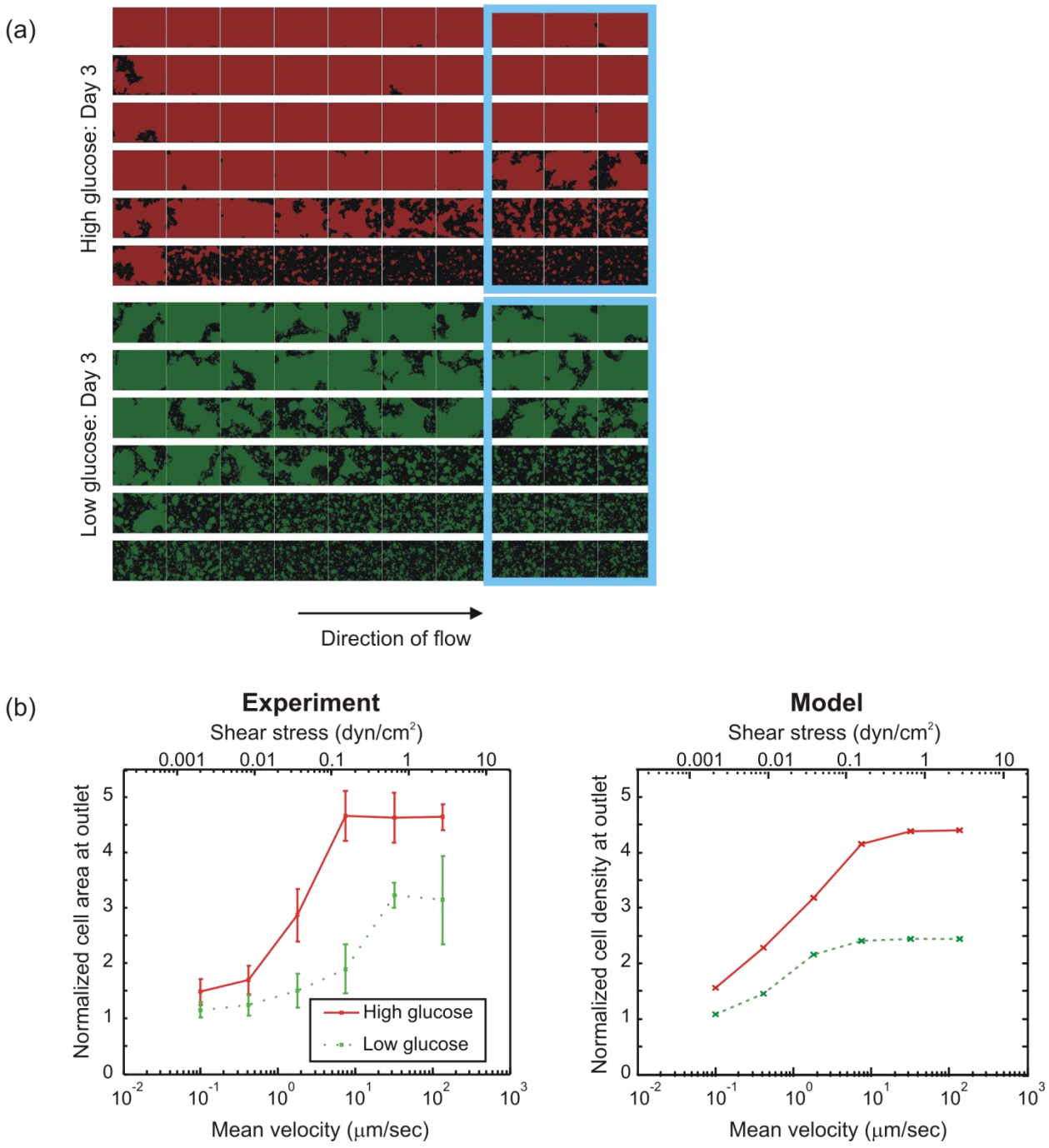

Figure 4.9: Experimental vs. modeled colony area on day 3. (a) Experiment results: Typical day 3 images from a high-glucose (red) and low-glucose (green) experiment. The blue rectangles show the image samples that were averaged to form the data points in (b-left). (b-left) Experimental results: averaged total cell area at channel outputs as a function of flow rate. This data is the mean over three independent experiments, with error bars showing the standard deviation. (b-right) shows results of modeling glucose depletion and cell proliferation. Using two fitting parameters, the normalized cell areas at the outlets show similar trends to the experimental data.

4.3.3 Modeling cell proliferation and glucose and oxygen profiles

In section 4.3.2 I observed that both the glucose concentration and the flow rate affected the colony area along the length of the culture channels. To explore the involvement of glucose depletion in creating the proliferation patterns seen in Figure 4.8, I modeled both glucose depletion and cell proliferation using the conditions applied in section 4.3.2. For simplicity, I modeled glucose depletion and glucose-dependent cell proliferation separately and assumed that the glucose profile was quasistatic with respect to the cell density. Because the mESC cell division time is roughly 18~24 hours, the cell density should not change significantly over 4 hours. Therefore, I simulated the glucose depletion that would occur over 4-hour time periods, assuming a temporally constant cell density. In between these 4-hour simulations, I updated the cell density based on the latest glucose concentrations. I continued this iterative process to cover the full 3-day time period. The next subsections describe these simulations. COMSOL simulation scripts are included in Appendix A.

Modeling glucose depletion: static attachment period

First I modeled glucose depletion during the 4-hour static attachment period. For simplicity, I assumed that the glucose concentration was independent of chamber width, enabling a 2D model shown in Figure 4.10.

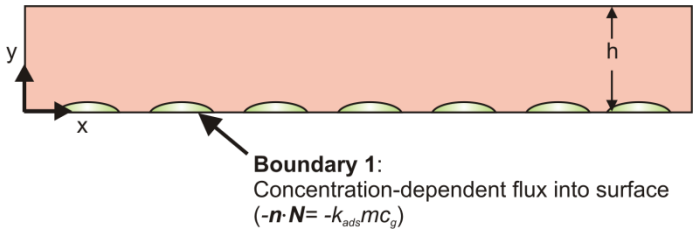

Figure 4.10: Static attachment period: boundary conditions for glucose concentration in FEM simulation. All boundaries except boundary 1 were set to insulating conditions (*n•N=0*).

The rectangular geometry (0.25 mm high × 30 mm long) represents a cross section of a single culture chamber as shown in Figure 4.10, which also shows the applied boundary conditions. Because the glucose concentration was still evolving at 4 hours, I used time-dependent finite element simulations using COMSOL Multiphysics (Stockholm, Sweden), a MATLAB-based finite element solver. I ran a finite element simulation using the time-dependent diffusion/convection mode that solved for the convection-diffusion equation (4.1). Because there is no convection in static culture, the fluid velocity is zero (equation (4.2)) and equation (4.1) reduces to the diffusion equation. Equations (4.3)-(4.4) describe the boundary condition applied at boundary 1. The glucose consumption rate is valid for partial pressures of oxygen level > 15 mmHg[93], which I confirmed by a separate simulation of oxygen depletion (not shown).

$$\frac{\partial c_g}{\partial t} + \boldsymbol{\nabla} \cdot \left(-D_g \nabla c_g\right) = -\boldsymbol{u} \cdot \nabla c_g \tag{4.1}$$

$$\boldsymbol{u} = \mathbf{0} \tag{4.2}$$

$$-\boldsymbol{n} \cdot \boldsymbol{N} = -k_{ads} m c_g \tag{4.3}$$

$$\boldsymbol{N} = -D_g \nabla c_g + c_g \boldsymbol{u} \tag{4.4}$$

where D_g=diffusivity of glucose (9×10^{-10} m^2 sec^{-1} from Cochran *et al.*[93]), c_g=glucose concentration (mol m^{-3}), $\boldsymbol{u}$=fluid velocity (m sec^{-1}), $\boldsymbol{n}$=normal vector, $\boldsymbol{N}$=glucose flux (mol m^{-2} s^{-1}), k_{ads}=rate constant for glucose consumption (5.4167×10^{-18} m^3 sec^{-1}), m=cell density (m^{-2}). The glucose consumption rate k_{ads} coefficient was calculated to result in the same glucose consumption rate reported in the literature[93]. I set c_0= initial glucose concentration to be 1000 mg/L (low-glucose media) or 4500 mg/L (high-glucose media). Finally, I set m=cell density (areal, cells cm^{-2}) to be equivalent to 100% of cells settling and attaching from a volumetric seeding density of 3×10^6 cells/mL, as was used during the experiment. (Note that these values were converted to have units using mol, m, and sec for the simulation.) Throughout I assumed that the cells form a monolayer culture, and that the glucose consumption rate per cell is independent of time and cell location.

Modeling cell proliferation

The next step was to use the results (c_g) of the previous simulation to estimate how the changes in glucose concentration may affect cell density throughout the channel. To estimate cell proliferation as a function of glucose concentration, I used experimental data from the literature. Kim *et al.* measured mESC proliferation when cultured in various levels of glucose[90]. They exposed mESC to different levels of glucose for 12 hours, then measured proliferation using two means – cell counting and BrdU incorporation.

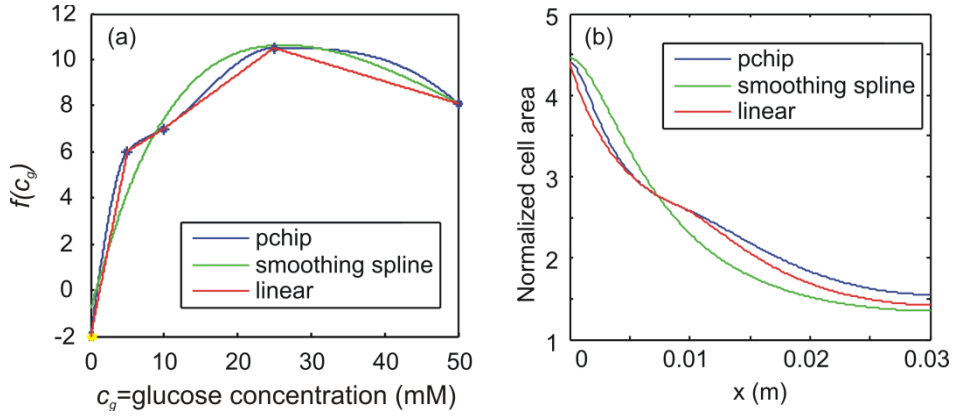

Figure 4.11: Effect of proliferation function shape on modeling results. (a) Three different curve fits for $f(c_g)$, where the blue data points were taken from literature[90], and the yellow point (at $f(0)=-2$) was a fitting parameter for describing cell death at low glucose levels. (The pchip interpolation was used throughout the rest of the data) (b) Corresponding cell area modeling results at day 3 at a velocity of using the three different fitted curves $f(c_g)$. The shape of $f(c_g)$ corresponds to the resulting shape of the normalized cell area versus distance along the channel in the x-direction.

Using both methods they found similar curves relating proliferation to glucose level. I used data points from their work to create an interpolated function $f(c_g)$, shown in Figure 4.11(a). I tried using three types of curve fits included in MATLAB: pchip interpolation (shape-preserving), linear interpolation (connect-the-dots), and smoothing spline. The shape of the cell proliferation as a function of position in Figure 4.11(b) mimics the corresponding shape of the interpolated function from Figure 4.11(a) that was used in the model. To choose the most appropriate curve fit, I compared the modeling results in Figure 4.11(b) with experimental results, but the experimental error was too large to favor any one particular fit. I chose to use the pchip interpolation here, as it matched the data most closely while maintaining a smooth shape. However, all three curves produced results similar to those in Figure 4.9(b). What is important is not the exact fit of the interpolation, but the overall trend of increasing $f(c_g)$ with increasing glucose concentration. If $f(c_g)$ were completely flat for any level of glucose, then the proliferation at all flow rates and locations would be the same. In order for this curve to produce results similar to the experiments, $f(c_g)$ must be generally increasing—larger for large c_g, smaller for small c_g. I designated $f(c_g)$ to be unitless and incorporated units into the coefficient, m_{coeff} in equation (4.5).

$$\frac{dm}{dt} = m_{coeff}\, f(c_g) \tag{4.5}$$

$$m_{new} = \frac{dm}{dt}\Delta t + m_{old} \tag{4.6}$$

where m=cell density as a function of distance along the channel (cells m^{-2}), m_{coeff}=fitting parameter (cells m^{-2} sec^{-1}) to adjust overall magnitude and units. To enable cell death in this model, I chose $f(0)<0$. Thus, there were two main fitting parameters in this model: m_{coeff} and $f(0)$. To prevent unphysical values of $m_{new} < 0$, if any values of m_{new} were negative, I reset them to zero. I used the same proliferation function, $f(c_g)$, throughout the entire simulation (during both

attachment and perfusion conditions). In reality, it is likely that cell proliferation is altered during the attachment phase, since it is known the cell attachment affects cell cycle[94].

The two fitting parameters adjusted the response curves in a predictable manner. Increasing m_{coeff} caused an increase in the overall magnitude of cell proliferation at high flow rates for both high- and low-glucose conditions, making both curves in Figure 4.9(c) steeper. This makes sense, because a larger m_{coeff} translates to a larger cell proliferation rate in equations (4.5)-(4.6). It also makes sense that it would have an effect of steepening the curve rather than causing a shift upwards, because $f(c_g)$ has both positive and negative portions. Increasing m_{coeff} has the effect of proportionally increasing the proliferation rate for $f(c_g)>0$ and proportionally increasing the death rate for $f(c_g)<0$. The second fitting parameter, $f(0)$, did not affect results at high flow rates, but did affect results at the lowest two flow rates. Decreasing $f(0)$ (making it more negative) lowered the cell numbers for the entire low glucose curve and the two lowest flow rates of the high glucose curve, which made sense because decreasing $f(0)$ was effectively increasing the cell death rate at low glucose. Likewise, increasing $f(0)$ (making it less negative) had the effect of boosting the cell numbers at low flow rates, because it was effectively decreasing the cell death rate at low glucose. Thus using these principles, I chose values of m_{coeff} and $f(0)=-2$ to fit the experimental data in Figure 4.9.

Modeling glucose depletion: perfusion culture

The next step was to use the updated cell density (m_{new}) to run another finite element glucose depletion simulation, using the same procedures above, except with parabolic flow (equation (4.7)). In addition, the boundary conditions at boundaries 2 and 4 had to be modified to accommodate the flow (Figure 4.12).

$$\boldsymbol{u} = 1.5U\left(1 - \left(\frac{y - 0.5h}{0.5h}\right)^2\right)\boldsymbol{i_x} \tag{4.7}$$

where $\boldsymbol{u}$=velocity in the x-direction (m s^{-1}), U=mean velocity in the x-direction (m s^{-1}), h=channel height (m). Also, the starting glucose concentration throughout the channel was the glucose concentration solution found during the simulation of the static attachment period. I simulated all six velocities used in the experiment, as well as both high and low glucose conditions (c_0).

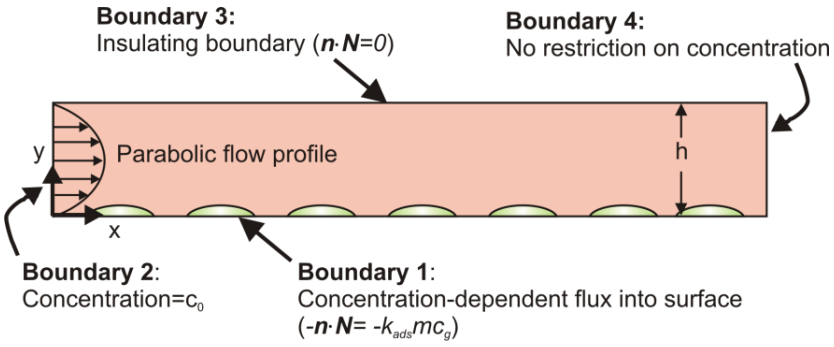

Figure 4.12: Boundary conditions for finite element modeling of glucose depletion during perfusion culture.

Again, I chose to simulate a 4-hour period of time. Using the results of this simulation (c_g), I calculated new cell densities (m_{new}). I continued simulating 4-hour time periods and updating the cell densities in-between simulations until the entire time period of the experiment (76 hours) had been simulated. The modeling process is summarized below:

Summary of modeling steps

1. **Model the static attachment period**
    a. **Compute glucose profile after t_{attach}=4 hours:**
    b. **Calculate cell proliferation:** Use the glucose concentration at t_{attach} hours to calculate a glucose-dependent proliferation rate and update the cell density using equations (4.5)-(4.6). Set fluid velocity $\boldsymbol{u}$=**0**.

2. **Model the perfusion period**
    a. **Compute glucose profile at $t+\Delta t$ hours, where Δt=4 hours,** setting the initial glucose concentration profile and cell density to the results calculated at the previous time step.
    b. **Calculate cell proliferation**: Use the glucose concentration at $t+\Delta t$ hours to calculate a glucose-dependent proliferation rate and update the cell density.

3. **Repeat steps 2a-2b until desired endpoint**: 76 hours in this case.

Model results

The modeling results are shown in Figure 4.9(c), Figure 4.14, and Figure 4.13. First I generated modeling results for the conditions used in the experimental data of Figure 4.9(a) and (b). For each experimental flow rate, I modeled both the high and low-glucose conditions over three days. To be consistent with the experimental data, I normalized the model cell density at the channel outputs on day 3 by the output cell densities on day 1, shown in Figure 4.9(b). By adjusting the two fitting parameters, the model shows similar trends to the experimental data of Figure 4.9(a), with low cell areas at low flow rates in both low and high-glucose conditions. As the flow rates increase, the output cell areas also increase for both low and high glucose. However, the overall slope of the high-glucose curve is steeper and saturates at a higher level than the low-glucose curve, again reflecting similar trends to the experimental data.

In addition to replicating the experimental trends seen in Figure 4.11, the model also allows one to investigate beyond the experimental observations to predict what the glucose concentration profile may be throughout the channel during various conditions. For example, Figure 4.13 shows typical 2D surface color plots of glucose concentration at high glucose, over three flow rates, for days 1-3. The color plots in Figure 4.13 correspond to the same channel cross-section from Figure 4.12. Corresponding normalized cell density profiles are also plotted under each color plot. At the two lower flow rates, at day 1 there is already a glucose concentration gradient throughout the length of the channel; the gradient is caused by depletion of glucose by upstream cells. Because of the increasing shape of the proliferation function $f(c_g)$, the glucose

concentration gradient causes a cell-density gradient. As time progresses from day 1 to day 3, the glucose gradient and the cell density gradient both steepen with respect to the length of the channel. At the highest flow rate, the glucose delivery rate is so high that it dominates any glucose uptake by cells, and there is negligible glucose depletion throughout day 1-2. Since all cells at the highest flow rate are seeing the same (~25 mM) glucose concentration, there is a level cell area profile along the length of the channel, similar to experimental observation from Figure 4.10. Interestingly, we also note that at the lower two flow rates, diffusion has made the glucose concentration roughly equal throughout the bulk height of the channel.

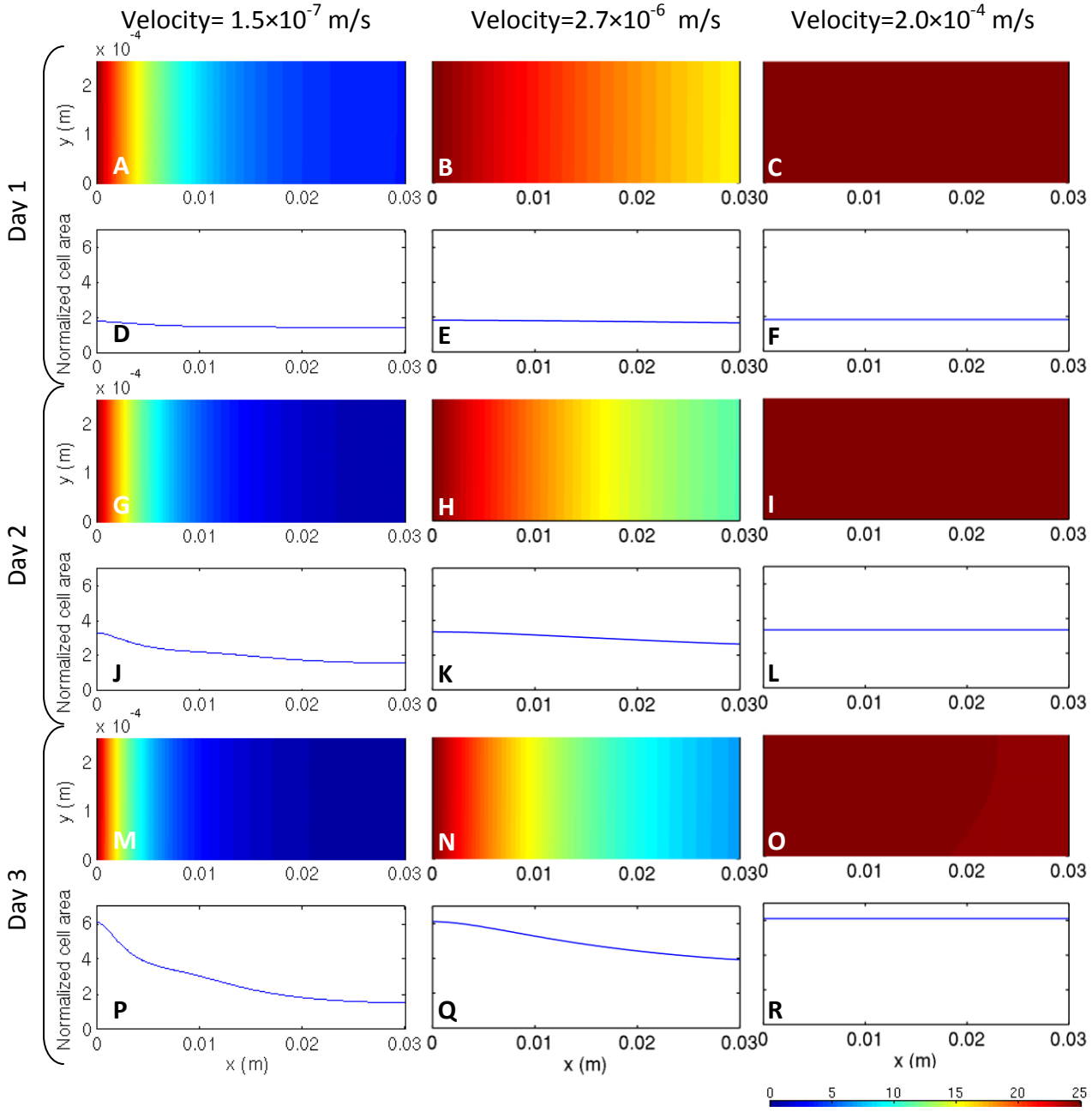

Figure 4.13: Modeling results for high glucose condition at three flow rates. Each colored graph (A-C, G-I, M-O) shows the glucose concentration at a particular time point (day 1-3) and velocity. The color scale at the lower right shows the glucose concentration (mM). Each line graph (D-F, J-L, P-R) shows the normalized cell area at a particular time point (day 1-3) and velocity.

To gain evidence that glucose depletion was indeed occurring, I designed an experiment to measure glucose concentration at the output of a 3-channel microfluidic device perfused at the same flow rate through all three channels. I then used the same modeling results to estimate the amount of glucose depletion predicted under the various flow rates, using the same fitting parameter values chosen to fit the data from Figure 4.11. Here I looked only at the high-glucose condition. I integrated the glucose flux at the input of the channel and the output of the channel, and normalized the glucose concentration at the output by the glucose concentration at the input. This normalized glucose concentration at the output was calculated for different flow rates and time points, shown in Figure 4.14. These results imply that there is significant glucose depletion at low flow rates, even as early as day 1, lending more weight to the idea that glucose depletion may be responsible for the nutritional effects seen at low flow rates. Interestingly, these results predict significant glucose depletion already at day 1 at low flow rates, even though in day 1 cultures, not much difference is seen between low and high flow-rate conditions. This delay may have occurred because it takes some time before glucose deprivation appears in the colony morphology.

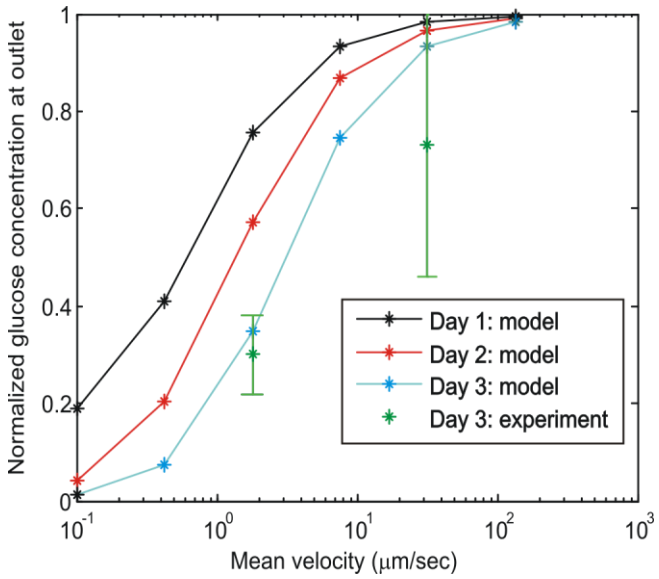

Figure 4.14: Predicted glucose depletion over time, calculated using the model described above for the high-glucose condition with the same fitting parameters. Data points show experimental data, with three trials per velocity condition.

Finally, to have an experimental measure of glucose depletion under various conditions, I compared input vs. output glucose concentration in high-glucose perfusion. Performing the protocol of section 4.2.7, I compared three conditions: low flow-rate cell culture, high flow-rate cell culture, and low flow-rate blank device with no cells. The results for the low and high-flow cell culture conditions are shown as data points in Figure 4.14. Each data point is the mean value from three trials per condition, where each trial value was itself averaged over three absorbance readings. Each trial was performed using a separate microfluidic device and setup. We see that

both the data points for the low and high flow-rate conditions match model predictions, although the data at the high flow-rate condition shows a large error. The control condition confirms that glucose is not depleted from the media when no cells are present in the device, with a mean normalized output glucose of 0.96 ± 0.11 (one standard deviation). An independent 1000 mg/L standard was used to calibrate the measurement. Considering the fact that the experimental conditions did not exactly match that of the model (there were cells upstream of the culture channels because the single flow-rate device did not have valves for selective cell placement during seeding), the match between experimental data and model predictions further supports the model.

4.4 Discussion

4.4.1 1×6 valved logarithmic flow-rate device design and operation

The 1×6 valved logarithmic flow-rate device successfully enabled further investigation of how flow rate affects mESC proliferation in perfusion culture. The return to using a polystyrene cell culture substrate improved cell attachment, with morphologies qualitatively similar to those in standard static culture. The incorporation of an active debubbler reduced the number of experiments that failed due to bubble generation within the device. The long culture channels enabled investigation of how total cell area varied along the length of the channel during flow. Finally, the incorporation of valves enabled selectively seeding cells only in the culture channels, with no cells upstream. This ability was crucial to performing glucose depletion studies, as it was important to establish a precise upstream boundary condition with a known glucose concentration.

The 1×6 device also incorporated additional, improved fabrication techniques. Using stereolithography to fabricate the mold has the advantages of convenience, lower cost, quick turnaround (~4 days), and more accurate reproduction of features, because it is difficult to achieve thick (> 150 μm), uniform layers using SU-8. One limitation is that the Viper Hi-Res process requires minimum features of ~50 μm in z and minimum wall thickness of ~100 μm in-plane. Therefore, in general, SU-8 is better suited to molds for microstructures requiring fine features and thin layers, whereas stereolithographic prototyping is better suited to larger-scale structures. In addition, the Smooth-Cast plastic does not require silanization before use with PDMS, and it also enables faster curing of thin PDMS layers when compared to the Prototherm molds. Using Prototherm 12120 molds, thin layers of PDMS take 24 hours to cure at 60°C instead of the usual 2 hours as with Smooth-Cast/SU-8/silicon molds. Using Smooth-Cast plastics to generate more molds was both cost- and time-efficient, enabling the creation of many plastic molds from a single Prototherm master.

Although the 1×6 device incorporates much functionality, the main challenge to using this device was a difficulty in achieving a uniform, repeatable clamping pressure. As mentioned earlier, if the clamping pressure is too low, the device leaks, and if it is too high, the valves will not open. In addition, I found that cell attachment seemed also to depend on clamping pressure. In several studies when I temporarily tightened the clamps during the attachment period only, I observed better, more consistent cell attachment. It is possible that if the device was not clamped tightly enough during cell attachment that temperature changes (transporting the device between room

temperature and the incubator) might have caused differential thermal expansion, causing movement of the PDMS relative to the polystyrene substrate, or causing mechanical/fluidic motion that disturbed cell attachment. Achieving good attachment is one of the most challenging and important practical aspects of performing microfluidic perfusion culture of mESCs. Both the substrate (polystyrene) and the mechanical environment (clamping setup) are important for achieving good attachment. One possible future direction to address this issue would be to develop a fabrication process enabling bonding of the PDMS to a polystyrene-coated glass substrate.

4.4.2 Glucose depletion consistent with experimental and model results

The evidence in this chapter supports the hypothesis that flow-rate-dependent glucose depletion can significantly affect mESC cell proliferation in microfluidic culture. In Figure 4.9(b), if one assumes that glucose depletion is responsible for the pattern, it is consistent that in the low-glucose condition, higher flow rates would be required to achieve the same glucose delivery that one could achieve with lower flow rates in high-glucose media. However, the observations in the low vs. high-glucose experiment of Figure 4.9(b) are correlations and do not necessarily imply a causal relationship. The further experimental evidence that the glucose concentration at the outlet was more depleted at low flow-rates than at high flow-rates makes it more likely that glucose depletion plays a significant role in establishing the cell proliferation patterns observed. Recently, Susan Lindquist's group has used a technique of incubating cells in the presence of a fluorescent, non-cleavable glucose analog (2-NBDG) to monitor glucose uptake[95]. The Lindquist group used flow cytometry to quantitatively assess fluorescence per cell. This would be an especially interesting approach to directly monitor glucose uptake while the cells are still in the device, such that the fluorescence could be monitored while preserving the spatial information of cell location. It is not clear whether conventional fluorescence microscopy would have sufficient quantitative resolution for this technique.

Reports from the literature further strengthen the case for the hypothesis of glucose-based proliferation patterns. It has been observed that mESCs do exhibit glucose-dependent proliferation, with higher proliferation in higher levels of glucose, and that these effects may be attributed to glucose-dependent upregulation of cell-cycle regulatory proteins[90].

Finally, although the model presented here is simple, it exhibited similar patterns of cell proliferation as were seen in the device, using only two fitting parameters. In addition, the model predictions for the amount of glucose depletion at different flow rates agreed with the preliminary experimental results. However, there were still several points of disagreement. The low-glucose model showed cell death at the lowest flow rate, which was not seen in the experimental data. Increasing the fitting parameter *f(0)* may improve the fit. Also, when I adjusted m_{coeff} such that the normalized cell area at high-glucose matched the experimental values, the model results for the low-glucose case were lower than in the experiments. In addition to the simplifying assumptions mentioned earlier, many of the parameters used in the model were taken during static experiments, and may not represent the parameters during perfusion. For example, the glucose consumption rate I used was experimentally verified in the literature, but it was measured in static culture. For mesenchymal stem cells, there is evidence

that the glucose consumption rate is much higher in perfused culture than in static culture[96], and it is quite possible that the same is true of mESCs. The data from the literature used to form the proliferation curve $f(c_g)$ was also measured in static culture, and thus the shape of the proliferation curve maybe different in perfusion. The perfused environment itself could cause many changes in the microenvironment, changing the overall state of the cell.

The implications of these results for future designs is that for long channels, fairly high flow rates are needed to avoid significant changes in the content of the media in the upstream vs. downstream portions of the culture chambers. However, if long culture chambers are not needed, using shorter channels may allow a slower flow rate while maintaining uniform culture along the length of the channel. In addition, if lower flow rates are desired while maintaining uniform cell proliferation along the length of the channels, another option is to increase the channel height. For the experiments in Chapter 5, I chose to apply flow rates that fell within the range of the three fastest flow rates used here. If glucose depletion does contribute to the flow-dependent proliferation patterns seen in the device, this does not exclude other mechanisms. It is possible that flow-dependent transport of growth factors, other nutrients, or waste products such as lactate, may also contribute.

4.5 Chapter Summary

In this chapter I further investigated the dependence of mESC proliferation on flow rate and location within the channel. I verified the flow-rate and position-dependent proliferation patterns observed in Chapter 3, and I investigated whether glucose depletion might be a cause of these proliferation patterns. I found that both the experimental evidence and modeling suggested that glucose depletion likely plays a significant role in establishing these patterns. In the process of investigation, I developed a microfluidic device with valves for selectively seeding cells, long culture channels for improved observation of potential effects of media depletion, higher culture chambers, improved cell adhesion to the substrate, and an active debubbler to reduce experimental failure. I also extended work from the literature to develop a basic model of mESC glucose consumption and cell proliferation, and used this model to predict flow rates at which glucose would be depleted at the output. Finally, the work in this chapter confirmed previous results from Chapters 2-3 on establishing a general flow-rate range for successful mESC culture in microfluidic perfusion.

Chapter 5. Using perfusion to modulate cell-cell diffusible signaling

The work of Chapters 2-4 established a viable flow-rate range for mESC culture in microfluidic, non-recirculating, serum-containing perfusion culture. Chapter 5 goes beyond looking at nutritional effects and investigates whether perfusion culture in this flow-rate range affects diffusible signaling in a biologically significant way.

I first explored whether the perfusion rates applied would indeed sweep away typical secreted factors, such as LIF. I experimentally measured LIF from the output of a microfluidic cell culture that had been perfused with LIF-free media. I also used modeling results from the literature to estimate the spatial range of signaling for LIF, and determined that the spatial range of signaling was on the same order as the channel height. I then estimated the Peclet number for LIF at typical flow rates to be >20 , supporting the idea that perfusion culture in the flow-rate range established in Chapters 2-4 can sweep away typical signaling molecules such as LIF.

Next I investigated the effect of perfusion on the neuronal differentiation protocol for adherent monoculture that was developed in Austin Smith's lab[17]. In these experiments, performed by Katarina Blagović, perfused mESCs did not survive in a perfused serum-free neuronal differentiation medium as they did in static culture. However, when the mESCs were perfused with a conditioned media mixture, they did proliferate and expressed a GFP reporter for Sox-1, an indicator of neuronal differentiation. These results strongly suggest that perfusion culture may affect the biological state of cells by removing secreted factors (which culturing in the conditioned media mixture restores). To further investigate this phenomenon, we then cultured mESCs in perfusion in the neuronal differentiation medium, but added LIF and BMP4. Together this media is known in static culture to be sufficient for mESC self-renewal[9]. However, here this serum-free formulation did not support mESC cultures, while a control formula with added serum did support colony proliferation. This suggested that added LIF and BMP4 were not sufficient to overcome the effects of perfusion on the mESC culture. To perform all of the serum-free culture experiments, we designed a new 2×3 side-by-side valved device which enabled investigation of two culture conditions on the same chip. This was important because it enabled the addition of a control condition in each experiment.

Together, the results of Chapter 5 strongly suggest that microfluidic perfusion culture can indeed affect diffusible signaling in the soluble microenvironment. These results lay the foundation for future studies into autocrine signaling in self-renewal and neuronal differentiation, and establish microfluidic perfusion culture as a new tool in investigating autocrine signaling.

Katarina Blagović carried out the neuronal differentiation experiments in this chapter.

5.1 Removing LIF by perfusion: modeling estimates

To investigate whether perfusion at the flow rates found in Chapters 2-4 would theoretically be able to sweep away typical secreted factors such as LIF, I used a two-step approach. I first estimated the spatial range of signaling of LIF in static culture using a model from the literature and known parameters. I then used this spatial range to calculate a local Peclet number

determining the relative influence of convection and diffusion on LIF transport in perfusion. The reason for using this two-step approach is that without knowing the spatial range of signaling, it is difficult to know what velocities are typically experienced by the ligands. If the spatial range of signaling is very small, then ligands will stay close to the cells and will experience low velocities, whereas if the spatial range is large, ligands may travel to the center of the flow chamber where they would experience the maximum channel velocity.

Assuming a random 2-D distribution of adherent cells on a surface under a standard media layer height of 2-3 mm, Batsilas *et al.*[97] traced the fate of a ligand released from the surface of a cell and tracked its progress before being trapped by a receptor on the originating cell (autocrine effect) or another cell (paracrine effect). They first developed a computational, Brownian-dynamics algorithm which allowed them to generate ligand trajectories. This algorithm used an adaptive timestep strategy which calculated the timestep differently depending on the location of the ligand (close to the cell-covered plane or in the bulk media).

When calculating the paracrine trajectories, they found that they could make the simplifying assumption that the surface was a homogeneous field with an effective trapping strength κ_{eff} (instead of an inhomogeneous field of randomly distributed cells).

$$\kappa_{eff} = \frac{\kappa\sigma}{1 + \frac{\pi\kappa r_{cell}}{4D_L}} \tag{5.1}$$

$$\sigma = \pi r_{cell}^2 n \tag{5.2}$$

$$\kappa = \frac{k_{on} R_{total}}{\pi r_{cell}^2 N_A} \tag{5.3}$$

where n=1/(average distance between cells)^2 (m^{-2}), r_{cell}=cell radius (m), σ=fraction of the surface occupied by the traps, D_L=ligand diffusivity (m^2 s^{-1}), k_{on}=ligand-receptor binding constant (L s^{-1} mol^{-1}), R_{total}=total number of receptors on the cell surface, and N_A=Avogadro's number. The simplifying assumption of a homogenous boundary condition allowed them to treat the problem analytically, and they derived the cumulative probability distribution function for r, the radial distance traversed by the paracrine trajectory, expressed in equation (5.4).

$$F(r) \approx \frac{r}{r + \frac{1.1D_L}{\kappa_{eff}}} \tag{5.4}$$

$F(r)$ is the fraction of paracrine trajectories captured at distances $\leq r$. One sees from equation (5.4), if the effective trapping strength, k_{eff}, is very large, $CDF(r) \approx 1$, even for small r. Thus, if the effective trapping strength is high, the spatial range of signaling will be small. Likewise, a larger ligand diffusivity D_L results in a larger spatial range of signaling.

To reach the compact expression in equation (5.4), Batsilas *et al.* assumed a medium layer thickness of 2-3 mm typically used in conventional cell culture. These dimensions are large compared to the medium layer thickness in our microfluidic systems (250 μm), however this model is still closer to the experimental situation than their previous models, which assumed cell culture in an infinite half-plane[3]. However, it is still useful for estimating the order of magnitude of the spatial range of paracrine signaling. Although the radial distance described is the in-plane radial distance to recapture, one can consider this value to be on the same order as the 3D spatial range of the ligand, because the simulation takes place in static culture, where the motion of the ligand is due solely to diffusion.

I calculated $F(r)$ using the following constants for LIF and mESCs: r_{cell}=5 μm, n^2=0.1 μm^{-1} (corresponding to an intercell spacing of 10 μm) $D_L=1\times10^{-4}$ mm^2/sec (typical diffusivity for 20 kDa molecule), $k_{on}=1.3\times10^{13}$ μL $(sec^{-1})(mol^{-1})$[98], R_{total}=1000. The value for R_{total} was chosen conservatively based on a value of ~270 receptors per cell measured in mESCs [98]. Because those measurements were obtained at 4°C with the mESCs cultured under specific conditions, it is possible that the value of R_{total} may be different under microfluidic conditions. The resulting probability distribution is shown in Figure 5.1. The channel height in the 2×3 side-by-side perfusion device used in this chapter is 0.25 mm. According to Figure 5.1, only ~25% of paracrine trajectories would stay within this height of 0.25 mm if cultured in a standard static dish with a medium layer height of 2-3 mm. Therefore the spatial range of signaling for LIF is quite large–on the same length scale as the microfluidic channel itself.

This implies that under normal circumstances, LIF is able to travel far enough away from the cells such that it may stray toward the center of the channel where the flow is the highest. Although these results will not be exactly the same in our device because the layer height is smaller, the result still provides valuable information on the general spatial range of signaling of LIF and other signaling molecules.

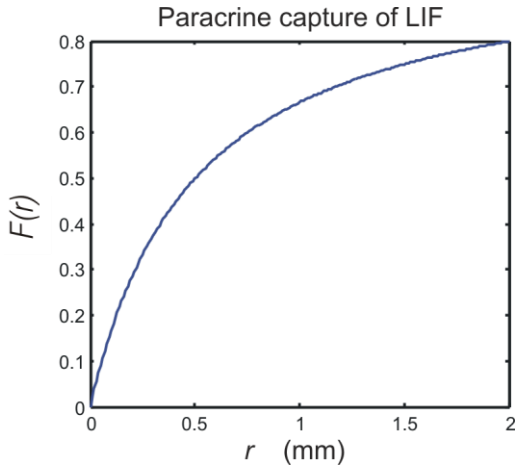

Figure 5.1: Estimate of the spatial range of signaling of LIF in static culture, assuming a large media layer height (>2 mm). *F(r)* is the cumulative probability that a paracrine trajectory will have a spatial range ≤ r.

Having found that the spatial range of signaling for LIF is on the same scale as the chamber height, I calculated the Peclet number assuming a characteristic length, *h*, of half the chamber height (0.125 mm) and a typical velocity range of v_{max}= found in Chapter 4.

$$Peclet\ number = \frac{v_{max}\, h}{D_L} \tag{5.5}$$

This calculation yielded a range of Peclet numbers of 14, 60, and 255 for the three highest flow rates of Chapter 4. The corresponding Peclet numbers for the 0.1 mL/hr and 0.2 mL/hr flow rates used in this chapter are 62.5 and 125 respectively. Since the Peclet numbers are substantially greater than 1, the transport of the released LIF is convection-dominated. Therefore, modeling estimates support the idea that cell culture in microfluidic perfusion can remove secreted factors from the soluble microenvironment. These estimates are in agreement with those performed by Figallo *et al.*[49] for their microbioreactor operated under similar conditions.

5.2 Experimental

5.2.1 Cell culture

Throughout Chapter 5 we used D3 mESCs (cultured as described in Chapter 4) and 46C mESCs (with a stably integrated GFP reporter for Sox-1, generously donated from Austin Smith's lab). We followed the Smith lab protocols for mESC culture in serum-containing- and serum-free media, and neuronal differentiation[17]. The passage number of 46C cells used was lower than 36, and the passage number of D3 cells used was lower than 22.

46C cells were cultured in **GMEM-based ES media**: GMEM (11710035, Invitrogen, Carlsbad, CA) supplemented with 10% ES-qualified fetal bovine serum (SH30070.03, Hyclone), 50 U/mL penicillin, 50 μg/mL streptomycin (15140122, Invitrogen), 100 μM β-mercaptoethanol (M7522, Sigma,,St. Louis, MO), and 10 ng/ml leukemia inhibitory factor (ESG1107, Chemicon, Temecula, CA).). We cultured cells directly on tissue-culture plastic (150679, Nunc) in a 37° C humidified environment with 7.5% CO_2. For maintenance of mESCs, we fed cells daily and passaged every other day using TrypLE Express (12604013, Invitrogen) at a density of ~$8x10^4$ cells/cm^2.

LIF-free ES media: This media had the same composition as the ES media of Chapters 2-4, however, without LIF.

5.2.2 Protocols for neuronal differentiation

Three different types of media were used during neuronal differentiation experiments. In preliminary experiments, for convenience we attempted to use an off-the-shelf N2 supplement (17502048, Invitrogen), as well as a partially customized N2 supplement using an off-the shelf insulin-transferrin-selenium mixture (41400045 Invitrogen). The off-the shelf N2 supplement did not produce substantial neuronal differential. While the ITS mixture was an improvement, the

exact formulation from Ying *et al.*[17] produced the most Sox-1 GFP expression, and so we duplicated the exact formulation throughout the experiments described here.

N2B27 media: was duplicated from Ying *et al.*[17], but with added penicillin-streptomycin, and consisted of a 1:1 mixture of Neurobasal medium (21103049, Invitrogen) supplemented with B27 (17504044, Invitrogen) and DMEM/F12 (21041025, Invitrogen) supplemented with a custom N2 mixture developed by the Smith lab: (25 µg/ml insulin (I1882 , Sigma Aldrich), 30 nM sodium selenite (S5261, Sigma Aldrich), 100 µg/ml apo-transferrin (T2036 , Sigma Aldrich), 6 ng/ml progesterone (P6149, Sigma Aldrich), 16 µg/ml putrescine (P5780 Sigma Aldrich), and 50 µg/ml bovine serum albumin fraction V (15260037, Invitrogen). Thus the final concentrations in N2B27 media of the N2 components are half the concentrations listed above. We also added 50 U/mL penicillin with 50 µg/mL streptomycin (15140122, Invitrogen).

N2B27+LIF media: N2B27 media with 10 ng/ml LIF (ESG1107, Chemicon) added.

N2B27/CM: Day 2-3 media was collected from 46C cells undergoing neuronal differentiation (as described below) and spun down for ~40 minutes using an Amicon Ultra centrifugal filter unit with a 3 kDa membrane (UFC900324, Millipore) until reduced to ~10% of its original volume, then supplemented with fresh N2B27 media to reach the original volume.

Neuronal differentiation protocol
The protocol from Ying *et al.*[17] was used for adherent, monoculture neuronal differentiation. For comparison the same numbering system for days was used as in Ying *et al.* 46C cells were cultured in serum-containing GMEM-based ES media, trypsinized, spun down and resuspended into N2B27+LIF medium. On day –1 the cells were then plated onto gelatin-coated dishes (ES-006-B Embryomax ES qualified gelatin, Millipore); the day numbering scheme was adopted to be consistent with that used by Ying *et al.*[17]. On day 0, the dish was washed twice with PBS to remove traces of LIF, and the cells were fed with N2B27 media. Cells were fed again with N2B27 media every two days (days 2, 4, 6).

5.2.3 Protocols for serum-free culture for self-renewal

N2B27+LIF+BMP4 media: N2B27 media supplemented with 10 ng/ml leukemia inhibitory factor (LIF, ESGRO, Chemicon) and 10 ng/ml BMP4 (314-BP-010, R&D Systems, Minneapolis, MN). This media was used only during perfusion experiments, not general culturing.

N2B27+LIF+BMP4/serum: This media was made by diluting the existing serum-free ES media (=N2B27+LIF+BMP4) by adding 10% ES-qualified fetal bovine serum (SH30070.03, Hyclone). This media was used only during perfusion experiments, not general culturing.

Because the initial neuronal differentiation protocol of Ying *et al.* used mESCs that had been routinely cultured in serum-containing media, we also adopted this procedure throughout this chapter, even when culturing in the serum-free self-renewal media N2B27+LIF+BMP4. Thus, we were able to directly compare the effects of adding LIF and BMP4 to the same protocols used for the perfusion culture neuronal differentiation.

5.2.4 Microfluidic fabrication

Two devices were used in this chapter, a 2×3 valved device, and the 1×3 single-layer device from Chapter 4. The 2×3 valved device was fabricated using the same procedures in section 4.1.2.1, and is shown in Figure 5.2(b).

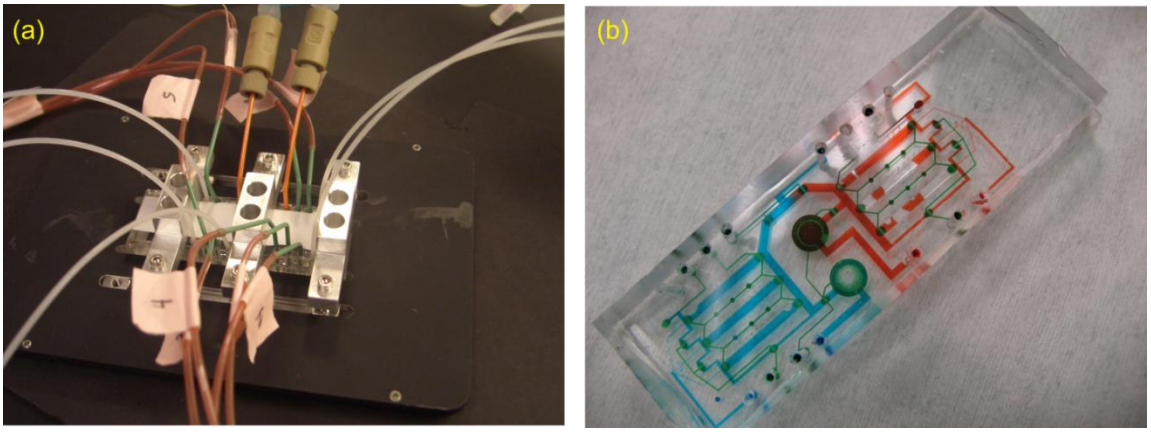

Figure 5.2: (a) Experimental setup of 2×3 device clamped into custom stage insert. (b) Photograph of 2×3 device filled with dye to illustrate channels. The green dye shows the pneumatic channels, and the red and blue dyes show how two different media types can be perfused on the same device.

5.2.5 Optics

The same optics setup was used here as in Chapter 4.

5.2.6 Serum-free perfusion culture in 2×3 side-by side device: protocols

The experimental setup is shown in Figure 5.2(a) and was similar to the setup used in Figure 4.3(b). In this setup, there were two duplicated media input streams with media input syringes connected to the same syringe pump, as well as additional separately addressable valves, each with separate pneumatic connections controlled using the custom pneumatic switchbox described in Chapter 4. The protocol for conducting the perfusion experiments was also similar to those of Chapter 4, the main difference being that here we were simultaneously setting up two parallel cultures on the same chip. Again, it was critical to adjust the clamping pressure holding the PDMS to the polystyrene during device assembly and testing to make sure the valves were operating, but there were no leaks.

On the day before loading cells, we prepared the device by perfusing and debubbling overnight with 0.1% ES-qualified gelatin solution (ES-006-B Embryomax ES qualified gelatin, Millipore).). Then ~2 hours before loading cells, we perfused with the attachment media solution (N2B27+LIF for neuronal experiments, and GMEM-based ES media for serum-free self-renewal).

The next day (designated day -1) we prepared and loaded the mESC suspension into the microfluidic device, using the same techniques from Chapter 4. The 2×3 device used here

enabled loading of cells through a single input into all chambers on the chip, shown in Figure 5.3(b.1). After the cells were loaded into the 6 culture chambers, we closed off the valves to the culture chambers using a positive pressure of ~2 PSI and flushed all extra cells from the device (Figure 5.3(b.2)). Finally, we removed all pneumatic vacuum/pressure control lines, allowing all valves to relax into the normally closed position, isolating cells in the device (Figure 5.3(b.3)). Using cells from the same cell suspension, we plated a static control culture in three wells of a 6-well plate, maintaining the roughly same areal density as on the device. We allowed the cells in the device and in the static dish to attach for 24 hours before beginning perfusion on day 0. A flow rate of 0.1 mL/hr for each side of the device was used for both neuronal and serum-free self-renewal perfusion culture experiments. Each day we disconnected the device from perfusion for ~30 minutes to take photographs, then reconnected it.

5.2.7 LIF measurements and mESC perfusion culture: protocols

The protocol for measuring LIF collected from perfusion cultures was similar to that for measuring glucose from perfusion culture wastes in Chapter 4. To measure LIF concentration at the output of mESC perfusion culture, I cultured D3 mESCs (passage number lower than 22) in a 1×3 single-flow-rate device with three parallel identical chambers (shown in Figure 4.5(d)). Here the goal was to perfuse LIF-free media and to measure the concentration of LIF in the waste media collected at the outlet.

All experiments were performed using LIF-free ES media. As in Chapter 4, I fabricated, assembled and prepared the 1×3 devices, filling the chambers with LIF-free ES media and incubating overnight to eliminate bubbles. On day 0, I loaded a 5×10^6 cells/mL suspension of D3 mESCs in high glucose ES media into the devices. At the chip output I connected a 15-mL tube to collect media. I allowed the cells to attach for 4 hours in static culture before starting perfusion culture, which continued to day 2. I also used the same cell suspension to culture cells in static culture at a density of 5.6×10^5 cells/mL in 35-mm Petri dishes. On each day I collected and replaced all waste tubes from the perfusion cultures and collected and fed the static cultures with 4 mL LIF-free ES media. In the perfused devices, the flow rate was 0.2 mL/hr. I repeated these experiments three times.

As a control, I also performed the same procedure with a blank device with no cells to gauge how the system itself affected LIF concentration. I perfused the blank devices with a low concentration of LIF (~4 pg/mL), also repeating this experiment three times.

Immediately after collecting media from both static and perfused cultures on day 1 and 2, I centrifuged the samples at 1500 rcf for 10 minutes to remove particles (such as cells and cell debris) from the solution by extracting only the supernatant. I then froze the samples at -20°C for storage. To measure LIF I performed a two-step process. I first concentrated the thawed collected media using an Amicon Ultra centrifugal filter with a 10 kDa cutoff (UFC801024, Millipore) by spinning down raw samples of 3.5 mL at 3200 rcf for 17 minutes. I chose a 10 kDa filter cutoff because the LIF molecule is 20 kDa[99].

I then measured the amount of LIF in the concentrated samples using a quantitative ELISA kit (MLF00, R&D Systems), calibrating the data using a standard curve provided in the kit. To

gauge the average amount of concentration, I centrifuged samples and measured the amount of LIF in the un-concentrated vs. the concentrated sample. All ELISA measurements were performed in triplicate to control for variations in the ELISA measurement itself.

5.3 Results

5.3.1 2×3 side-by-side device design

The purpose of the 2×3 side-by-side device was to enable triplicate perfusion cultures under two media conditions on the same device. However, because the valves are independently addressable, the design is actually more versatile and can be used under a wider variety of conditions, with any combination of the following: one/two cells types or densities, one/two media types, one/two flow rates. In this chapter we were interested in comparing only the two media types but kept cells types, densities, and flow rates constant throughout the rest of the device. Figure 5.3(a) shows the overall layout of the device, with the fluidic channels in gray and the pneumatic channels in orange. Because this device did not require a logarithmic range of fluidic resistances, the fluidic layer here was a single thickness of 250 μm. The valve and debubbler geometries were similar to those in the 1×6 valved device of Chapter 4. As described above in section 5.2.6, the device was operated in four stages, shown below in Figure 5.3(b).

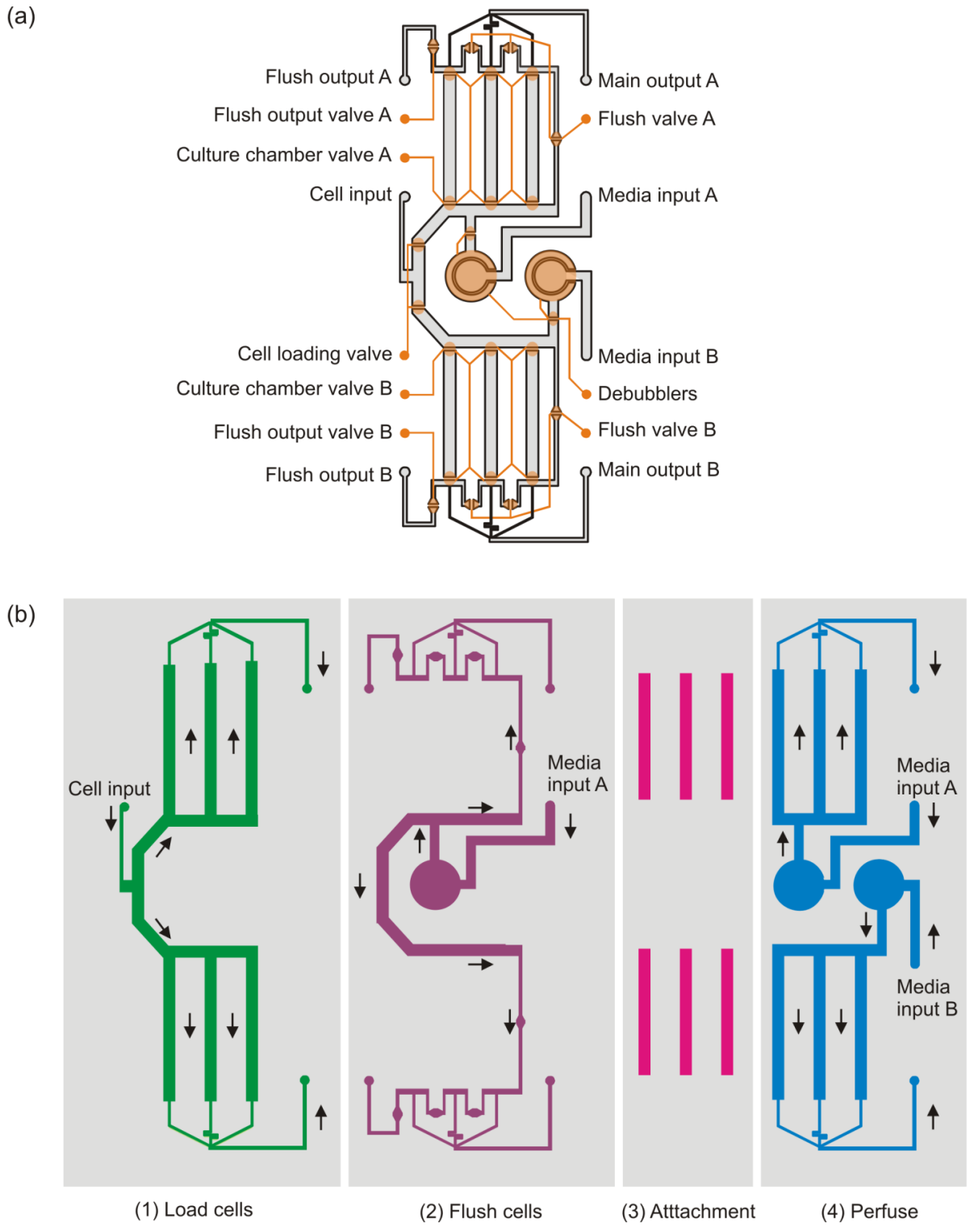

Figure 5.3 Design and operation of 2×3 side-by-side device. (a) shows the fluidic channels in gray and the pneumatic channels in orange. The device has eight separately addressable valves which can be used in various combinations throughout the loading and perfusion process. (b) shows how we used the valves in a typical perfusion experiment to load cells (b.1), flush extra cells (b.2), close off culture channels to encourage attachment (b.3), and finally, to perfuse each side of the chip with a different type of media (b.3).

5.3.2 Removing LIF by perfusion: experimental evidence

Next, to experimentally measure whether LIF could be swept away during standard microfluidic perfusion, I cultured D3 mESCs cells in LIF-free ES media and collected the media at the waste output each day, as described in section 5.2.7. Figure 5.4 shows the results from measuring LIF from perfused devices as from static dishes. For comparison between perfused and static measurement, the seeding cell densities were used to calculate a LIF production rate per cell. Because these normalizations made it difficult to visualize the static dish results, I replotted them in the inset of Figure 5.4. The day 1 and 2 bars show respective measurements from media collected on days 1 and 2 for chip (perfused) and dish (static) conditions. The "Chip neg. control" indicates the low-end resolution of the ELISA measurement, and was found by measuring a known LIF-free sample, then normalizing that by the seeding cell number in a device. Thus, the "Chip neg. control" is an indicator of the noise level of this measurement. A similar normalization was performed for the seeding cell density in the dish, producing the "Dish neg. control" values. For both the chip and the dish, the LIF in the day 1 and 2 samples registered above the noise level of the measurement. The error bars represent the standard deviation from three replicate experimental conditions. The large error bars in the "Chip day 1" sample may have been due to residual LIF in the microfluidic tubing which was flushed out on day 1 from a single sample. Regardless of whether the LIF collected was produced by cells or was residual in the system, this experiment demonstrates the ability of perfusion culture to remove LIF from the microfluidic perfusion setup, confirming the modeling predictions of section 5.1.

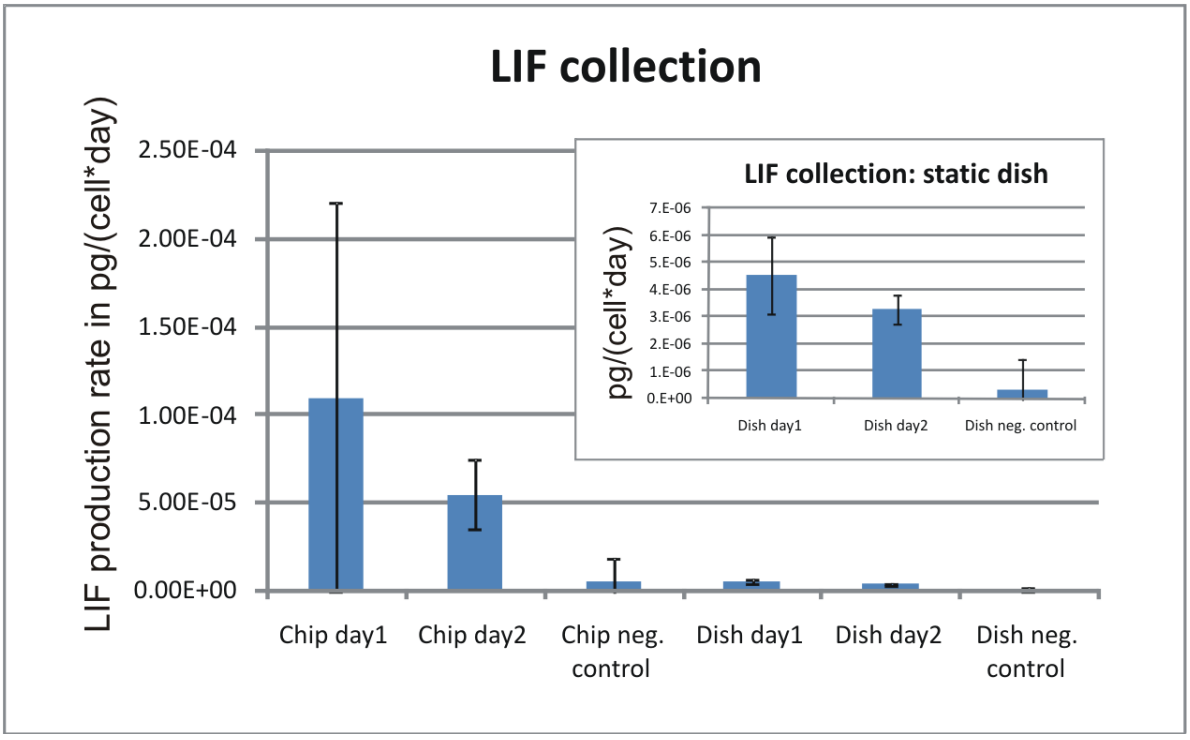

Figure 5.4: LIF production rate per cell in perfused chips vs. in a static dish, calculated based on the initial cell number at the time of plating on day 0. The error bars show variation across three culture trials. The

"Chip negative control" and "Dish negative control" show the lower limit of resolution of the measurement, and were calculated by dividing the measurement of the original LIF-free input media by the respective cell densities in perfusion and static. For both the static and perfused cases, the LIF measurements are above the lower limit of resolution.

To further establish the role of the microfluidic perfusion culture system in the LIF measurement, I also performed a control experiment using a blank microfluidic device without cells. Because of the permeable nature of PDMS, one hypothesis was that evaporation through the PDMS might cause an increase in LIF concentration at the output. Another hypothesis was that LIF molecules might stick to the inner surfaces of the microfluidic system, resulting in a decrease in LIF concentration at the output. Thus, this experiment was designed to show whether the microfluidic system might be increasing or decreasing the amount of LIF detected at the output. Because the point of this experiment was to be able to measure not only increases but also decreases in the LIF concentration, instead of perfusing the systems with LIF-free media, I perfused them with a known concentration of LIF and compared the output LIF concentrations to the input concentration. To avoid the same large error bars seen in the Chip day 1 measurement of Figure 5.4, I perfused and autoclaved the system to remove residual LIF prior to starting the experiment. The results (Figure 5.5) indicate that the day 1-3 measurements are not significantly different from the initial input LIF concentration (using the t-test), implying that the microfluidic system has a negligible effect on LIF concentration.

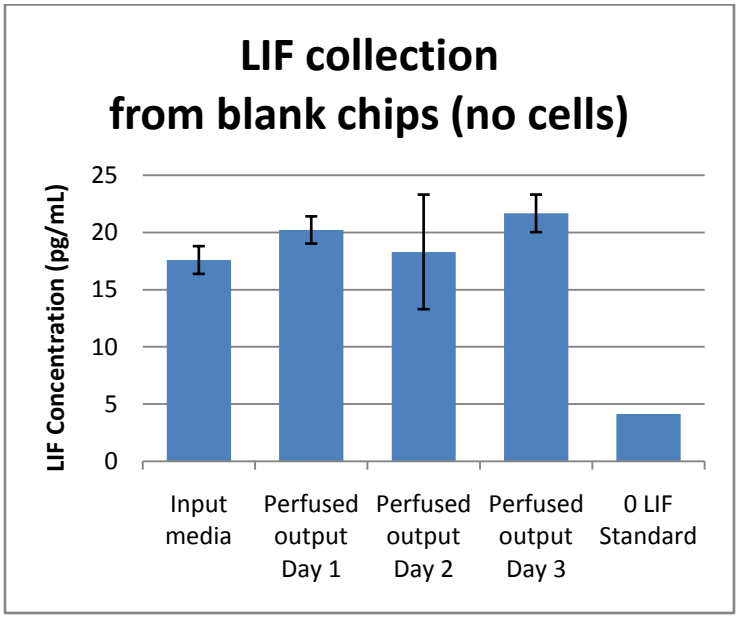

Figure 5.5: LIF measurements from perfusing blank chips without cells. Three devices were perfused with a low (~ 4 pg/mL) concentration of LIF. The graph shows the mean and standard deviation of the post-concentrated amounts of LIF in the Input media vs. perfused, collected outputs from a blank chip on days 1-3. For comparison, the value for a 0 LIF standard is also shown to demonstrate the lower limit of this measurement. The Perfusion culture in N2B27 media vs. N2B27 conditioned media.

5.3.3 Monoculture neuronal differentiation in microfluidic perfusion

The next goal was to show that culturing cells in microfluidic perfusion can change the soluble microenvironment in a biologically significant manner. To explore this, I chose the system of serum-free monoculture differentiation of mESCs developed by Austin Smith's group and described in Chapter 1[17]. The reason for choosing the N2B27 neuronal differentiation system was that Ying *et al.* had already demonstrated a measurable effect of autocrine fibroblast growth factor 4 (FGF4) on neuronal differentiation. They showed that cells cultured at low densities exhibited a lower amount of neuronal differentiation, which was boosted with the addition of exogenous FGF4. They also found that addition of SU5042, a pharmacological inhibitor of the FGF receptor, caused a reduction in neuronal differentiation. Therefore they concluded that neuronal differentiation is not merely a default differentiation pathway, but requires autocrine FGF4. This neuronal differentiation protocol was also especially appropriate because it is already performed under some of the most controlled conditions available in static culture (serum-free media, monoculture, differentiation without the use of embryoid body cellular aggregates).

The experiment in this section was designed to ensure that results were due to the removal/restoration of secreted factors and not to altered nutrition or shear stress. The concept for the experiment is illustrated in Figure 5.6. Two separate conditions are applied, one perfusing defined N2B27 neuronal-differentiation media (upper illustration), the other applying conditioned N2B27 media (N2B27/CM) at the same perfusion rate (lower illustration). In a process similar to dialysis, the conditioned media is modified to restore nutrients while retaining the original concentration of large molecules. Thus, when comparing the two conditions, both conditions experience the same mechanical forces (same flow rate) and the same nutrient delivery (since nutrients were replenished in the conditioned media). The only difference between these two conditions is that if we assume secreted factors are being removed by flow, the upper condition has reduced diffusible signaling, whereas the lower condition should be more similar to conditions in static culture. Applying this experiment to neuronal differentiation, assuming that the mESCs survived in perfusion, the hypothesis was that the mESCs in perfused N2B27 culture would show lower differentiation than mESCs in perfused N2B27/CM.

Although similar to the experiment of Chung *et al.*[31], the key difference is that here conditioned media has been used as a comparison condition to restore those same secreted factors that may be swept away by flow. Because Chung *et al.* did not use conditioned media, but used specific exogenously added factors, it could be argued that the differences they saw between the two conditions were due to effects of artificial levels/combinations of exogenous factors, rather than restoration of endogenous factors that had been swept away.

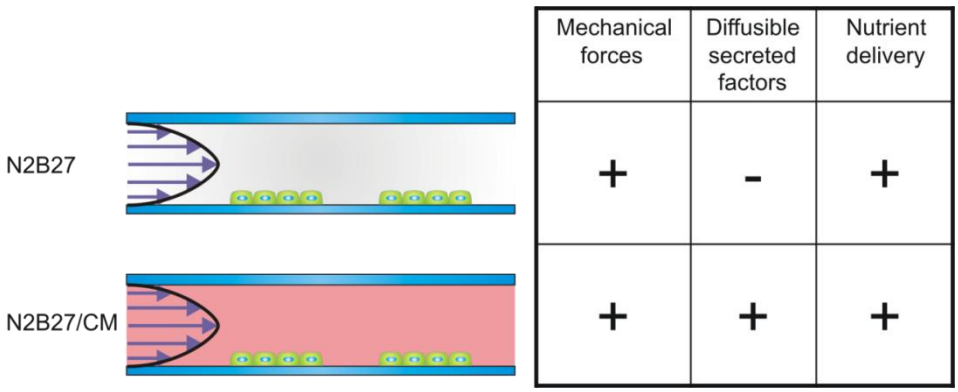

Figure 5.6: Concept for neuronal differentiation/conditioned media experiment.

To assess the effects of microfluidic perfusion culture on the biological state of cells, we compared the perfusion culture of cells in N2B27 serum-free neuronal differentiation media with cells in N2B27/CM media that contained a mixture of conditioned media from differentiating cells and fresh N2B27. We seeded 46C cells in N2B27+LIF overnight and began perfusion the next day (day 0) with N2B27 on one side of the device and N2B27/CM on the other side of the device. Both sides were otherwise treated the same (seeded at the same density and perfused at the same flow rate of 0.1 mL/hr).

We repeated this experiment four times, with representative results shown in Figure 5.7. Perfusion culture at these densities did not support proliferation of mESCs in N2B27 alone (Figure 5.7(e)), unlike in static culture, where colonies proliferated and differentiated (Figure 5.7(f)). However, when cultured in the N2B27/CM media during perfusion, colonies proliferated (Figure 5.7(d)).

If we assume that diffusible secreted factors are removed by perfusion at, the main difference between the conditions in Figure 5.7(d) and Figure 5.7(e) was the presence of secreted factors. Because the N2B27/CM media was nutritionally replenished and the same flow rates were used in both conditions, the nutritionally delivery and shear stress conditions were equivalent in both Figure 5.7(d) and Figure 5.7(e). The fact that the perfused conditioned media was able to restore the high proliferation seen in the static condition strongly support the idea that perfusion culture did remove secreted factors, and that these autocrine/paracrine factors are critical for survival of mESCs in serum-free monoculture neuronal differentiation. Finally, the results strongly suggest that not only can perfusion remove soluble factors from the microenvironment, but it does so to such an extent that significant biological effects are observed.

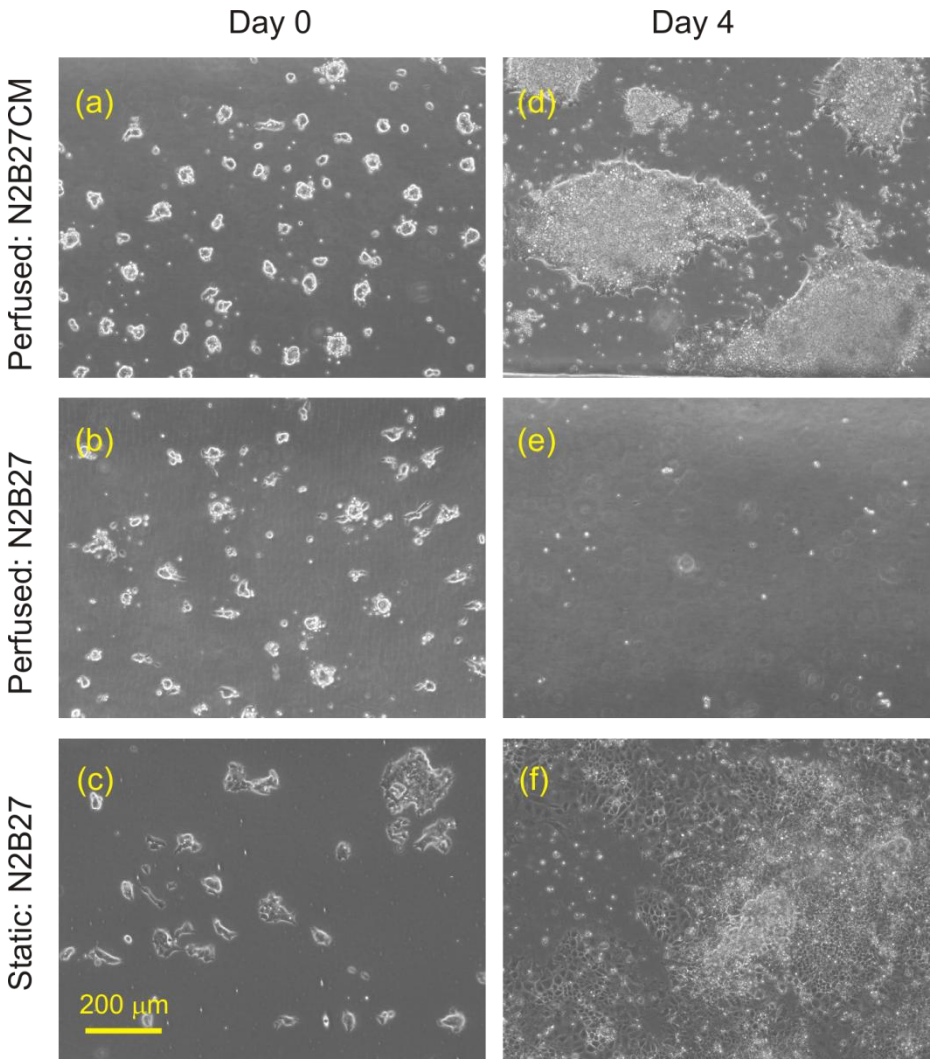

Figure 5.7: Microfluidic perfusion culture of 46C mESCs in N2B27 and N2B27 conditioned media, compared with static culture in N2B27. (a)-(c) show typical colonies on day 0 before perfusion begins. (d)-(f) show results after 4 days of perfusion (d,e) or static (f) culture. All photos are the same scale.

Although we performed the same procedure each time, variations in cell attachment caused some variation in the results, summarized in Figure 5.8, which shows results from the perfused N2B27 conditions and Figure 5.9, which shows perfused results in N2B27/CM. The results shown are representative images for each trial, using images from the middle of the 3 chambers for each condition. Overall we found that the middle chamber repeatedly had the best initial attachment and overall results, while the cell attachment and proliferation in the outer two channels was usually worse. In general, we found that achieving successful attachment was more challenging in serum-free conditions than in the experiments in Chapter 4. These figures give a general sense of the amount of variability from trial to trial and also indicate the influence of initial attachment on the day 5 results. The trials are numbered consistently in both Figure 5.8 and Figure 5.9; that is, Trial 1 in both figures refers to the same experiment, with the N2B27 on one side of the side-by-side device, and with the N2B27/CM condition on the other side of the device.

Figure 5.8 shows that in all four trials, there was indeed no cell proliferation observed on day 5 despite attachment seen on day 0 in all trials. Not only was there no proliferation, but the cells seen on day 0 seem to have died or disappeared, leaving only debris.

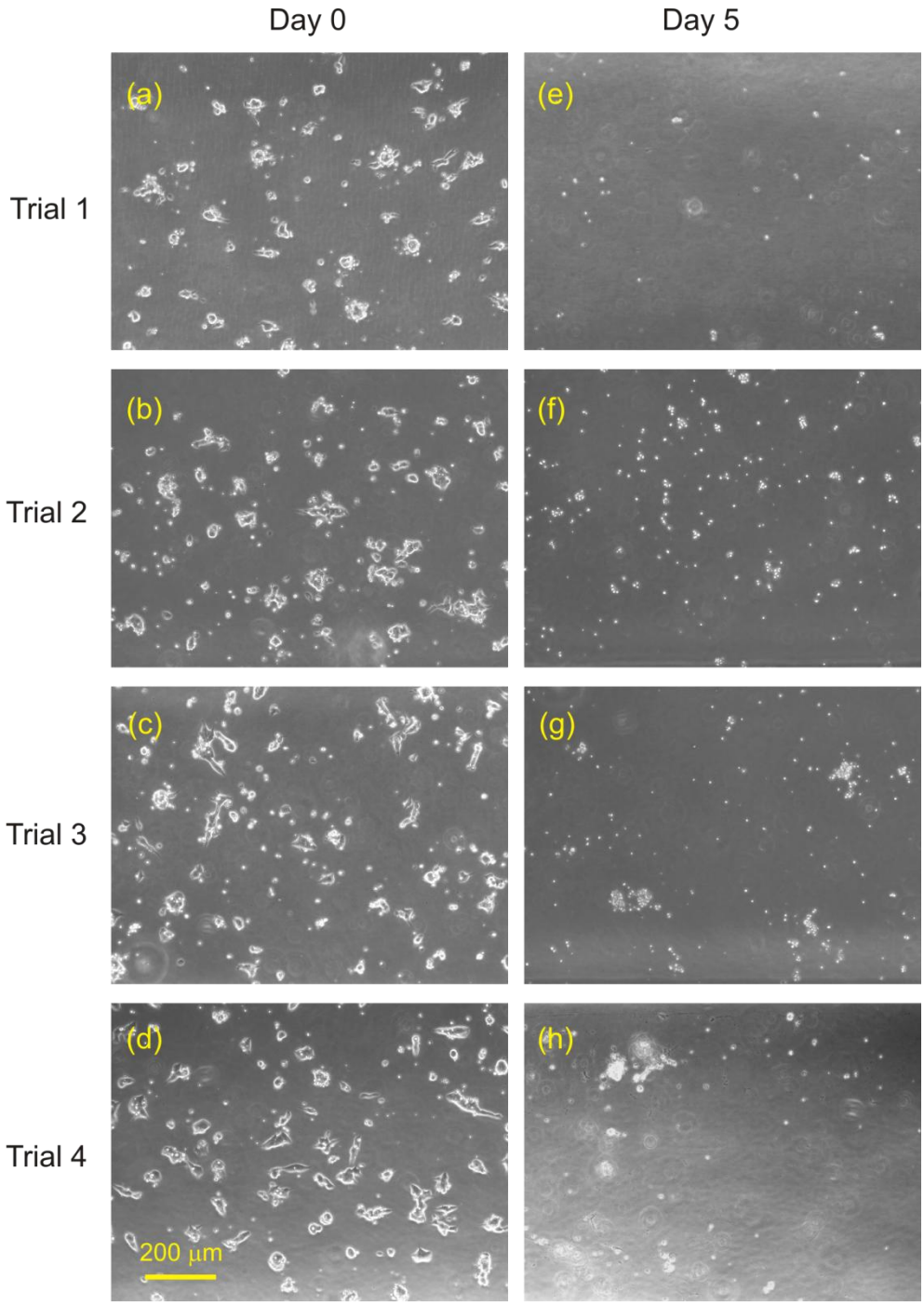

Figure 5.8: Microfludic perfusion culture of mESCs in serum-free N2B27 neuronal differentiation medium. (a)-(d) show cells from four repeated trials on day 0, before perfusion had started. (e)-(h) show images of those same fields of view after four days of perfusion. All photos are the same scale.

Figure 5.9 shows the amount of variability in the N2B27/CM results. Here we see there was significant proliferation in Trials 1,3, and 4. Trial 2 showed poor proliferation on day 5. A possible explanation for this is the low density on day 0, seen in Figure 5.9(b). It is possible that there is a threshold for the level of endogenous factors required to maintain cell survival and proliferation. In this hypothesis, cell survival may have resulted from a combination of adequate initial cell density with the additional factors delivered by the conditioned media. This hypothesis could be tested by performing repeated experiments using different cell densities and conditioned media concentrations. From Figure 5.9 we also see that the amount of proliferation and colony morphologies differ from trial to trial. Trials 3 and 4 show confluent cultures at day 5, whereas Trial 1 shows smaller colonies. One possible explanation for this is that the initial colonies in Figure 5.9(a) are rounder and less spread-out compared with those in Figure 5.9(c) and Figure 5.9(d), perhaps corresponding to the smaller colonies in (e) compared with the confluent growth in (g) and (h). Despite these variations, the results clearly indicate that the addition of N2B27/CM is able to restore cell survival and proliferation when compared with mESCs perfused in N2B27 alone.

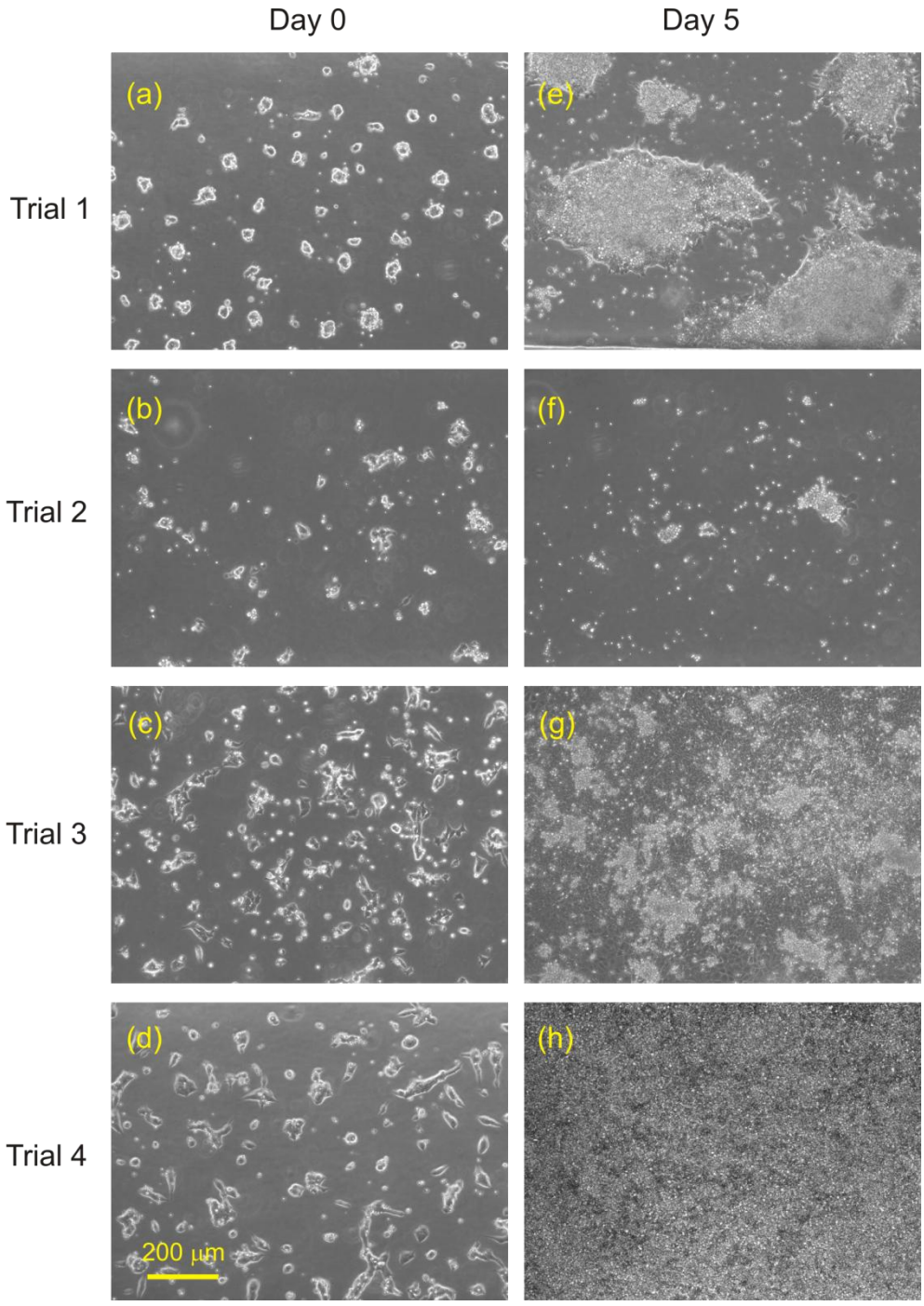

Figure 5.9: Microfluidic perfusion culture of mESCs in N2B27 conditioned media. (a)-(d) show cells from four repeated trials on day 0, before perfusion had started. (e)-(h) show images of those same fields of view after four days of perfusion. Photographs were taken from middle field of the middle channel for each trial, which was a representative image. All photos are the same scale.

Finally, in a separate experiment, we also observed expression of the Sox-1 GFP reporter in day 7 cultures perfused in N2B27/CM media when cultured under the same conditions, side-by-side with mESCs cultured in GMEM-based ES media which did not express measureable GFP

(Figure 5.10). Interestingly, the emergence of the Sox-1 signal on day 7 was delayed when compared to static neuronal differentiation, where we observed measurable Sox-1 signal as early as day 4-5. Throughout the entire experiment we perfused with conditioned media collected from day 2-3, and it is possible this may have affected the timing of the appearance of the Sox-1 signal. These results strongly suggest that not only can N2B27/CM restore proliferation of the mESC culture, but that the perfused N2B27/CM condition is sufficient to induce neuronal differentiation.

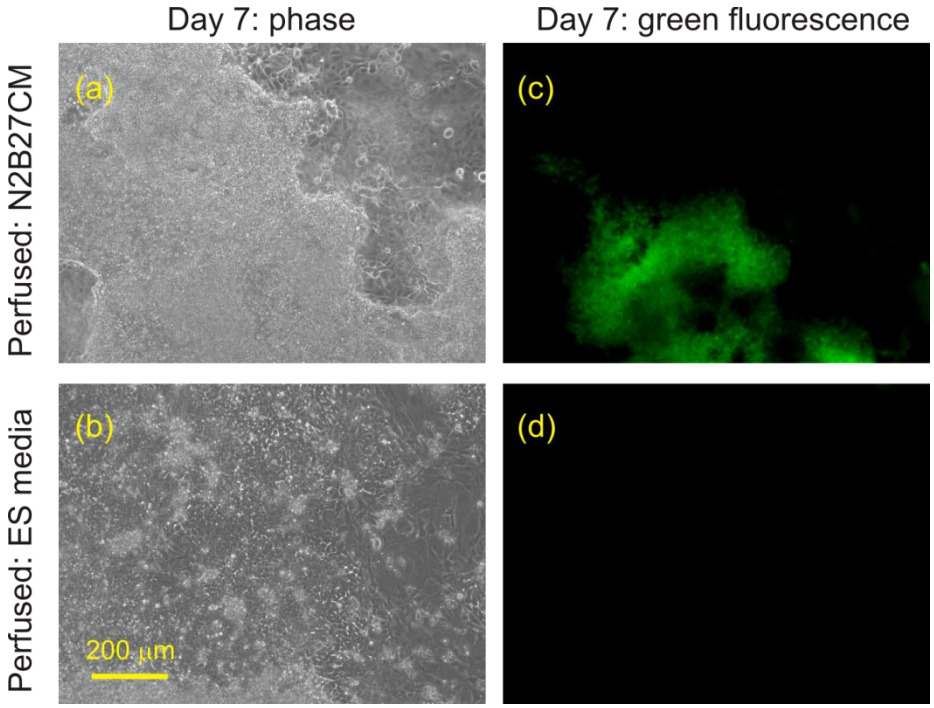

Figure 5.10: Expression of Sox-1 GFP reporter in 46C mESCs on day 7 in perfusion culture. (a,c) show phase and fluorescence results in N2B27 CM media, while (b,d) show results for cells perfused with GMEM-based ES-media as a control. Fluorescence images were taken using the same exposure times and were processed using the same procedures. Comparing (c) and (d), we observe measurable Sox-1 GFP expression in the N2B27 CM culture, indicating neuronal differentiation. All photos are the same scale.

5.3.4 Perfusion culture of mESCs in serum-free N2B27+LIF+BMP4

The results of section 5.3.3 imply that perfusion culture of mESCs in N2B27 alone is not sufficient for cell survival and proliferation, suggesting that there are diffusible secreted factors essential to survival/proliferation. The next question: what are these factors? As discussed in Chapter 1, N2B27 is a base media which, on its own causes neuronal differentiation in static culture[17], but when LIF and BMP4 are added to N2B27, the N2B27+LIF+BMP4 combination is sufficient to inhibit neuronal as well as mesodermal/endodermal fates and direct cells to maintain pluripotency in the absence of serum[9]. In other words, N2B27+LIF+BMP4 has been established as a serum-free medium sufficient for self-renewal of mESCs in static culture. For this reason, I proceeded to investigate whether adding LIF (10 ng/ml) and BMP4 (10 ng/ml) would restore the

perfusion culture such that comparable results would be seen in perfused and static samples. Such an experiment would test two things at once: 1) whether N2B27+LIF+BMP4 was a sufficient medium for mESC self-renewal in perfusion culture at typical densities and 2) whether the addition of LIF and BMP4, both of which are known to be secreted by mESCs, would cause the cells to survive.

To investigate this, I seeded 46C cells that had been routinely cultured in serum-containing GMEM-based ES media into that same media into the microfluidic 2×3 side-by-side device and in static 6-well plates. I seeded in serum-containing GMEM-based ES media because results from section 0 had shown that obtaining good cell attachment was more challenging in serum-free condition. On day 0, I began perfusing one side of the 2×3 device with N2B27+LIF+BMP4, and the other side with N2B27+LIF+BMP4/Serum (a mixture of 1 part serum to 9 parts N2B27+LIF+BMP4), and continued perfusing until day 4. The purpose for perfusing serum-containing media on one side of the chip was to provide a known control condition. The results from Chapter 2-3 had demonstrated mESC perfusion culture in serum-containing media., therefore it was expected that the cells in this condition should proliferate.

I repeated this experiment four times, and a representative result is shown in Figure 5.11. Given good attachment on day 0, the perfused N2B27+LIF+BMP4/serum condition (Figure 5.11(d)) produced proliferation on day 4 comparable to static controls in serum-free media (Figure 5.11(f)) as expected. The serum-free perfused condition (Figure 5.11(e)) did show some small colonies, which was more than was seen in the experiments involving perfused N2B27, but with nowhere near the same proliferation as seen in static or serum-containing conditions. Therefore, these results show that N2B27+LIF+BMP4 is not a sufficient medium for serum-free perfusion culture of mESCs, and that there are significant autocrine/paracrine effects related to the survival/proliferation of mESCs in static, serum-free culture.

As in the neuronal differentiation experiments, I found that in general, the best attachment and most consistent results were again found in the middle chamber. I repeated this experiment four times (data not shown) with similar results. In one of the trials that had a slightly higher initial seeding density and excellent initial attachment, I did observe regions of proliferation in perfused N2B27+LIF+BMP4 that were comparable to static culture. Interestingly, these regions were located in the downstream section of the channel. It is not known whether there was some altered flow condition that caused these results, but it may be possible that if mESCs were cultured at a higher density, proliferation would occur even in perfused serum-free conditions. It is also of note that the experiments in this section differ from those of section 5.3.3 in that the cells were seeded in serum-containing media (to alleviate attachment issues), which may have increased the survival rate of the cells when compared to the N2B27 experiments, in which they were seeded in N2B27+LIF.

I also repeated this experiment once using ABJ1 mESCs, with similar results (data not shown), implying that this phenomenon is not restricted to the 46C line of mESCs.

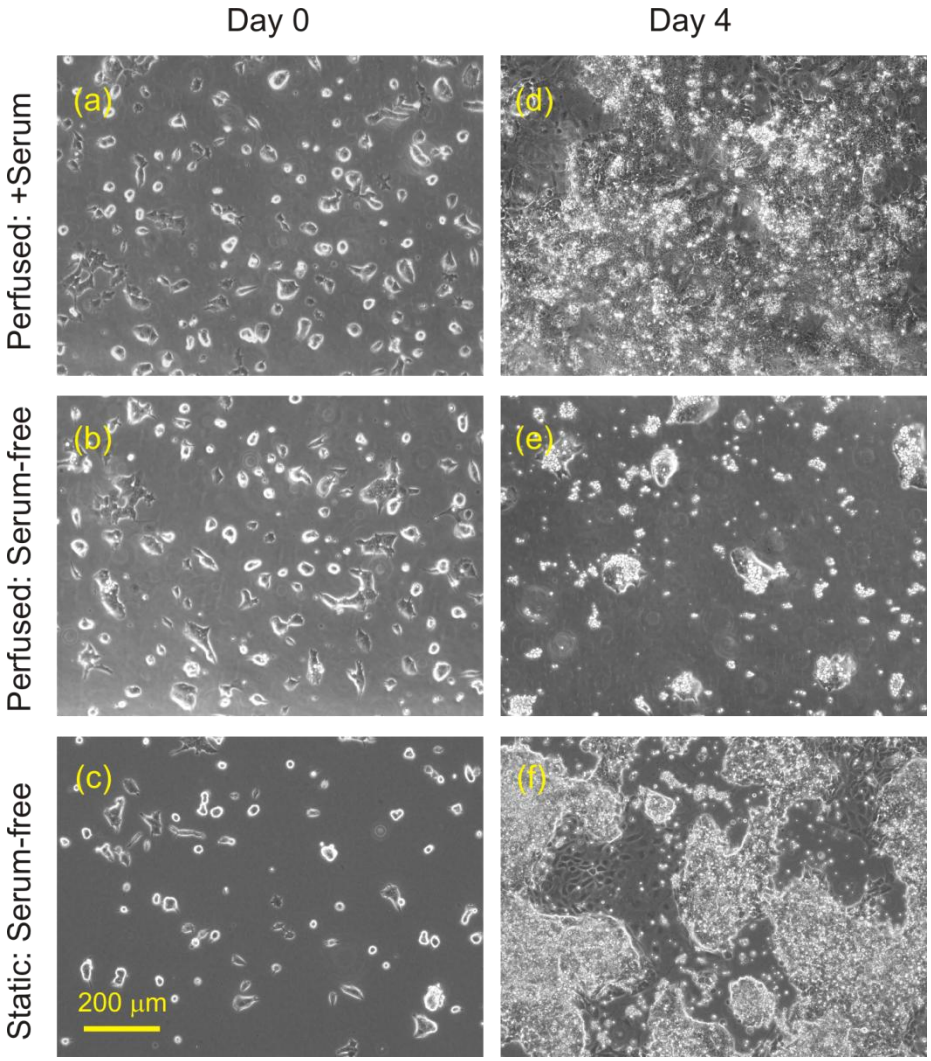

Figure 5.11: Microfluidic perfusion culture of 46C mESCs in serum-free N2B27+LIF+BMP4 and Defined ES media + serum. (a)-(c) show typical colonies on day 0 before perfusion begins. (d)-(f) show results after 4 days of perfusion (d,e) or static (f) culture. Although some colonies exist in perfused, serum-free culture (3), they are fewer and smaller when compared with results in perfused serum-containing culture (d) or static, serum-free culture (f). All photos are the same scale.

5.4 Discussion

5.4.1 2×3 side-by-side device design

The 2×3 device incorporated the advantageous features of the 1×6 valved logarithmic device in Chapter 4, such as an active debubbler, higher-ceiling chambers, selective seeding within the culture channels, and culture on a polystyrene substrate. It achieved the goal of enabling side-by-side culture of mESCs under two conditions on the same device, with convenient simultaneous loading of both sides at once, and relatively bubble-free operation. In addition, this device design was flexible enough to enable other applications not used here: culture of different cell types/densities on each side, perfusing at different flow rates on each side, etc. However, the design also inherited the packaging system of the 1×6 valved device involving hand-adjusted

clamping of the PDMS microfluidics to the polystyrene base. The variability of this clamping seemed to affect the success rate of cell attachment, and this was even more pronounced in the serum-free studies in this chapter, despite the use of gelatin to condition the surface before seeding cells. It is unknown why for all the serum-free experiments, better attachment and repeatability were found in the middle of the three chambers. As in Chapter 4, one possible explanation is that thermal expansion/contraction of the PDMS relative to the polystyrene base may have preferentially caused motion or disruption in the outer chambers, whereas the middle chambers were less affected because of their location. Indeed, in failed experiments where cells did not attach in any chambers, we often observed a repeatable pattern of unattached cells in the outer chambers that had migrated toward the center, whereas the cells in the center were evenly spaced (although still not well attached). This implies a physical disruption of cells in the outer chambers, even before starting perfusion that was not observed to the same extent in the middle chambers. As with the valved devices in the previous chapter, developing improved methods for attaching the PDMS upper to the polystyrene is an area for future work.

5.4.2 Demonstrating LIF is removed by flow

The results of sections 5.1 and 5.3.2 strongly suggest that when culturing cells under typical flow rates established in Chapters 2-4, it is possible for secreted factors such as LIF to be removed by the flow. Although there were several assumptions made in estimating the spatial range of signaling, the overall result that secreted LIF could travel far enough from the cell surface to be swept away in convection-dominated transport was confirmed by the experimental results of section 5.3.2. Measureable quantities of LIF were found at the output of a perfused microfluidic mESC culture which had been perfused with LIF-free ES media. Regardless of whether this LIF was generated solely by the cells or was a combination of cell-generated and residual LIF in the system, these results showed the perfusion culture can sweep away LIF.

Because of the many assumptions used here (for example, the assumption that the cell number stayed constant over the entire 2-day assay), it is difficult to make conclusions about the actual net LIF secretion/uptake rate in perfused vs. static systems. Although at first glance, one may think that the data indicates net LIF secretion is greater in perfused vs. static cultures, more work would need to be done to establish this. For example, the numbers in Figure 5.4 are based on the initial cell seeding number in both static and perfused conditions. It is possible that proliferation in the perfused condition was higher, thus explaining the higher amount of LIF collected per initial cell compared with static. It is also possible that secreted factor production and uptake are both affected. Therefore, the main conclusion to be drawn from this experiment is simply, but profoundly, that microfluidic perfusion can remove secreted factors from a typical culture. Investigating the exact net LIF production per cell and the balance of secretion vs. uptake (for example, the number of LIF receptors expressed at the cell surface) is an area for future work.

Although these results have been found in the specific case of the ligand LIF, since many other secreted factors such as FGF and BMP have similar characteristics (diffusivity, binding constants), it is reasonable to assume this phenomenon extends to other secreted factors as well. However, secreted factors such as Wnt signaling molecules which have a high propensity to bind to the ECM[2] are less likely to be affected. Likewise, secreted factors which have an especially high affinity for their corresponding receptors (and/or situations where there is an extremely high

receptor density) will have a shorter spatial range of signaling (assuming the same diffusivity) and may bind locally before they have a chance to move away from the walls of the channel and be swept into the flow. Therefore, in general, we would expect diffusible signaling to be affected by flow in cases where the ligand/receptor binding state is such that secreted ligands regularly travel far enough from the cells that they are swept away before they can bind. As mentioned earlier, the device must be operated in a flow regime that a) sustains cell culture by avoiding nutrient depletion as well as shear effects b) effects a large local Peclet number, such that transport of ligands is convection-dominated when estimated using the spatial range of signaling for the particular ligand.

5.4.3 Serum-free neuronal differentiation in perfusion

The results of the side-by-side perfusion culture of 46C mESCs with N2B27 vs. N2B27/CM suggest that there exist molecules that are not present in N2B27 that are required for colony survival and proliferation, but that are present in N2B27/CM. Because both sides of the perfused culture experience the same flow rates, and because the N2B27/CM media was replenished with fresh N2B27, it is unlikely that nutrient-related or shear-related effects played a significant role in this phenomenon.

Which molecules in the N2B27/CM media enabled the proliferation of the cells? Because the N2B27/CM was not strictly dialyzed, but was composed of concentrated conditioned media that was replenished with full-strength N2B27 to reach the original concentration, it contained not only all secreted factors > 3 kDa, but also may have doubled the strength of large molecules in the original N2B27 formulation, such as BSA, insulin, or transferrin. While it is theoretically possible that these N2B27-originating molecules may have affected colony establishment and proliferation, this possibility is unlikely. In static culture, mESCs survive and proliferate under a wide variety of different media formulations, including different levels of BSA, insulin, and transferrin. For example, in the work for this thesis I experimented with three variations of the N2B27 formula, all with different amounts of insulin and transferrin. Although I did observe different levels of differentiation using the different formulations, none of the N2B27 formulas caused any problem with cell survival and proliferation. However, to be strictly certain that cell-secreted factors were the main difference in the behavior of the N2B27-perfused vs. the N2B27/CM-perfused cells, one could repeat these experiments but mix the concentrated conditioned media with large-molecule-depleted N2B27.

The conclusion that cell-secreted factors may be essential in establishing mESC survival and proliferation in neuronal differentiation agrees with the general observations from the literature that it can be difficult to establish mESC cultures at very low densities[5, 11]. In particular, Ying *et al.* who developed the N2B27 neuronal differentiation protocol also observed difficulty establishing cultures at low plating densities, suggesting that autocrine/paracrine factors may be necessary for cell survival and attachment. Furthermore, Austin Smith's group has shown that autocrine signaling via FGF4 is necessary for neuronal differentiation[17]. Although autocrine factors for survival/proliferation may be different from those specifying neural commitment, it is possible that FGF4 may also play a role in establishing mESC survival and proliferation in N2B27.

5.4.4 Serum-free self-renewal in perfusion: adding LIF+BMP4

Again, the results from the side-by-side perfusion of mESCs with N2B27+LIF+BMP4 compared with serum-added N2B27+LIF+BMP4 strongly suggest that there exist molecules not present in N2B27+LIF+BMP4 that are required for cell survival and/or proliferation. Again, because mESCs in static culture can proliferate in N2B27+LIF+BMP4 alone, this suggests that necessary cell-secreted factors present in static culture have been removed in perfusion culture. The restoration of the perfused culture with the addition of 10% serum implies that serum contains some factors which are able to overcome the loss of the cell-secreted factors to establish a proliferating culture. However, it remains unknown what specific factors in the serum may be causing this effect, and also whether they are the same as the cell-secreted factors that may have been removed by flow.

In particular, recent work from the lab of Hitoshi Niwa has demonstrated that activin-Nodal signaling plays an important role in mESC propagation in serum-free culture[100]. Ogawa *et al.*[100] found that in serum-free media, when activin-Nodal signaling was inhibited, proliferation dramatically decreased (but pluripotency remained the same). When they supplemented serum-free mESC culture with recombinant activin and Nodal (both members of the TGF-β superfamily of cytokines)[5], cell proliferation increased while maintaining pluripotency. They also found that autocrine activin-Nodal signaling was constitutively on in serum-free culture of mESCs. Interestingly, they found that neither TGF-β nor BMP increased proliferation without affecting pluripotency. These findings fit with our observations that adding BMP4 did not improve cell survival/proliferation. Therefore, it may be interesting in future work to add activin or Nodal to the N2B27 or N2B27+LIF+BMP4 media formulations and observe whether this restores cell proliferation in serum-free perfusion.

Finally, we also observed that in one higher-density, downstream case, we did see greater proliferation, comparable to that in static culture. If we also look at the Trial 2 result from Figure 5.9(b,f), it is possible that the initial seeding density in perfusion has an effect on colony proliferation. These preliminary observations suggest that by adjusting the plating density/perfusion rate, we may see a variety of proliferation effects.

5.5 Chapter Summary

Both the modeling and experimental results from this chapter strongly suggest that microfluidic perfusion culture performed at typical flow rates can remove secreted factors such as LIF from the soluble microenvironment. Using a custom-developed side-by-side, valved microfluidic perfusion device, we found results that strongly support the idea that perfusion does affect the soluble microenvironment of mESCs in a biologically significant way, making serum-free culture that is possible in static conditions, unsupportable at equivalent densities in perfusion. Specifically, we found that neither N2B27 nor N2B27+LIF+BMP4 alone were sufficient for perfusion culture at typical densities, while using N2B27/CM or serum-added media restored the culture. Finally, for the first time, we demonstrated neuronal differentiation of mESCs in microfluidic perfusion using conditioned media. This works sets the stage for using microfluidic perfusion as a tool to investigate autocrine/paracrine signaling in mESCs and other adherent cells.

Chapter 6. Conclusions

6.1 Thesis Contributions

In this thesis I have contributed to both the biomicrosystems community as well as to the stem cell community. The main contributions of this thesis: 1) the development of microfluidic systems tailored to meet the needs of biological experimentation 2) the establishment and characterization of conditions for successful microfluidic perfusion culture of mESCs, 3) the demonstration of the concept that perfusion culture can significantly affect diffusible cell-cell signaling in the soluble microenvironment, and thus the cell's biological state 4) the confirmation that autocrine/paracrine loops are important for establishment of mESCs in serum-free culture (both in self-renewal and neuronal differentiation conditions). These contributions establish a new type of experimental tool for probing autocrine signaling in mESC culture. Although the work I have done in this thesis has focused on mouse embryonic stem cells, this experimental approach could be applied to any adherent cell type.

Microfluidic devices
While the fabrication of the devices in this thesis was based on existing techniques, the device designs were novel and specifically addressed the needs of biological research. I developed and characterized two novel microfluidic devices (1×4 and 1×6) for culturing adherent cells over a logarithmic range of flow rates. This type of device is useful because it enables application of a wide range of flow rates in a single experiment. While logarithmic ranges are commonly used in biology, they have been less commonly incorporated into engineered devices. In particular, the 1×6 valved logarithmic flow-rate device also enabled quantitative characterization of mESC proliferation by incorporating valves for selectively seeding cells and long culture channels for improved observation of potential effects of media depletion. I also developed a 2×3 microfluidic culture device that enabled the incorporation of a control condition on the same device as the test condition. As with the logarithmic flow-rate devices, the incorporation of a simultaneous, on-chip control condition is another feature that takes into account the needs of the specific biological application.

Microfluidic culture of mESCs
I established the first demonstration of sufficient conditions for successful microfluidic perfusion culture of mESCs (D3 and ABJ1 lines). While there are examples of culturing other cell types (fibroblasts, myoblasts, neural cells) in microfluidic perfusion, mESCs, especially monocultured mESCs, are significantly more challenging to culture in microfluidic perfusion and require specific protocols to achieve success. To date, this work remains the only demonstration of mESC self-renewal in microfluidic perfusion, and paves the way for further work in mESC microfluidic perfusion.

Using a custom logarithmic flow-rate device, I found an optimal flow-rate range for mESC proliferation and characterized the dependence of mESC proliferation on flow rate and location within the channel. I then investigated the role of glucose depletion in generating these proliferation patterns by first developing a basic model of mESC glucose consumption and cell proliferation. The results give insight into how the proliferation patterns may have developed,

although other mechanisms may be involved. This thesis establishes a basis for further investigation into how perfusion culture conditions affect basic mESC proliferation and culture.

Many practical aspects were involved in achieving successful culture of mESCs on chip. In addition to finding an optimal flow-rate range for proliferation, I also developed and incorporated methods for assembly of a sterile microfluidic system, methods for bubble-free loading of cells at a uniform density throughout the device, methods for achieving cell attachment, and methods for maintaining a bubble-free system throughout a multi-day experiment. I included many of these techniques in the paper "A practical guide to microfluidic perfusion culture of adherent cells"[86] to make this knowledge available to the community.

Effect of perfusion culture on mESC soluble microenvironment and biology
Finally, I showed that continuous, non-recirculating perfusion can be used as a tool for modulating diffusible cell-cell signaling, and can have significant effects on the biological state mESCs in serum-free self-renewal and differentiation conditions. Using both modeling and experiments, I showed for the first time that microfluidic perfusion culture performed at typical flow rates can remove secreted factors such as LIF. Our results strongly suggest that enough diffusible factors are removed that perfusion does affect mESC culture, making serum-free culture that is possible in static conditions, unsupportable at equivalent densities in perfusion. Specifically, we found that neither N2B27 nor N2B27+LIF+BMP4 alone are sufficient for perfusion culture at typical densities, while using enhanced media (N2B27/CM or N2B27+LIF+BMP4/serum) restored proliferation to be comparable to static conditions. Because all perfused conditions experienced the same mechanical forces and similar nutrient content, the observed results are likely due to differences in the large molecule content of the perfused environments. These results imply that autocrine/paracrine loops are important for establishment of mESCs in serum-free culture in N2B27 and N2B27+LIF+BMP4.

Additionally, we performed the first demonstration of neuronal differentiation of mESCs in microfluidic perfusion using conditioned media. This work opens up new questions on the role of paracrine signaling in mESC self-renewal and differentiation, on what particular large molecules caused the effects observed, and sets the stage for using microfluidic perfusion as a tool to investigate paracrine signaling. Although I have focused on diffusible signaling in mESCs, the methods developed here are more general and could work other adherent cell types.

6.2 Outlook, challenges, and future work

6.2.1 Technological directions

Cell attachment
The main practical issue I encountered throughout the experimental work was the challenge of achieving consistent cell attachment, especially under serum-free conditions. Although the measures I took (using a polystyrene substrate, seeding in serum-containing media, allowing longer times for static attachment in serum-free media, tightening the clamps only during the attachment period) did improve attachment, there was still a great enough failure rate such that for every one successful experiment, roughly two failed due to attachment issues.

The first step toward improving cell attachment would be to perform experiments to understand the cause of variable attachment. Because the substrate surface and preparation of the cell suspension were the same for both perfused and static samples, it is unlikely that either of these caused the variable attachment. Our current hypothesis is that thermal expansion/contraction of the PDMS microfluidic block relative to the polystyrene base caused mechanical disturbance when culturing cells in clamped setups. Preliminary evidence for this hypothesis: 1) the cell migration patterns observed during failed experiments are consistent with the hypothesis 2) these cell migration patterns were observed only in clamped devices 3) when care was taken to maintain the setup at 37°C at all times, even during cell loading (using a heated microscope stage incubator), attachment problems were minimized 4) tightening clamping during attachment minimized attachment problems. Salil Desai and Katarina Blagovic in our lab are currently investigating the technique of patterning polystyrene on glass to create bondable devices that maintain a polystyrene base for culturing cells. They are currently characterizing how the patterned polystyrene surfaces compare to standard tissue-culture polystyrene surfaces such as Nunclon Δ.

Integrating perfusion culture with other microsystems
Another direction for the technology is to create methods for combining perfusion culture with other microsystems tools to enable further control over the cell-culture microenvironment or to enable microscale sensing. For example, our lab has developed several methods for cell patterning to create fine control over cell-cell contact[33, 36, 101]. Combination of these methods with perfusion culture could enable investigation of the role of diffusible signaling vs. direct cell-cell contact.

Because of the generally small numbers of cells used in microfluidic cultures, there is currently a mismatch between the ability to grow small numbers of cells on a device and the ability to quantitatively gather information from these cells *in situ*. Currently, imaging-based methods continue to grow in sophistication, both in methods for quantification and sensors[15]. However, in addition to improving image-based assays, it is also possible to directly integrate technologies such as PCR and ELISA into microfluidic devices[102]. Another direction for future work involves integrating microfluidic perfusion culture with such assays. Our lab is looking into a collaboration with Professors Jongyoon Han and Paula Hammond at MIT to develop devices that marry cell culture on chip with preconcentration and protein detection via an integrated ELISA. This type of device could perform more sensitive measurements over time of the net LIF production per cell.

6.2.2 Biological directions

Perfusion culture and nutrient delivery
Although the results presented here provide evidence that glucose depletion may affect proliferation of mESCs in microfluidic perfusion culture, the role of glucose could be investigated in more detail. As mentioned earlier, while it is known that culturing cells in perfused environments may change net uptake rates, it is not clear how the glucose uptake rate compares in perfused vs. static cultures, and if the uptake rate is different, what the mechanism is for creating this difference (for example, increased expression of glucose transporters at the

surface of the cell). As mentioned in Chapter 4, it may be possible to incubate cells in the presence of a fluorescent, non-cleavable glucose analog (2-NBDG) to monitor glucose uptake[95]. It would be an especially interesting approach to directly monitor glucose uptake in situ, such that the fluorescence could be monitored while preserving the spatial information of cell location. In addition, Tonack *et al*.[89] used immunohistochemical staining to assess expression of glucose transporter (GLUT) isoforms in differentiating mESCs. It may be interesting to also use this experimental technique to investigate whether GLUT expression is changed in perfusion culture.

It is also possible and likely that other mechanisms, such as concentration of diffusible growth factors, may be involved in explaining the proliferation patterns observed. There is evidence that culturing mESCs at higher densities encourages growth[11], however, there is also evidence that culturing mESCs in perfusion (albeit recirculating), which may remove or dilute growth factors, can also enhance proliferation[18]. It is possible and likely that these mechanisms are happening simultaneously, and that the overall level of proliferation depends on the balance of nutrient delivery and autocrine growth factor conditions. One hypothesis would be that high perfusion rates may remove secreted growth factors but increase glucose uptake. It is possible that the necessary growth factors are removed by perfusion but redelivered via serum-containing media. Investigating this leads to the next topic of further work on serum-free perfusion culture.

6.2.3 Serum-free neuronal differentiation and self-renewal

The results from Chapter 5 strongly suggest that cell-secreted factors missing from the N2B27 and N2B27+LIF+BMP4 formulation are necessary for establishment of mESCs in perfusion culture. To gather more evidence, the next step could be to repeat both differentiation and self-renewal experiments using traditionally dialyzed conditioned media. In this way, we could be certain that the addition or subtraction of only the cell-secreted molecules was causing the failure to proliferate.

However, as discussed in Chapter 5, it is unlikely that small changes in the nutritional content caused the significant failure in the ability of the mESCs to proliferate in perfusion at typical densities. If we assume that cell-secreted factors missing from N2B27+LIF+BMP4 are responsible for the different results in perfused vs. static cultures, there are two basic questions: 1) which factors are required to simply have the cells *survive and proliferate* and 2) which additional factors are necessary to reach levels of *neuronal differentiation / serum-free self-renewal* that are comparable to those in static conditions? In addition, these two questions generate a host of sub-questions, for example, if a minimal set of factors in defined media is found to support proliferation in perfused culture, are these the same factors that play the critical role in static culture? What downstream pathways are activated by these factors, and what levels (or combinations of levels) of different factors are required to create these conditions? When the colonies fail to proliferate in N2B27 or N2B27+LIF+BMP4 alone, what mechanisms cause this failure? Is it truly a failure to proliferate, or is it that the cells simply cannot survive, let alone proliferate, in that condition? Preliminary evidence would suggest that it may be a matter of survival, since the initially well-attached cells seem to vanish by day 4.

What are potential strategies for identifying these factors? One possibility would be to perform a proteomic analysis on the N2B27-based, mESC-conditioned media to identify potential cell-secreted factors[10]. However, because these methods tend to generate long lists of factors, it would still be necessary to narrow down the search to tease out which of the factors were responsible for the effects seen in Chapter 5.

As mentioned in Chapter 5, some candidates include members of the TGF-β superfamily of cytokines and basic fibroblast growth factor (FGF) as well as FGF4[5]. The work by Ogawa *et al.*[100] in demonstrating the role of activin-Nodal in mESC proliferation in serum-free conditions is compelling and suggests activin-Nodal would be a prime candidate for initial studies. One approach would be to first perfuse groups of factors (added to N2B27 or N2B27+LIF+BMP4) to determine whether they contained the necessary subset, then to tease out which individual combinations might produce a sufficient defined media for perfusion culture.

Appendix A: COMSOL scripts for glucose modeling

Initialization file: init_run.m

```
% Custom definitions
dt=60*60*4;                 % (sec) Total duration of one time-dependent
solver run
dt_attachment=60*60*4;      % (sec) Total duration of one time-dependent
solver run (static attachment period)
femtimestep=60*5;           % (sec) Timestep used by time-dependent solver
during one solver run

solverruns_init=ceil(dt_attachment./dt);% Number of solver runs (static
attachment period)
solverruns_perf=ceil(60*60*(24*3)./dt); % Number of solver runs (perfusion)

day1index=ceil(60*60*(24*1)./dt);
day2index=ceil(60*60*(24*2)./dt);
day3index=ceil(60*60*(24*3)./dt);

DensityVector=[0.5e6 1.5e6 3e6 6e6].*0.025.*1e4;          % (cells/m^2) Areal
cell density
ncoeff=0.87e-6;              % Fitting parameter related to cell
proliferation magnitude
prolif_x=[0 5 10 25 50];    % (mM) glucose concentrations from J. Cell.
Physiol. Vol.209, 1 Pages: 94-102
prolif_y=[-2 6 7 10.5 8.1]; % dNdt from J. Cell. Physiol. Vol.209, 1 Pages:
94-102
GlucoseArray={'5.56' '25'}; % Glucose concentration (mM=mol/m3)
VelocityArray={'1.4730e-007' '6.2605e-007' '2.6607e-006' '1.1308e-005'
'4.8059e-005' '2.0425e-004'}; % (m/s) Max velocity
HeightArray={'50e-6' '125e-6' '250e-6' '500e-6'};    % (m) Channel height
LengthArray={'.03'};    % (m) Channel length
lengthindex=1;
heightindex=3;
densityindex=2;

% Choose interpolation method for proliferation function
fittedmodel=fit(prolif_x',prolif_y',fitmethod);

% Run static culture glucose depletion simulations
glucoseindex=1;             % Low Glucose
d3glucose_coupled_attachment;
glucoseindex=2;             % High Glucose
d3glucose_coupled_attachment;

% For each velocity (1-6) run perfusion culture glucose depletion simulation
for velocityindex=1:6,
    for glucoseindex=1:2,
        d3glucose_coupled_perfusion;
        velocityindex
    end
end
```

COMSOL script file for static attachment period: d3glucose_coupled_attachment.m

```
% COMSOL Multiphysics Model M-file
% Generated by COMSOL 3.2 (COMSOL 3.2.0.222, $Date: 2005/09/01 18:02:30 $)

flclear fem
pause(5)

% COMSOL version
clear vrsn
vrsn.name = 'COMSOL 3.2';
vrsn.ext = '';
vrsn.major = 0;
vrsn.build = 222;
vrsn.rcs = '$Name:  $';
vrsn.date = '$Date: 2005/09/01 18:02:30 $';
fem.version = vrsn;

n0=DensityVector(densityindex);
GlucoseString=char(GlucoseArray(glucoseindex))
HeightString=char(HeightArray(heightindex));           % Retrieve height
string
LengthString=char(LengthArray(lengthindex));
channel_height=eval(HeightString);
channel_length=eval(LengthString);

% Constants
fem.const = {'D','9e-10', ...       % Diffusivity of glucose (m2/s) from
David Cochran paper
    'c0',GlucoseString, ...         % Media glucose concentration
(mM=mol/m3))
    'Qg','1.95e-14/(3600)', ...     % Glucose consumption rate m3/(cell*sec)
    'molw','180.16', ...            % Molecular weight glucose (g/mol)
    'kads','Qg', ...                % Glucose consumption rate
(m3/(cell*sec))
    'H',HeightString, ...              % Channel height (m)
    'velmax','0'};                  % Max velocity (m/s)

% Geometry
g1=rect2(LengthString,HeightString,'base','corner','pos',{'0','0'},'rot','0')
;    % Channel geometry (m)
s.objs={g1};
s.name={'R1'};
s.tags={'g1'};
fem.draw=struct('s',s);
fem.geom = geomcsg(fem);

% Create mapped quad mesh
fem.mesh=meshmap(fem, ...
    'edgegroups',{{[2],[4],[3],[1]}}, ...
    'edgelem',{1,[0:0.1:1],2,[0:0.002:1],3,[0:0.002:1],4,[0:0.1:1]}, ...
    'hauto',5);

% Write n_new_highinit to file for first iteration
```

```
x0=[0:.0001:channel_length];
y0=zeros(1,length(x0));
n_seedinit=n0.*ones(1,length(x0));
n_new=n_seedinit;
p_boundarywithcells = [x0(:)'; y0(:)'];

delete 'results_temp.mat'
save -v6 'results_temp.mat' n_new x0    % Initialize file

for solverrun_index=1:solverruns_init,
    % Application mode 1
    clear appl
    appl.mode.class = 'FlConvDiff';
    appl.assignsuffix = '_cd';
    clear prop
    prop.analysis='static';
    appl.prop = prop;
    clear bnd
    bnd.type = {'N0','N0','N','N0'};
    bnd.c0 = {0,'c0',0,'c'};
    bnd.N = {0,0,'react_surf',0};
    bnd.ind = [2,3,1,4];
    appl.bnd = bnd;
    clear equ
    equ.D = 'D';
    equ.init='c0';
    equ.u = '0';                              % Static culture (set velocity to
0)
    equ.ind = [1];
    appl.equ = equ;
    fem.appl{1} = appl;
    fem.border = 1;
    fem.outform = 'general';
    fem.units = 'SI';

    % Boundary expression
    bnd.ind = [1,2,1,1];
    bnd.dim = {'c'};
    bnd.expr = {'react_surf',{'','-kads*interpolate_nnew(x)*c'}};
    fem.bnd = bnd;

    % Descriptions
    clear descr
    descr.const= {'D','Diffusivity of glucose (m/s)','velmax','Max velocity
(m/s)','c0','initial concentration (mM)','H','Channel height
(m)','Qg','Glucose consumption rate L/(cell*sec)','dt','Timestep
(s)','kads','Glucose consumption rate (mmol/(cell*sec))','molw','Molecular
weight glucose (g/mol)','n0','Starting cell density (cells/m2)'};
    fem.descr = descr;

    % Multiphysics
    fem=multiphysics(fem);

    % Extend mesh
    fem.xmesh=meshextend(fem);
```

```
    % Solve problem
    fem.sol=femtime(fem, ...
        'solcomp',{'c'}, ...
        'outcomp',{'c'}, ...
        'tlist',[0:femtimestep:dt_attachment], ...n_init
        'tout','tlist');

    % Save current fem structure for restart purposes
    fem0=fem;
    eval(['fem' num2str(solverrun_index) '=fem;']);

    % Save concentration at boundary to create new value of n
    c_boundary(solverrun_index,:)=postinterp(fem,'c',p_boundarywithcells);
    n_save(solverrun_index,:)=n_new;
    dndt=ncoeff.*feval(fittedmodel,c_boundary(solverrun_index,:));
    dndt=dndt';
    n_new=(1+dndt.*dt_attachment).*n_new;
    neg_indices=find(n_new<0)
    n_new(neg_indices)=0;
    n_norm(solverrun_index,:)=n_new./n_seedinit;

    delete 'results_temp.mat'
    save -v6 'results_temp.mat' n_new x0
end

eval(strcat('save -v6 results_init_glucose',num2str(glucoseindex),
'_',fitmethod,'_density',num2str(densityindex),'_height',num2str(heightindex)
,'.mat n_seedinit n_norm n_new x0 fem0'));   % Write static results to file
for cataloging
```

COMSOL script for perfusion culture: d3glucose_coupled_perfusion.m

```
% COMSOL Multiphysics Model M-file
% Generated by COMSOL 3.2 (COMSOL 3.2.0.222, $Date: 2005/09/01 18:02:30 $)

flclear fem
pause(5)

% COMSOL version
clear vrsn
vrsn.name = 'COMSOL 3.2';
vrsn.ext = '';
vrsn.major = 0;
vrsn.build = 222;
vrsn.rcs = '$Name:  $';
vrsn.date = '$Date: 2005/09/01 18:02:30 $';
fem.version = vrsn;

n0=DensityVector(densityindex);
GlucoseString=char(GlucoseArray(glucoseindex));        % Retrieve glucose
string
VelocityString=char(VelocityArray(velocityindex));     % Retrieve velocity
string
HeightString=char(HeightArray(heightindex));           % Retrieve height
string
LengthString=char(LengthArray(lengthindex));
channel_height=eval(HeightString);
channel_length=eval(LengthString);

% Load n_new from static attachment results file for first iteration
eval(strcat('load results_init_glucose',num2str(glucoseindex),
'_',fitmethod,'_density',num2str(densityindex),'_height',num2str(heightindex)
))
n_day0=n_new;
n_norm_day0=n_norm;
clear n_norm
x0=[0:.0001:channel_length];
y0=zeros(1,length(x0));
p_boundarywithcells = [x0(:)'; y0(:)'];

n_seedinit=n0.*ones(1,length(x0));
delete('results_temp.mat')
save -v6 'results_temp.mat' n_new x0  % Write n_new to file for next
iteration

for solverrun_index=1:solverruns_perf,
    flclear fem
    % Constants
    fem.const = {'D','9e-10', ...    % Diffusivity of glucose (m2/s) from
David Cochran paper
        'c0',GlucoseString, ...      % Media glucose concentration
(mM=mol/m3))
        'Qg','1.95e-14/(3600)', ...  % Glucose consumption rate m3/(cell*sec)
        'molw','180.16', ...         % Molecular weight glucose (g/mol)
```

```
        'kads','Qg', ...              % Glucose consumption rate
(m3/(cell*sec))
        'H',HeightString, ...         % Channel height (m)
        'velmax',VelocityString};     % Max velocity (m/s)

    % Geometry
    clear draw s

g1=rect2(LengthString,HeightString,'base','corner','pos',{'0','0'},'rot','0')
;     % Channel geometry (m)
    s.objs={g1};
    s.name={'R1'};
    s.tags={'g1'};
    fem.draw=struct('s',s);
    fem.geom = geomcsg(fem);

    % Create mapped quad mesh
    fem.mesh=meshmap(fem, ...
        'edgegroups',{{[2],[4],[3],[1]}}, ...
        'edgelem',{1,[0:0.1:1],2,[0:0.002:1],3,[0:0.002:1],4,[0:0.1:1]}, ...
        'hauto',5);

    % Application mode 1
    clear appl
    appl.mode.class = 'FlConvDiff';
    appl.assignsuffix = '_cd';
    clear prop
    prop.analysis='static';
    appl.prop = prop;
    clear bnd
    bnd.type = {'N0','C','N','C'};
    bnd.c0 = {0,'c0',0,'c'};
    bnd.N = {0,0,'react_surf',0};
    bnd.ind = [2,3,1,4];
    appl.bnd = bnd;
    clear equ
    equ.D = 'D';
    equ.u = 'velmax*(1-((y-0.5*H)/(0.5*H))^2)';
    equ.ind = [1];
    appl.equ = equ;
    fem.appl{1} = appl;
    fem.border = 1;
    fem.outform = 'general';
    fem.units = 'SI';

    % Boundary expressions
    bnd.ind = [1,2,1,1];
    bnd.dim = {'c'};
    bnd.expr = {'react_surf',{'','-kads*interpolate_nnew(x)*c'}};
    fem.bnd = bnd;

    % Descriptions
    clear descr
    descr.const= {'D','Diffusivity of glucose (m/s)','velmax','Max velocity
(m/s)','c0','initial concentration (mM)','H','Channel height
```

```
(m)','Qg','Glucose consumption rate L/(cell*sec)','dt','Timestep
(s)','kads','Glucose consumption rate (mmol/(cell*sec))','molw','Molecular
weight glucose (g/mol)','n0','Starting cell density (cells/m2)'};
    fem.descr = descr;

    % Multiphysics
    fem=multiphysics(fem);

    % Extend mesh
    fem.xmesh=meshextend(fem);

    % Mapping stored solution to extended mesh (Start new run using
    % solution from previous run
    if  solverrun_index==1,
        solution_number=dt_attachment./femtimestep;
    else
        solution_number=dt./femtimestep;
    end

    init = asseminit(fem, 'init', fem0.sol, 'solnum', solution_number);

    % Solve problem
    fem.sol=femtime(fem, ...
        'init', init, ...
        'solcomp',{'c'}, ...
        'outcomp',{'c'}, ...
        'tlist',[0:femtimestep:dt], ...
        'tout','tlist');

    % Save current fem structure for restart purposes
    fem0=fem;
    eval(['fem' num2str(solverrun_index) '=fem;']);

    % Save concentration at boundary to create new value of n
    c_boundary(solverrun_index,:)=postinterp(fem,'c',p_boundarywithcells,
'solnum', 'end');
    n_save(solverrun_index,:)=n_new;
    dndt=ncoeff.*feval(fittedmodel,c_boundary(solverrun_index,:));
    dndt=dndt';
    n_new=(1+dndt.*dt).*n_new;
    neg_indices=find(n_new<0);
    n_new(neg_indices)=0;
    n_seedinit=n0.*ones(1,length(x0));
    n_norm(solverrun_index,:)=n_new./n_seedinit;

    % Integrate input glucose flux across the cross section
    input_glucose_flux(solverrun_index)=postint(fem,'ntflux_c_cd', ...
        'unit','mol/(m*s)', ...
        'dl',[1], ...
        'edim',1);

    % Integrate output glucose flux across the cross section
    output_glucose_flux(solverrun_index)=postint(fem,'ntflux_c_cd', ...
        'unit','mol/(m*s)', ...
```

```
        'dl',[4], ...
        'edim',1);

    delete 'results_temp.mat'
    save -v6 'results_temp.mat' n_new x0      % Write n_new to file for next
iteration
end

GlucoseVelocityFilename=strcat('
results_glucose',num2str(glucoseindex),'_flowrate',num2str(velocityindex),
'_',fitmethod,'_density',num2str(densityindex),'_height',num2str(heightindex)
,'.mat');
eval(strcat('delete ', GlucoseVelocityFilename));
savestring=strcat('save ',GlucoseVelocityFilename, ' x0 input_glucose_flux
output_glucose_flux n_norm_day0 n_norm fem',num2str(day1index),'
fem',num2str(day2index),' fem',num2str(day3index),' -v6 ');
eval(savestring)
```

Bibliography

1. Lodish, H.B., Arnold; Zipursky, S. Lawrence; Matsudaira, Paul; Baltimore, David; Darnell, James E. Molecular Cell Biology. (W.H. Freeman & Co., 1999).
2. Hsieh, J.C., Rattner, A., Smallwood, P.M. & Nathans, J. Biochemical characterization of Wnt-Frizzled interactions using a soluble, biologically active vertebrate Wnt protein. *Proceedings of the National Academy of Sciences of the United States of America* **96**, 3546-3551 (1999).
3. Shvartsman, S.Y., Wiley, H.S., Deen, W.M. & Lauffenburger, D.A. Spatial Range of Autocrine Signaling: Modeling and Computational Analysis. *Biophys. J.* **81**, 1854-1867 (2001).
4. DeWitt, A.E., Dong, J.Y., Wiley, H.S. & Lauffenburger, D.A. Quantitative analysis of the EGF receptor autocrine system reveals cryptic regulation of cell response by ligand capture. *J Cell Sci* **114**, 2301-2313 (2001).
5. Lensch, M.W., Daheron, L. & Schlaeger, T.M. Pluripotent stem cells and their niches. *Stem Cell Reviews* **2**, 185-201 (2006).
6. Niwa, H. How is pluripotency determined and maintained? *Development* **134**, 635-646 (2007).
7. Smith, A.G. Embryo-Derived Stem Cells: of Mice and Men. *Annual Review of Cell and Developmental Biology* **17**, 435-462 (2001).
8. Koestenbauer, S. et al. Embryonic stem cells: Similarities and differences between human and murine embryonic stem cells. *American Journal of Reproductive Immunology* **55**, 169-180 (2006).
9. Ying, Q.L., Nichols, J., Chambers, I. & Smith, A. Bmp Induction of Id Proteins Suppresses Differentiation and Sustains Embryonic Stem Cell Self-Renewal in Collaboration With Stat3. *Cell* **115**, 281-292 (2003).
10. Prudhomme, W., Daley, G.Q., Zandstra, P. & Lauffenburger, D.A. Multivariate proteomic analysis of murine embryonic stem cell self-renewal versus differentiation signaling. *Proceedings of the National Academy of Sciences of the United States of America* **101**, 2900–2905 (2004).
11. Zandstra, P.W., Le, H.V., Daley, G.Q., Griffith, L.G. & Lauffenburger, D.A. Leukemia Inhibitory Factor (Lif) Concentration Modulates Embryonic Stem Cell Self-Renewal and Differentiation Independently of Proliferation. *Biotechnology and Bioengineering* **69**, 607-617 (2000).
12. Sato, N., Meijer, L., Skaltsounis, L., Greengard, P. & Brivanlou, A.H. Maintenance of Pluripotency in Human and Mouse Embryonic Stem Cells Through Activation of Wnt Signaling by a Pharmacological Gsk-3-Specific Inhibitor. *Nature Medicine* **10**, 55-63 (2004).
13. Viswanathan, S., Benatar, T., Rose-John, S., Lauffenburger, D.A. & Zandstra, P.W. Ligand/Receptor Signaling Threshold (List) Model Accounts for Gp130-Mediated Embryonic Stem Cell Self-Renewal Responses to Lif and Hil-6. *Stem Cells* **20**, 119-138 (2002).
14. Davey, R.E., Onishi, K., Mahdavi, A. & Zandstra, P.W. LIF-mediated control of embryonic stem cell self-renewal emerges due to an autoregulatory loop. *Faseb Journal* **21**, 2020-2032 (2007).

15. Davey, R.E. & Zandstra, P.W. Spatial organization of embryonic stem cell responsiveness to autocrine gp130 ligands reveals an autoregulatory stem cell niche. *Stem Cells* **24**, 2538-2548 (2006).
16. Keller, G. Embryonic stem cell differentiation: emergence of a new era in biology and medicine. *Genes & Development* **19**, 1129-1155 (2005).
17. Ying, Q.L., Stavridis, M., Griffiths, D., Li, M. & Smith, A. Conversion of embryonic stem cells into neuroectodermal precursors in adherent monoculture. *Nature Biotechnology* **21**, 183-186 (2003).
18. Fong, W., Tan, H., Choo, A. & Oh, S. Perfusion cultures of human embryonic stem cells. *Bioprocess and Biosystems Engineering* **27**, 381-387 (2005).
19. Fok, E.Y.L. & Zandstra, P.W. Shear-Controlled Single-Step Mouse Embryonic Stem Cell Expansion and Embryoid Body-Based Differentiation. *Stem Cells* **23**, 1333-1342 (2005).
20. Dang, S.M., Gerecht-Nir, S., Chen, J., Itskovitz-Eldor, J. & Zandstra, P.W. Controlled, Scalable Embryonic Stem Cell Differentiation Culture. *Stem Cells* **22**, 275-282 (2004).
21. Fernandes, A.M. et al. Mouse embryonic stem cell expansion in a microcarrier-based stirred culture system. *Journal of Biotechnology* **132**, 227-236 (2007).
22. Li, Y., Kniss, D.A., Lasky, L.C. & Yang, S.T. Culturing and differentiation of murine embryonic stem cells in a three-dimensional fibrous matrix. *Cytotechnology* **41**, 23-35 (2003).
23. El-Ali, J., Sorger, P.K. & Jensen, K.F. Cells on chips. *Nature* **442**, 403-411 (2006).
24. Khademhosseini, A., Langer, R., Borenstein, J. & Vacanti, J.P. Microscale technologies for tissue engineering and biology. *Proceedings of the National Academy of Sciences of the United States of America* **103**, 2480–2487 (2006).
25. Hung, P.J., Lee, P.J., Sabounchi, P., Lin, R. & Lee, L.P. Continuous Perfusion Microfluidic Cell Culture Array for High-Throughput Cell-Based Assays. *Biotechnology and Bioengineering* **89**, 1-8 (2005).
26. Shackman, J.G., Dahlgren, G.M., Peters, J.L. & Kennedy, R.T. Perfusion and chemical monitoring of living cells on a microfluidic chip. *Lab on a Chip* **5**, 56-63 (2005).
27. Thompson, D.M. et al. Dynamic gene expression profiling using a microfabricated living cell array. *Anal. Chem.* **76**, 4098-4103 (2004).
28. Saadi, W., Wang, S.J., Lin, F. & Jeon, N.L. A parallel-gradient microfluidic chamber for quantitative analysis of breast cancer cell chemotaxis. *Biomed. Microdevices* **8**, 109-118 (2006).
29. Lin, F. et al. Generation of Dynamic Temporal and Spatial Concentration Gradients Using Microfluidic Devices. *Lab on a Chip* **4**, 164-167 (2004).
30. Abhyankar, V.V., Lokuta, M.A., Huttenlocher, A. & Beebe, D.J. Characterization of a membrane-based gradient generator for use in cell-signaling studies. *Lab on a Chip* **6**, 389-393 (2006).
31. Chung, B.G. et al. Human Neural Stem Cell Growth and Differentiation in a Gradient-Generating Microfluidic Device. *Lab on a Chip* **5**, 401-406 (2005).
32. Takayama, S. et al. Selective chemical treatment of cellular microdomains using multiple laminar streams. *Chemistry & Biology* **10**, 123-130 (2003).
33. Rosenthal, A., Macdonald, A. & Voldman, J. Cell patterning chip for controlling the stem cell microenvironment. *Biomaterials* **28**, 3208-3216 (2007).
34. Khetani, S.R. & Bhatia, S.N. Microscale culture of human liver cells for drug development. *Nat Biotech* **26**, 120-126 (2008).

35. Bhatia, S.N., Balis, U.J., Yarmush, M.L. & Toner, M. Effect of Cell-Cell Interactions in Preservation of Cellular Phenotype: Cocultivation of Hepatocytes and Nonparenchymal Cells. *Faseb Journal* **13**, 1883-1900 (1999).
36. Rosenthal, A. & Voldman, J. Dielectrophoretic traps for single-particle patterning. *Biophys. J.* **88**, 2193-2205 (2005).
37. Albrecht, D.R., Underhill, G.H., Wassermann, T.B., Sah, R.L. & Bhatia, S.N. Probing the role of multicellular organization in three-dimensional microenvironments. *Nature Methods* **3**, 369-375 (2006).
38. Folch, A., Jo, B.H., Hurtado, O., Beebe, D.J. & Toner, M. Microfabricated Elastomeric Stencils for Micropatterning Cell Cultures. *Journal of Biomedical Materials Research* **52**, 346-353 (2000).
39. Wright, D., Rajalingam, B., Selvarasah, S., Dokmeci, M.R. & Khademhosseini, A. Generation of static and dynamic patterned co-cultures using microfabricated parylene-C stencils. *Lab on a Chip* **7**, 1272-1279 (2007).
40. Abhyankar, V.V. & Beebe, D.J. Spatiotemporal micropatterning of cells on arbitrary substrates. *Anal. Chem.* **79**, 4066-4073 (2007).
41. Albrecht, D.R., Liu, V., Saha, R.L. & Bhatia, S.N. Photo- and electropatterning of hydrogel-encapsulated living cell arrays. *Lab on a Chip* **5**, 111-118 (2005).
42. Leclerc, E., Sakai, Y. & Fujii, T. Cell culture in 3-dimensional microfluidic structure of PDMS (polydimethylsiloxane). *Biomed. Microdevices* **5**, 109-114 (2003).
43. Kane, B.J., Zinner, M.J., Yarmush, M.L. & Toner, M. Liver-specific functional studies in a microfluidic array of primary mammalian hepatocytes. *Anal. Chem.* **78**, 4291-4298 (2006).
44. Bettinger, C.J. et al. Three-dimensional microfluidic tissue-engineering scaffolds using a flexible biodegradable polymer. *Advanced Materials* **18**, 165-169 (2006).
45. Gu, W., Zhu, X.Y., Futai, N., Cho, B.S. & Takayama, S. Computerized microfluidic cell culture using elastomeric channels and Braille displays. *Proceedings of the National Academy of Sciences of the United States of America* **101**, 15861-15866 (2004).
46. Tourovskaia, A., Figueroa-Masot, X. & Folch, A. Differentiation-on-a-chip: A microfluidic platform for long-term cell culture studies. *Lab on a Chip* **5** (2005).
47. Hung, P.J. et al. A novel high aspect ratio microfluidic design to provide a stable and uniform microenvironment for cell growth in a high throughput mammalian cell culture array. *Lab on a Chip* **5**, 44-48 (2005).
48. Toh, Y.C. et al. A novel 3D mammalian cell perfusion-culture system in microfluidic channels. *Lab on a Chip* **7**, 302-309 (2007).
49. Figallo, E. et al. Micro-bioreactor array for controlling cellular microenvironments. *Lab on a Chip* **7**, 710-719 (2007).
50. Powers, M.J. et al. A microfabricated array bioreactor for perfused 3D liver culture. *Biotechnology and Bioengineering* **78**, 257-269 (2002).
51. Sivaraman, A. et al. A Microscale In Vitro Physiological Model of the Liver: Predictive Screens for Drug Metabolism and Enzyme Induction. *Current Drug Metabolism* **6**, 569-591 (2005).
52. Hu, G.Q., Quaranta, V. & Li, D.Q. Modeling of effects of nutrient gradients on cell proliferation in microfluidic bioreactor. *Biotechnology Progress* **23**, 1347-1354 (2007).

53. Mehta, G. et al. Quantitative measurement and control of oxygen levels in microfluidic poly(dimethylsiloxane) bioreactors during cell culture. *Biomed. Microdevices* **9**, 123-134 (2007).
54. Curran, S.J., Chen, R., Oates, M. & Hunt, J.A. Human mesenchymal stem cell differentiation on modified thin polymer films in a hypoxic microfluidic bioreactor: An experimental and computational modelling study. *Tissue Engineering* **12**, 1024-1024 (2006).
55. Mehta, K. & Linderman, J.J. Model-based analysis and design of a microchannel reactor for tissue engineering. *Biotechnology and Bioengineering* **94**, 596-609 (2006).
56. Roy, P., Baskaran, H., Tilles, A.W., Yarmush, M.L. & Toner, M. Analysis of oxygen transport to hepatocytes in a flat-plate microchannel bioreactor. *Ann. Biomed. Eng.* **29**, 947-955 (2001).
57. Yu, H.M., Meyvantsson, I., Shkel, I.A. & Beebe, D.J. Diffusion Dependent Cell Behavior in Microenvironments. *Lab on a Chip* **5**, 1089-1095 (2005).
58. Lee, P.J., Hung, P.J., Rao, V.M. & Lee, L.P. Nanoliter scale microbioreactor array for quantitative cell biology. *Biotechnology and Bioengineering* **94**, 5-14 (2006).
59. Khademhosseini, A. et al. Cell docking inside microwells within reversibly sealed microfluidic channels for fabricating multiphenotype cell arrays. *Lab on a Chip* **5**, 1380-1386 (2005).
60. Gray, B.L., Lieu, D.K., Collins, S.D., Smith, R.L. & Barakat, A.I. Microchannel Platform for the Study of Endothelial Cell Shape and Function. *Biomed. Microdevices* **4**, 9-16 (2002).
61. Lu, H. et al. Microfluidic shear devices for quantitative analysis of cell adhesion. *Anal. Chem.* **76**, 5257-5264 (2004).
62. Deen, W.M. Analysis of Transport Phenomena. (Oxford University Press, New York; 1998).
63. Ranjan, V., Waterbury, R., Xiao, Z.H. & Diamond, S.L. Fluid shear stress induction of the transcriptional activator c-fos in human and bovine endothelial cells, HeLa, and Chinese hamster ovary cells. *Biotechnology and Bioengineering* **49**, 383-390 (1996).
64. Tilles, A.W., Baskaran, H., Roy, P., Yarmush, M.L. & Toner, M. Effects of oxygenation and flow on the viability and function of rat hepatocytes cocultured in a microchannel flat-plate bioreactor. *Biotechnology and Bioengineering* **73**, 379 – 389 (2001).
65. Yamamoto, K. et al. Fluid shear stress induces differentiation of Flk-1-positive embryonic stem cells into vascular endothelial cells in vitro. *American Journal of Physiology-Heart and Circulatory Physiology* **288**, H1915-H1924 (2005).
66. Wang, H. et al. Shear stress induces endothelial differentiation from a murine embryonic mesenchymal progenitor cell line. *Arteriosclerosis Thrombosis and Vascular Biology* **25**, 1817-1823 (2005).
67. Tourovskaia, A., Kosar, T.F. & Folch, A. Local Induction of Acetylcholine Receptor Clustering in Myotube Cultures Using Microfluidic Application of Agrin. *Biophys. J.* **90**, 2192-2198 (2006).
68. Kim, L., Vahey, M.D., Lee, H.Y. & Voldman, J. Microfluidic arrays for logarithmically perfused embryonic stem cell culture. *Lab on a Chip* **6**, 394-406 (2006).
69. Lee, J.N., Jiang, X., Ryan, D. & Whitesides, G.M. Compatibility of Mammalian Cells on Surfaces of Poly(Dimethylsiloxane). *Langmuir* **20**, 11684-11691 (2004).

70. Thorsen, T., Maerkl, S.J. & Quake, S.R. Microfluidic Large-Scale Integration. *Science* **298**, 580-584 (2002).
71. Song, J.W. et al. Computer-controlled microcirculatory support system for endothelial cell culture and shearing. *Anal. Chem.* **77**, 3993-3999 (2005).
72. Piruska, A. et al. The autofluorescence of plastic materials and chips measured under laser irradiation. *Lab on a Chip* **5**, 1348-1354 (2005).
73. Heo, Y.S. et al. Characterization and resolution of evaporation-mediated osmolality shifts that constrain microfluidic cell culture in poly(dimethylsiloxane) devices. *Anal. Chem.* **79**, 1126-1134 (2007).
74. Toepke, M.W. & Beebe, D.J. PDMS absorption of small molecules and consequences in microfluidic applications. *Lab on a Chip* **6**, 1484-1486 (2006).
75. Randall, G.C. & Doyle, P.S. Permeation-driven flow in poly(dimethylsiloxane) microfluidic devices. *Proceedings of the National Academy of Sciences of the United States of America* **102**, 10813-10818 (2005).
76. Edmond W.K. Young, A.R.W.a.C.A.S. Chips & Tips: Avoiding bubble injection by droplet merging *Lab on a Chip* (2006).
77. Chappell, M.A. & Payne, S.J. A physiological model of the release of gas bubbles from crevices under decompression. *Respiratory Physiology & Neurobiology* **153**, 166–180 (2006).
78. Liu, H.B. et al. Micro air bubble formation and its control during polymerase chain reaction (PCR) in polydimethylsiloxane (PDMS) microreactors. *J. Micromech. Microeng.* **17**, 2055-2064 (2007).
79. Chen, S.S., Fitzgerald, W., Zimmerberg, J., Kleinman, H.K. & Margolis, L. Cell-cell and cell-extracellular matrix interactions regulate embryonic stem cell differentiation. *Stem Cells* **25**, 553-561 (2007).
80. Pihl, J. et al. Microfluidic Gradient-Generating Device for Pharmacological Profiling. *Anal. Chem.* **77**, 3897-3903 (2005).
81. Beebe, D.J., Mensing, G.A. & Walker, G.M. Physics and Applications of Microfluidics in Biology. *Annual Review of Biomedical Engineering* **4**, 261-286 (2002).
82. Gaver, D.P. & Kute, S.M. A Theoretical Model Study of the Influence of Fluid Stresses on a Cell Adhering to a Microchannel Wall. *Biophys. J.* **75**, 721-733 (1998).
83. McDonald, J.C. & Whitesides, G.M. Poly(Dimethylsiloxane) as a Material for Fabricating Microfluidic Devices. *Accounts of Chemical Research* **35**, 491-499 (2002).
84. Juncker, D. et al. Soft and Rigid Two-Level Microfluidic Networks for Patterning Surfaces. *J. Micromech. Microeng.* **11**, 532-541 (2001).
85. Wu, H.K., Odom, T.W., Chiu, D.T. & Whitesides, G.M. Fabrication of Complex Three-Dimensional Microchannel Systems in Pdms. *Journal of the American Chemical Society* **125**, 554-559 (2003).
86. Kim, L., Toh, Y.C., Voldman, J. & Yu, H. A practical guide to microfluidic perfusion culture of adherent mammalian cells. *Lab on a Chip* **7**, 681-694 (2007).
87. Stroock, A.D. et al. Chaotic Mixer for Microchannels. *Science* **295**, 647-651 (2002).
88. Bettger, W.J. & McKeehan, W.L. MECHANISMS OF CELLULAR NUTRITION. *Physiological Reviews* **66**, 1-35 (1986).
89. Tonack, S., Rolletschek, A., Wobus, A.M., Fischer, B. & Santos, A.N. Differential expression of glucose transporter isoforms during embryonic stem cell differentiation. *Differentiation* **74**, 499-509 (2006).

90. Kim, Y.H., Heo, J.S. & Han, H.J. High glucose increase cell cycle regulatory proteins level of mouse embryonic stem cells via PI3-K/Akt and MAPKs signal pathways. *Journal of Cellular Physiology* **209**, 94-102 (2006).
91. Irimia, D. et al. Microfluidic system for measuring neutrophil migratory responses to fast switches of chemical gradients. *Lab on a Chip* **6**, 191-198 (2006).
92. Sigma-Aldrich 2008).
93. Cochran, D.M., Fukumura, D., Ancukiewicz, M., Carmeliet, P. & Jain, R.K. Evolution of oxygen and glucose concentration profiles in a tissue-mimetic culture system of embryonic stem cells. *Ann. Biomed. Eng.* **34**, 1247-1258 (2006).
94. Pugacheva, E.N., Roegiers, F. & Golemis, E.A. Interdependence of cell attachment and cell cycle signaling. *Current Opinion in Cell Biology* **18**, 507-515 (2006).
95. Dai, C., Whitesell, L., Rogers, A.B. & Lindquist, S. Heat shock factor 1 is a powerful multifaceted modifier of carcinogenesis. *Cell* **130**, 1005-1018 (2007).
96. Xie, Y.Z. et al. Three-dimensional flow perfusion culture system for stem cell proliferation inside the critical-size beta-tricalcium phosphate scaffold. *Tissue Engineering* **12**, 3535-3543 (2006).
97. Batsilas, L., Berezhkovskii, A.M. & Shvartsman, S.Y. Stochastic Model of Autocrine and Paracrine Signals in Cell Culture Assays. *Biophys. J.* **85**, 3659-3665 (2003).
98. Hilton, D.J. & Nicola, N.A. Kinetic Analyses of the Binding of Leukemia Inhibitory Factor to Receptors on Cells and Membranes and in Detergent Solution. *Journal of Biological Chemistry* **267**, 10238-10247 (1992).
99. Millipore 2008).
100. Ogawa, K. et al. Activin-nodal signaling is involved in propagation of mouse embryonic stem cells. *Journal of Cell Science* **120**, 55-65 (2007).
101. Mittal, N., Rosenthal, A. & Voldman, J. NDEP microwells for single-cell patterning in physiological media. *Lab on a Chip* **7**, 1146-1153 (2007).
102. Herrmann, M., Veres, T. & Tabrizian, M. Enzymatically-generated fluorescent detection in micro-channels with internal magnetic mixing for the development of parallel microfluidic ELISA. *Lab on a Chip* **6**, 555-560 (2006).